Modelling Channel Morphodynamics: The Effects of Large Wood and Bed Grain Size Distribution

by

Lucy MacKenzie

B.Sc., University of British Columbia, 2012

A THESIS SUBMITTED IN PARTIAL FULFILLMENT
OF THE REQUIREMENTS FOR THE DEGREE OF

Master of Science

in

THE FACULTY OF ARTS
(Geography)

The University Of British Columbia
(Vancouver)

August 2014

Abstract

Within this thesis the results of a set of four stream table experiments are presented in order to examine the role that bed texture adjustments play in the development of a equilibrium channel form in the presence of large wood. Experiments were conducted using two physical models of Fishtrap Creek, an intermediate sized stream in the interior of British Columbia. While both flumes were Froude-scaled models with fixed banks and mobile beds, Model 1 contained a single grain size representative of the D_{50} of the prototype stream while Model 2 contained a scaled grain size distribution (GSD) of Fishtrap Creek. Two treatments of wood load were run in each model: a moderate wood load (a scale equivalent of 160 m^3/m^2) and a high wood load (a scale equivalent of 220 m^3/m^2). Channel morphology was captured at five-hour intervals in order to create DEMs of the evolving bed surface. The results of this study show that bed grain size composition plays a dominant role in shaping channel morphology, even in the presence of large wood. The addition of large wood increased sediment storage which resulted in an increase in reach-averaged bed slope, the magnitude of which was proportional to the wood load added. Large wood also caused new areas of scour and deposition to be imposed onto the channel morphology that had been established prior to the addition of wood, causing an overall decrease in pool spacing and median pool area. The presence of a grain size distribution constrained the range of depth values in the flume as it allowed the bed to self-stabilize by limiting scour depth through the process of armouring. Regardless of the presence of large wood, maximum depths were approximately twice as deep in the single grain size flume and pools were deeper relative to their area. These results highlight the necessity of considering the full grain size distribution when modelling channel response to changes in the governing variables that influence channel morphology.

Preface

This dissertation is based on a set of four experiments that were designed by Brett Eaton. Experiment 1 was run by Siri Hermanski as part of a work study position in 2011. Experiment 2 was run by Lucy MacKenzie as part of a work study in 2012. Experiments 3 and 4 were run by Sarah Davidson as part of her M Sc Thesis in 2009 and 2010. All of the analysis and writing presented in this dissertation was done by Lucy MacKenzie and none of the text is taken directly from previously published or collaborative articles, including Davidson's M Sc thesis.

Table of Contents

Abstract . . . . . **ii**

Preface . . . . . **iii**

Table of Contents . . . . . **iv**

List of Tables . . . . . **vi**

List of Figures . . . . . **vii**

Acknowledgments . . . . . **ix**

1 Introduction **1**

1.1 How Rivers Work 1

1.2 How Have We Studied Rivers 4

1.3 Objectives and Research Questions 9

1.4 Thesis Organization 10

2 Experimental Design **11**

2.1 Issues of Scale in Physical Modelling 11

2.1.1 Types of Scale Models 13

2.1.2 Modeling Large Wood in Stream Channels 15

2.2 Prototype Stream: Fishtrap Creek 15

2.3 Model Design 18

2.4 Experimental Design and Data Collection 24

3 Data Analysis **27**

3.1 Bed Elevation 27

3.2 Water Surface Elevation and Water Depth . . . 30
3.3 Pool Identification . . . 34
3.4 Wood Location Data . . . 36

4 Results . . . 37
4.1 Experiment 1 . . . 37
4.2 Experiment 2 . . . 41
4.3 Experiment 3 . . . 43
4.4 Experiment 4 . . . 45
4.5 Synthesis of Results . . . 46

5 Discussion . . . 53
5.1 Equilibrium Without Wood . . . 53
5.2 The Addition of Large Wood . . . 55
5.3 Equilibrium with Wood Present . . . 56
5.4 The Role of a GSD . . . 58

6 Conclusions . . . 62
6.1 Grain Size Distribution . . . 62
6.2 The Presence of Large Wood . . . 63
6.3 Wood Load . . . 64
6.4 Applications of this Study . . . 64
6.5 Future Work . . . 65

Bibliography . . . 66

A LiDAR Visualization . . . 77
A.1 LiDAR: Remotely Sensed Data . . . 77
A.1.1 Research Objectives . . . 78
A.2 LiDAR Visualization Methods . . . 79
A.3 Proposed Method of Visualization . . . 81
A.3.1 Comparison of Visualization Methods . . . 88

B Digital Elevation Models . . . 92

C DEMs of Difference . . . 105

List of Tables

Table 2.1 Model and Prototype Parameters 23
Table 2.2 Model Wood Piece Characteristics 23
Table 2.3 Summary of Experiments 24
Table 2.4 Facies Grain Size Categories 26

Table 3.1 DEM Uncertainty 29

Table 4.1 Comparison of Sediment Storage and Bed Slope 37
Table 4.2 Summary of Steady State Morphology 38
Table 4.3 Within-Pool Bed Surface Texture 45

Table 5.1 Summary of the Effects of Wood Addition, Wood Load, and GSD 60

Table A.1 Summary of PCA Analysis 84

List of Figures

Figure 2.1 LiDAR Image of Fishtrap Creek Watershed and Surroundings 17
Figure 2.2 Location of Fishtrap Creek and the Study Reach 18
Figure 2.3 Study Reach at Fishtrap Creek in 2008 19
Figure 2.4 The Approximate Area of Fishtrap Creek Represented by the Two Models . . 20
Figure 2.5 Images of the Two Models 21
Figure 2.6 Grain Size Distributions of Prototype and Models 22
Figure 2.7 Examples of Bed Surface Texture from the Two Models 22
Figure 2.8 Model Wood Piece Forms 24
Figure 2.9 Laser Mount 26

Figure 3.1 Depth Distributions 31
Figure 3.1 Depth distributions continued 32
Figure 3.2 Pool Areas for Various Depth Criteria 33
Figure 3.3 Mean Pool Areas for Various Pool Depth Criteria 35

Figure 4.1 Example DEMs from Experiment 1 39
Figure 4.2 Longitudinal Profiles Prior to and Following Wood Addition 40
Figure 4.3 Example DEMs from Experiment 2 42
Figure 4.4 Example DEMs from Experiment 3 44
Figure 4.5 Example DEMs from Experiment 4 46
Figure 4.6 DoDs of Equilibrium Morphologies 48
Figure 4.7 Cumulative Sediment Storage Since Wood Addition 49
Figure 4.8 Pool Spacing and Area Through Time 50
Figure 4.9 Pool Morphologies Relative to Wood Load 51
Figure 4.10 Pool Morphologies Relative to Bed Textures 52

Figure 5.1 Wood Movement Through Time 55

Figure A.1 Components of a PCA 82
Figure A.2 Example of LiDAR Visualization Method 83
Figure A.3 Various Methods of PCA Visualization 85
Figure A.4 Flow Chart of LiDAR Visualization Method 87
Figure A.5 Visualization Methods Compared for Location 1 89
Figure A.6 Visualization Methods Compared for Location 2 90
Figure A.7 Visualization Methods Compared for Location 3 91

Figure B.1 DEM Legends 92
Figure B.2 Digital Elevation Models for Experiment 1 96
Figure B.3 Digital Elevation Models for Experiment 2 100
Figure B.4 Digital Elevation Models for Experiment 3 102
Figure B.5 Digital Elevation Models for Experiment 4 104

Figure C.1 DoD Legend 105
Figure C.2 DEMs of Difference for Experiment 1 109
Figure C.3 DEMs of Difference for Experiment 2 113
Figure C.4 DEMs of Difference for Experiment 3 115
Figure C.5 DEMs of Difference for Experiment 4 117

Acknowledgments

I would first of all like to thank my two supervisors, Dr Brett Eaton and Dr Michele Koppes, for the help and guidance they have provided throughout my academic career thus far. I am not sure that I would have pursued my master's degree without the encouragement and support of Dr Koppes. She has been an inspiring mentor throughout this process and I am thankful for her advice and support. I am also grateful to Dr Eaton who helped shape my background in geomorphology as well as fostered the development of my own ideas about the way things work. His knowledge and enthusiasm have motivated me to do my very best.

I would like to thank my office mates, Lawrence Bird, Matt Chernos, and Alexis Moyer, who have provided valuable help as well as valuable distractions throughout the process of my degree. Likewise, many, many thanks to Sarah Davidson who has been a true friend as well as a (future) collaborator. I would also like to thank the rest of my lab group, in particular Lea Zhecheva, Ariel Kettle, and Siri Hermanski, for their help in the lab, the field, and in our many brainstorming sessions.

Finally, I want to express how lucky I am to have the very best friends and family. Although I have encountered a number of tough and stressful challenges within this process I have always felt supported and well-loved; there is no way I could have succeeded without them.

Chapter 1

Introduction

1.1 How Rivers Work

From small mountaineous channels to huge rivers that cut through plateaus and plains, all streams act to shape the landscape. It is generally accepted that, regardless of size, the range of possible forms that channels may exhibit is constrained by the timing and magnitude of flows in the channel (Q), the material that is transported and deposited along its length (Q_b), and local boundary conditions such as bank strength and bed sedimentology (e.g. Mackin, 1948; Lane, 1957; Millar and Quick, 1993; Montgomery and Buffington, 1998; Eaton and Church, 2004). The relations between these three governing conditions have been described using both empirically-derived equations as well as physically-based theories. Predicting how a channel reacts to changes in one or several of these conditions has long been a source of interest, as changes to environmental drivers within fluvial systems is inevitable.

Although moderate flows can rework both bank and bed material, it is the peak annual discharge, or bankfull flow, that is the most geomorphically effective in shaping channel form (Wolman and Miller, 1960). The magnitude of discharge that a channel experiences is a function of the size of the contributing watershed area (Dunne and Leopold, 1978) and the hydrologic connectivity within the watershed (Jencso et al., 2009). The timing and duration of the peak flows are driven by the general climate of the area and the presence of glaciers or other anthropogenic diversions (e.g. dams or agricultural demands) in upstream areas (Déry et al., 2009).

Material found within a channel reach may either be transported in from upstream or eroded from banks and the surrounding area. The flux of sediment coming into the system, $Q_b(t)$, influences the relative magnitude of erosion and deposition that occurs within the channel (Montgomery and Buffington, 1998). However, because the ability of the channel to move sediment

through the system ultimately depends on $Q(t)$, the tendency for a channel to aggrade or degrade over a period of time is dictated by the relative ratio of sediment transport capacity to sediment supply (Montgomery and Buffington, 1997).

The size distribution of particles, $Q_b(D)$, that are transported in from upstream reaches or is eroded from channel banks also influence channel morphology. The size of particles relative to the discharge influences the amount of sediment transport that can occur (Buffington and Montgomery, 1999b) while the distribution of sizes present allows for stabilizing processes such as armouring and the development of other features, such as stone cells, to form (Church et al., 1998).

The range of boundary conditions that account for a huge amount of variability in channel morphologies worldwide. Consequently, it is important to consider the geological, fluvial, and, if applicable, glacial legacies of an area when examining channel morphologies. These processes play a part in forming the longitudinal valley slope, S_v, which constrains the range of channel slopes that are possible and thereby influences the sediment transport ability of the channel (Eaton and Church, 2004). Bank strength, which is dictated by the cohesiveness of bank sediment and the presence of vegetation, also influences channel form but must be considered relative to bed strength as well as in relation the the width to depth ratio of the channel (Eaton and Millar, 2004; Millar, 2005; Eaton and Giles, 2009).

Outside of the governing conditions, although partially linked to bank stability, in-stream large wood (LW), or wood pieces larger than 0.1 m in diameter and 1 m in length (Hassan et al., 2005), has also been found to influence channel morphology at a channel-unit, channel-reach, and watershed scale (Abbe and Montgomery, 2003; Thompson, 1995; Brummer et al., 2006). Input from adjacent forest areas or transported in from upstream reaches (Webb and Erskine, 2003; Bocchiola, 2011), LW plays a significant role in modifying reach-scale channel hydraulics and sediment transport by increasing flow resistance, and thereby decreasing flow velocity (Buffington and Montgomery, 1999a; Manga and Kirchner, 2000; Wilcox et al., 2006; Davidson and Eaton, 2012). Trapping over 150 % of the annual bed load and sediment yield (e.g.Megahan, 1982; Andreoli et al., 2007), in-stream LW accounts for the storage of more sediment than the amount that is stored in riffles or by other channel obstructions (Megahan, 1982; Thompson, 1995). The volume of sediment stored within a stream channel correlates to the amount of LW present in a stream channel: streams with higher wood loads store more sediment than those with little or no wood (Gomi et al., 2001; Tecle et al., 2001; May and Gresswell, 2003; Davidson and Eaton, 2012). In mountaineous terrain, where wood loads are high and streams are of intermediate size, log jams act as one of the dominant storage reservoirs for sediment at a watershed scale (May and Gresswell, 2003).

LW affects where within the stream channel sediment erosion and deposition will occur by altering flow patterns within a stream channel (e.g. Thompson, 1995; Abbe and Montgomery, 1996; Buffington et al., 2002; Montgomery et al., 2003). Erosion tends to occur in areas of vortices and flow compression whereas deposition occurs primarily in areas of flow divergence. The areas of backwater often caused by valley dams are key locations of deposition in stream channels as the channel-spanning jam imposes a new, higher base level which results in reduced flow velocities and decreased sediment transport (Lisle, 1986; Thompson, 1995; Lancaster et al., 2001; Wohl, 2011).

A fluvial system in equilibrium, or steady state, is defined as one in which the functional relationship between the input and output variable(s) is invariant for some period of time (Howard, 1982; Renwick, 1992). Streams in equilibrium often display an optimal channel form, one that is 'in regime' with the given hydraulic regime, which is dictated by $Q(t)$ and $Q_b(t,D)$. It must be noted however, that this is a dynamic equilibrium, meaning that although the overall channel dimensions remain relatively fixed (e.g. width-to-depth ratio), the location of bars, banks, pools, and meanders are not necessarily stable through time (Millar, 2005).

The time it takes for a system to respond to a change in one or several of the governing conditions is characterized by its response, or relaxation, time which is a function of the size of the channel network (or stream length), the hydraulic regime, and to a lesser extent, the magnitude of change itself (Howard, 1982, 1988). Systems tend to be insensitive to regime changes that cycle on time scales shorter than the response time (e.g. annual fluctuations in discharge and sediment yield) (Howard, 1982). Likewise, if input variables cycle at a lower frequency than the response time, the system has time to adjust while remaining in equilibrium (Howard, 1982).

Rapid changes in trends, step changes, pulse inputs, or an intermediate frequency input cycles can cause the morphology of a channel to alter (Howard, 1982). Such changes can be caused by processes and events such as mass movements from valley sides, upstream mining or forestry practices, dam construction or removal, forest fires, and watershed urbanization (Montgomery and Buffington, 1998). Due to the prevalence of such forcings in watersheds worldwide, the morphology of many real world streams are constantly adjusting to changes in their governing conditions.

Despite this, the concept of a steady state channel configuration is pervasive within the field of fluvial gemorphology and underlies much of our qualitative understanding of morphodynamics within fluvial systems (Lane, 1955). This is driven by the fact that studies have to assume morphological equilibrium of a channel in order to isolate the role that single variables play in dictating channel morphology.

Regime theory has been developed with the goal of better understanding how channel mor-

phology responds to environmental change (Eaton and Church, 2004). This approach applies the concept of governing conditions to stream channels in order to predict an optimized channel geometry for any given set of conditions. This is accomplished by utilizing relations that incorporate bed material transport, flow resistance, and bank stability (Kirkby, 1977; Chang, 1979; Davies and Sutherland, 1983; Millar and Quick, 1993). Using these, regime models attempt to find single solutions that represent an equilibrium stream geometry configuration for any given set of inputs. While empirical relations, derived from regression analysis of observed channel geometries, have been used to solve for the hydraulic geometry of simple channels, such as canals, rational regime models utilize physically-based equations to guide our understanding of channel response.

A rational regime model proposed by Eaton et al. (2004) predicts that channel stability, and therefore an equilibrium form, is achieved by adjustments made at three scales: grain scale, bedform scale, and reach scale. Adjustments occur at grain and bedform scales through changes to the surface texture and structure (e.g. Ashmore, 1991a; Church et al., 1998; Wilcox et al., 2006). In channels where banks are erodable, changes to flow resistance occur at a reach scale through adjustments to channel gradient achieved through changes to channel sinuosity (e.g. Eaton and Church, 2004).

Understanding how different processes act to shape channel morphology is important in a changing world as humans play a large role in modifying governing processes that act to shape fluvial systems at a range of scales. Development and land use change influence watersheds by increasing runoff in urban areas, by rerouting water for agricultural uses and by limiting sediment supply in areas downstream of dams, among other things (Stromberg et al., 2004). Overlaid on top of that are anthropogenic changes to the climate system which influence many geomorphic processes. Evidence for non-linear changes in cycles of stream discharge, in large part due to changes in precipitation patterns resulting from increased melt of permafrost and glaciers (e.g. Clarke, 2007; Shook and Pomeroy, 2012), have been observed on several continents. By altering temporal patterns of stream discharge, $Q(t)$, this "loss of hydrologic stationarity" in conjunction with increased pressure on our freshwater systems will continue to play a role in altering the morphology of many fluvial systems (Sandford, 2012).

1.2 How Have We Studied Rivers

Our current state of knowledge regarding fluvial systems has come from three principle methods of amassing data: field studies, numerical modelling, and physical modelling, or experimentation. All three methods have their own inherent strengths and weaknesses that must be considered when conducting analysis on the results. In many circumstances, the best understanding of physical

processes is acquired when all three are used in conjunction with one another.

Field studies are based on observations in which quantitative measurements and qualitative classifications are made on real-life systems. Case studies are a type of field-based method of data collection, conducted at one location, in which a single system is studied in depth to better understand the unique context that gave rise to its current state but also in order to get at the underlying processes that drive the system. Field studies may also be undertaken in the form of a survey in which many field sites are examined and the results are compared and contrasted between sites in order to understand the relationship between two or more variables. It is from the results of these multi-site field studies that many empirical relations are derived.

Field studies are very important in shaping our understanding of how the driving forces affect the actual morphology of stream channels, and for guiding the development of conceptual models regarding the functioning of fluvial systems. Additionally, measurements of real stream channels are commonly used to validate the results of numerical and physical models.

Numerical models use empirical and physical relations to model the functioning of systems over a long period of time or for a range of different scenarios. These types of studies rely on pre-existing concepts of how systems operate, which generally have been formed through field observations. Studies that employ numerical modelling are best used to assess patterns that exist within the real world and to construct hypotheses that may be tested using field studies.

While it is very appealing to take the results of numerical models at face value, it is important to recognize that their results are dictated by the choices made by the user as the conceptual model on which it is based as well as which the equations used in the model, whether physical or empirical, ultimately govern the results of the model. Furthermore, the high sensitivity of numerical models to their initial inputs demonstrates the necessity of having reliable measurements of existing systems derived from field work.

Many rational regime models are numerical models that use optimality criterion to obtain the solution for the hydraulic geometry of a channel for a given set of conditions (Millar and Quick, 1993; Eaton et al., 2004). The type of criterion used depends both on the extremal hypothesis is invoked as well as the processes under study. Extremal hypotheses attempt to describe which channel variable(s) is optimized by the fluvial system in order achieve an equilibrium geometry. Examples of such hypotheses include minimizing stream power (Chang, 1979), maximizing sediment transport efficiency (Kirkby, 1977), maximizing sediment transport capacity (White and Paris, 1982; Millar and Quick, 1993; Millar, 2005), maximizing friction factor (Davies and Sutherland, 1983) and maximizing resistance to flow (Eaton et al., 2004). In many ways all of these hypotheses are addressing the same fundamental processes and comparison of the results of different hypotheses for similar conditions have been shown to yield equivalent results (White and

Paris, 1982). While numerical modelling affords the ability to compare the results derived from the different hypotheses, it does not allow us to determine how river systems actually adjust to change.

Physical modelling is useful in investigating how well hypotheses explain or predict how fluvial systems come into equilibrium. Unlike in field studies, where the results are purely observations of the existing conditions, physical modelling is an experimental method and allows for single or multiple conditions to be varied. Additionally, because physical modelling allows for a decoupling of process from any specific environmental conditions, this type of model is useful for studying relationships and processes that are applicable to entire populations of phenomena rather than single case studies (Hooke, 1968).

Physical modeling has several advantages over data collection in the field. First of all, working in a laboratory or controlled environment reduces the hazards and technical difficulties associated with collecting field data. Many geomorphic and hydrologic processes of interest in fluvial environments occur predominantly during periods of high flow when the ability to collect data is compromised due to logistical and safety constraints (Braudrick and Grant, 2001). For example, high rates of discharge during high flows make stream crossing hazardous, while the increased ability of transport of sediment and debris poses threats to in-stream instruments. Physical experiments permit high flow conditions to be mimicked, allowing for hydraulic and geomorphic variables to be measured, while reducing the risk associated with measurement.

Secondly, physical modeling of stream channels allows us to address the role that specific variables have on complex processes as they allow us to alter a single variable while holding the rest of the system steady. Consequently, it is possible to determine the how changes to a specific variable may alter channel conditions. This type of control also allows us to deconstruct processes that are too complex to fully understand based on field data alone (Wallerstein et al., 2001).

Lastly, the scaling down of models from field prototypes in the field allows us to decrease not only the spatial dimensions of a stream channel, but also the temporal dimension as well, meaning that it becomes possible to study in the time frame of hours to days the effects of processes that, in real life, operate on time scales ranging from years to decades. This is important as the length of time series required to study certain fluvial processes are not readily available and inherently require long periods of time to acquire.

Stream tables, or flumes, are scaled-down physical models of stream channels. Two general types of models exist: prototype models and generic models. Prototype models are scaled versions of a specific stream channel and are used to examine how changes to certain variables affect the system as a whole. “Generic” models (which have also been called “analogue” or “similarity of process” models (Hooke, 1968)) are not models of any specific prototype stream, but instead obey

gross scaling relationships found in fluvial systems and are used to study general fluvial processes. Chapter 2 goes further into detail regarding the methods employed when creating physical models.

Flume experiments began to appear in the scientific literature around the late 1800s and early 1900s. In many of these first studies, the observations made from the models were qualitatively rather than quantitatively related back to the original system (Gilbert and Murphy, 1914). Some of the first modelling techniques that employed scaling equations through dimensional analysis were first described by Buckingham (1915) and later refined throughout the rest of the 1900s by both fluvial geomorphologists and hydraulics engineers alike (e.g. Bruun, 1966; Hooke, 1968; Hebertson, 1969; Schumm et al., 1987; Postma et al., 2008). Key findings from these early studies confirmed that if gross scaling relationships were met it could be assumed that the same morphodynamic processes operated in both the model and the prototype (Bruun, 1966; Hooke, 1968).

Physical models have been used to examine a range of processes in fluvial geomorphology including: sediment transport within channels (e.g. Ashmore, 1988; Young and Davies, 1991), the development of channel pattern (e.g. Schumm and Khan, 1972; Whiting and Dietrich, 1993; Termini, 2009), how channel patterns are sustained through time (e.g. Ashmore, 1991b; Braudrick et al., 2009), how channel patterns change (e.g. Schumm and Khan, 1972; Davies and Lee, 1988), and local scour patterns due to roughness elements within the channel (e.g. Cherry and Beschta, 1989; Kuhnle et al., 2002; Dey and Raikar, 2007; Pagliara and Carnacina, 2010; Bocchiola, 2011).

When designing a flume experiment to examine hypotheses within regime theory it is necessary to consider the conditions that govern channel morphology: water discharge, sediment flux and size distribution, and local environmental factors (e.g. valley slope, bank cohesion, geological history). Manipulating and isolating these many different components within a physical model allow the user to focus in on the relationships between different variables in the system.

Experiments conducted in a generic physical model of a laterally active gravel stream bed by Eaton and Church (2004) examined the relationship between channel geometry and three independent variables, discharge (Q), sediment discharge (Q_b), and valley slope (S_v), in order to investigate the hypothesis proposed by Eaton et al. (2004) that adjustments to governing conditions occurs at three different scales. When Q and Q_b were varied and changes to channel morphology were possible at all scales,Eaton and Church (2004) found that the primary channel adjustments occurred at a reach scale through the modification of channel slope. Changes in grain and bedform scale, such as surface armouring and changes in channel cross section geometry, were found to only contribute in a minor way to the overall changes in channel morphology.

While Eaton and Church (2004) found that adjustments to channel slope occurred through changes in channel sinuosity (i.e. channel length), a similar set of experiments conducted by Madej et al. (2009), found that although channel slope adjusted in response to changes in Q_b,

these adjustments occurred through changes in bed elevation driven by aggredation or degradation. Additionally, Madej et al. (2009) observed changes in bed armouring and channel geometry under high sediment feed and zero sediment feed conditions. This response was attributed to the fact that although the streams in both experiments were able to erode through the substrate, the flume bed used by Madej et al. (2009) was narrower than that used by Eaton and Church (2004), meaning that channel migration was limited by the flume walls. These results indicate that if a channel is limited at one scale, in this case at a reach scale, in its ability to respond to changes in governing conditions, this must be compensated for through changes to flow resistance at other scales.

In order to further examine the ability of the system to respond to changes in governing conditions at a bedform and grain scale, Eaton and Church (2009) conducted a set of experiments in which Q_b was varied in a flume with non-erodible banks. Like what was seen by Madej et al. (2009) in moderate sediment feed conditions, the results from these experiments showed that bed state adjustments were able to compensate for nearly a twofold range of Q_b without significant changes to channel gradient. However, at high and sediment feed rates, the system was found to experience net aggredation in the upper part of the study reach and was unable to establish a morphologic equilibrium form with respect to the governing conditions.

The results from experiments mentioned above contribute to our understanding of how stream channels adjust to changes in governing conditions. In unconstrained systems with erodible banks, stability is achieved by the channel adjusting its sinuosity to accommodate the imposed conditions (Eaton and Church, 2004). In systems where the channel is constrained or the banks are non-erodible, bed form adjustments can accommodate moderate changes in Q and Q_b, (Madej et al., 2009; Eaton and Church, 2009).

Given its influence on channel morphology and its prevalence in streams worldwide, large wood in stream channels is another important variable to study in relation to regime theory. In order to investigate the relationship between large wood and reach-scale channel morphology, a set of experiments were conducted on a non-erodible bank flume under the conditions of constant S_v, Q_b and Q (Davidson, 2011).

Davidson (2011) found the addition of LW resulted in decreased a reach-averaged flow velocity. This decrease in sediment transport lead to the aggradation of material in the flume, the magnitude of which corresponded to the wood load present in the channel. In the presence of high wood loading, this storage of sediment resulted in a higher reach-averaged bed gradient at equilibrium. Additionally, Davidson (2011) found that the higher spatial variability of local flow patterns around LW pieces increased the heterogeneity of the bed surface as evidenced through the development of a greater number of bed facies patches with wood present.

Altogether, the results of Davidson (2011) suggest that stream channels adapt to increases in

flow resistance caused by the addition of LW by adjusting both at a reach-scale, through changes to reach-averaged gradient, and at a bed form scale, through changes to bed facies. These findings contradict those of Eaton and Church (2009) which predict that, in a non-erodible bank flume, bed state alone should adjust to changes to governing variables and if changes to sediment supply are too large for the channel to adjust to by altering the bed state alone the system will be unable to achieve equilibrium.

1.3 Objectives and Research Questions

Studies that utilize physical models of stream channel reveal that, in highly simplified systems, the stability of the stream boundary dictates whether the channel will accommodate changes in governing conditions either through adjustments at a reach scale in systems where banks are erodible (Eaton and Church, 2004) or through changes in bed state where bank erosion is constrained (Eaton and Church, 2009). Introducing additional roughness elements into a non-erodible flume in the form of modelled large wood pieces, increases the complexity of the response of the system to the newly imposed conditions as both reach-scale and bed-scale adjustments are observed (Davidson, 2011).

This study aims to further examine the morphologic response of stream channels to the addition of wood by i) examining the changes in bed morphology that occur following the addition of large wood and ii) assessing the role that the bed grain size distribution has on channel morphodynamics. The following questions will be addressed in relation to these themes:

1. How does bed texture influence the progression of the channel into equilibrium in the absence of large wood?

2. What are the main differences in equilibrium channel morphology in the absence of large wood when only a single grain size is used compared to when a wide range of grain sizes are present?

3. What impacts does the addition of large wood have on channel morphodynamics?

4. In a non-erodible bank, mobile bed flume, how does the system adjust to accommodate the presence of large wood?

5. In the presence of large wood, what are the main differences in equilibrium channel morphology with and without a full grain size distribution?

6. How do different wood loads influence the resulting equilibrium channel morphology?

1.4 Thesis Organization

Chapter 2 discusses the experimental design of the flume experiments. Issues of scaling of both the prototype models and large wood pieces are introduced and addressed. The prototype stream, Fishtrap Creek, is described and previous work on the field site is summarized. Both the design of the models themselves and the design of the experiments are outlined and the methods of data collection are explained.

Chapter 3 presents the methods used in the analysis of the data. This includes the creation of digital elevation models of the bed surface elevation and depth maps from the bed elevation data and water surface elevations. It also presents a method for identifying pool areas from depth maps.

Chapter 4 presents the results from the flume experiments. Channel morphology is qualitatively assessed based on the digital elevation models of the bed surface. The temporal patterns of erosion and deposition are considered by examining the spatial correlation between subsequent runs. The relative amount and location of sediment storage that occurred in each experiment is presented. Pool morphology is compared between different wood loads and with and without a full grain size distribution.

Chapter 5 discusses the results of this study in relation to the questions outlined in the objectives. This chapter is organized into sections that examine the channel morphodynamics 1) associated with the development of an equilibrium morphology without wood present, 2) those related with the addition of wood, and 3) those linked to the flume coming into equilibrium with wood present.

Chapter 6 summarizes the results of this study and proposes areas of further study related to the main themes that are presented.

Appendix A presents a short study that outlines a LiDAR visualization method developed in order minimize the biasing associated with the hillshading of DEMs using a single angle of illumination.

Appendix B supplies the digital elevation models of the flume bed at the culmination of each run of each experiment.

Appendix C supplies DEMs of difference showing the change in elevation between each subsequent run for all experiments.

Chapter 2

Experimental Design

2.1 Issues of Scale in Physical Modelling

When utilizing flumes, especially prototype models, it is necessary to employ scaling techniques in order to assure that the types of processes and results observed during the experimental runs can be scaled up and applied to the real streams which they are attempting to model. Scaling techniques aim to properly scale key variables are commonly known as 'pi' (Π) terms (Peakall et al., 1996). The Π terms differ slightly on whether the model is attempting to simulate sediment transport or not.

For fixed-bed models with non erodible channel boundaries and no sediment transport (i.e. no loose substrate), the Π terms are: the flow Reynolds number (Re, Eqn. 2.1), the Froude number (Fr, Eqn. 2.2), the relative roughness (Eqn. 2.3), and the channel bed slope (Eqn. 2.4). Fixed-bed models have been used to examine processes that occur in stream channels but are separate from sediment movement, such as wood transport and movement (Braudrick and Grant, 2000; Bocchiola, 2011). The controlling variables that make up these equations for fixed-bed open channel flow model are (Yalin, 1971; Peakall et al., 1996):

- properties of the fluid: the dynamic viscosity (μ) and density (ρ)
- boundary conditions of the channel: hydraulic radius (R) and surface roughness (k_s)
- bed slope (S)
- average downstream velocity (U) and
- gravitational constant (g)

$$\Pi_1 = \frac{\rho R U}{\mu} = Re \tag{2.1}$$

$$\Pi_2 = \frac{U}{\sqrt{gR}} = Fr \tag{2.2}$$

$$\Pi_3 = \frac{k_s}{R} \tag{2.3}$$

$$\Pi_4 = S \tag{2.4}$$

Mobile-bed studies are more common in practice as they are used to examine key aspects of channel morphodynamics such as sediment transport and/or channel morphology (e.g. Madej et al., 2009; Malverti et al., 2008; Wallerstein et al., 2001; Whiting and Dietrich, 1993; Schumm and Khan, 1972). When a mobile bed model is used, the system is modelled as a two-phase flow comprised of the sediment particles and the overlying fluid. Consequently, in addition to the Re number and the Fr number, other Π terms, namely the relative roughness of the sediment (Eqn. 2.5), the relative density of the sediment (Eqn. 2.6), the grain Reynolds number (Eqn. 2.7), and an expression of the Shields relationship (Eqn. 2.8), must be considered. In mobile-bed experiments, two additional parameters, the sediment density (μ_s) and the characteristic grain size of the sediment (D) are employed in addition to μ, ρ, R, k_s, S, U, and g.

$$\Pi_1 = \frac{R}{D} \tag{2.5}$$

$$\Pi_2 = \frac{\rho_s}{\rho} \tag{2.6}$$

$$\Pi_3 = \frac{\rho U_* D}{\mu} = Re_* \tag{2.7}$$

$$\Pi_4 = \frac{\rho U_*^2}{\gamma_s D} \tag{2.8}$$

In mobile bed studies it is necessary mimic the sediment size distribution of the prototype stream in order to both assure a rough boundary layer and to correctly model sediment transport. The sediment size distribution of a flume is associated with flow and hydraulic constraints (as it dictates Re_*), bedload transport and deposition, and particle settling. It is also related to bank cohesion in flumes with unconstrained channels. Consequently it is necessary to scale the distri-

bution as accurately as possible. For most prototype–model relationships, this is done by scaling down grain size distribution of the prototype (Madej et al., 2009). It is, however, difficult to maintain accurate sediment scaling in cases where the lower end of the sediment size distribution scales down to less than 300 μm as past this point the $Re*$ drops lower than 70, meaning that the flow over these particles is no longer fully rough and the dimensionless shear stress of entrainment changes rapidly. This is mitigated against by using sediment only greater than 300 μm.

The cohesion of sediment, and therefore bank strength, can also be changed during scaling down of sediment as clay minerals have different intermolecular forces that sand or gravel. The increase in cohesion of sediment due to the addition of clay has been shown to limit channel erosion in flumes (Schumm and Khan, 1972). This issue is especially relevant for microscale river experiments as it is impossible to truncate the grain-size distribution at silt-sized particles, as is often done in other studies. In response to this issue, studies have shown that it is possible to use alternative materials, such as inert silica flour (Garcia, 1993), Urea type II plastic (Gaines and Maynord, 2001) or small glass beads (Malverti et al., 2008), to replace the clays without affecting the outcome of the experiment drastically.

Models can also be divided into experiments that use unconstrained (mobile banks) and those that use constrained channels (fixed banks). Constrained banks are often used to study the affects of a specific channel pattern on sediment transport and deposition processes, for example, the pattern of channel bars in a sinusoidal channel (Whiting and Dietrich, 1993; Eaton and Church, 2009). Flumes with unconstrained, erodible banks have been used to study how changes in channel pattern are related to changes in sediment discharge or other key variables (e.g. Schumm and Khan, 1972; Wallerstein et al., 2001; Eaton and Church, 2004; Malverti et al., 2008; Braudrick et al., 2009; Madej et al., 2009).

Studies that have used unconstrained channels have also experimented with using techniques to model the presence of vegetation in riparian areas (e.g. Tal and Paola, 2007). This may be done in order to model the elevated bank strength associated with near-channel vegetation and/or assess the that bank stability has on channel migration. Vegetation has been modeled using alfalfa sprouts, toothpicks, and other seeded plants (Tal et al., 2004; Pollen and Simon, 2006; Tal and Paola, 2007; Braudrick et al., 2009). There are still issues that arise when modeling vegetation as the change in bank and soil cohesion that is associated with the roots of riparian vegetation cannot be scaled (Pollen and Simon, 2006).

2.1.1 Types of Scale Models

In an ideal situation, all Π terms would maintain a 1:1 ratio between the model and the prototype. However, in most situations, it is not possible to accomplish this, meaning that there are one or

more scaling exceptions to be made. It is generally the research objective of a study that dictates which relationships may be relaxed and which must be preserved.

Froude-scale modeling is a commonly used method of scaling in which the flow conditions dictated by the Froude number (subcritical vs. supercritical flow) are preserved while those dictated by the flow Reynolds number (laminar vs. turbulent flow) are relaxed enough that a smaller experimental model can be created but that the resulting model still experiences fully turbulent flow (i.e. the flow Reynolds number must remain greater than 2000). This compromise is necessitated by the fact that, without changing the fluid viscosity between the model and the prototype, it is impossible to satisfy both the Froude and the Reynolds criteria for a scaled-down model.

In Froude-scale models, there is the assumption that the other channel parameters (i.e. relative roughness, channel slope), along with the Froude number, are correctly scaled between the model in the prototype. Studies may choose to distort scaling relationships for parameters other than the Re (and Re_*) number in order to build smaller models or to study larger prototypes (Madej et al., 2009; Peakall et al., 1996). An example of this are distorted Froude-scale models which increase the horizontal scale relative to the vertical scale while maintaining similarity of Froude number (Peakall et al., 1996).

While distorted Froude-scale models still attempt to maintain a high Re number (i.e. turbulent flow), ”microscale rivers” operate with laminar flows, meaning that the Re number falls below 2000 (Malverti et al., 2008). The main advantage to these laminar flow models is that time scales can be greatly reduced, allowing many experiments to be run in a short period of time. In addition, these ”microscale rivers” do not require large laboratories to be run in as are quite small in size, with flow depths of only millimeters and lengths and widths on the order of tens of centimeters to meters. There are, however, several issues that arise with this type of scaling technique: (1) these models are believed to have unrealistic friction coefficients, (2) suspended sediment transport is not possible due to the absence of turbulence, (3) surface tension at these scales is believed to effect the physics of channelized flow (Malverti et al., 2008). Despite the limitations that these issues seem to impose on microscale models, several studies have suggested that it is still possible to apply the findings from microscale studies to large scale fluvial systems (e.g. Lajeunesse et al., 2009; Malverti et al., 2008; Davies et al., 2003).

Generic models, which have also been called ”analogue” or ”similarity of process” models (Hooke, 1968), are used to examine the underlying processes of large-scale phenomena. As the name suggests, these models are not scaled from a specific prototype, instead they obey gross scaling relationships and model some processes present in natural systems. Generic models have been commonly used to examine fluvial responses to sea-level change (e.g. Van Heijst and Postma, 2002; Koss et al., 1994) and long-term landscape evolution (e.g. Postma et al., 2008; Van Hei-

jst et al., 2002). The main downfall of generic models are that, unlike Froude-scaled and even distorted-scale models, their results cannot be applied directly to any specific field example. The results from generic models are instead used to describe key trends and processes that underlie the fluvial systems that the model is simulating.

2.1.2 Modeling Large Wood in Stream Channels

When modeling LW in flume experiments, the physical characteristics of the wood pieces must be designed to replicate the properties of LW that makes them influential in channel morphodynamics. The characteristics that are relevant include: wood density (Bocchiola, 2011; Braudrick and Grant, 2001; Wallerstein et al., 2001), piece length (Wallerstein et al., 2001; Braudrick and Grant, 2000; Braudrick et al., 1997), "trunk" shape (Davidson, 2011; Braudrick and Grant, 2001; Wallerstein et al., 2001; Braudrick et al., 1997), and presence of branches and/or rootwads on the pieces (Davidson, 2011; Braudrick et al., 1997; Braudrick and Grant, 2001). Like bed sediment, LW pieces may be mobile (Davidson, 2011; Braudrick and Grant, 2001, 2000; Braudrick et al., 1997) or fixed (Bocchiola, 2011; Wallerstein et al., 2001) within the flume.

In studies that use mobile LW pieces, the quantity and the placement of pieces will influence channel dynamics, since individual pieces behave differently than log jams made up of several wood pieces (Bocchiola, 2011; Davidson, 2011). Two types of wood loading have been described by Bocchiola (2011): distributed wood loading and lumped wood loading. Distributed wood loading, in which individual pieces enter the stream at random intervals, tends to mimic the addition of wood due to processes such as tree senescence or bank erosion. Lumped wood loading, in which several LW pieces enter the channel at a single point, emulates the addition of wood due to a single event (e.g. forest fires, landslides and debris flows).

2.2 Prototype Stream: Fishtrap Creek

Fishtrap Creek, the prototype stream for the flume models used in this study, is located in the interior region of British Columbia near the town of Barriere and approximately 50 km north of Kamloops. The Fishtrap Creek watershed drains an area of about 158 km^2 (Eaton et al., 2010a).

Elevations within the area range from about 300 m a.s.l. to 1600 m a.s.l. The terrain is made up of incised stream channels, steep valley slopes, as well as gently sloping plateaus. Although a large portion of the surficial deposits present in the area are associated with the last glaciation which culminated around 11 500 years BP (Ryder et al., 1991), post-glacial fluvial activity, and mass movements have reworked many of these deposits resulting in a complex assortment of deposit types and landforms. This glacial and post-glacial legacy is indicated by the landforms,

such as drumlins and landslides, visible on the LiDAR image shown in Figure 2.1. The novel method of LiDAR data visualization developed during this thesis research project is described in depth in Appendix I. The relationship between the glacial legacy and the current fluvial processes is notable in Figure 2.1 as Fishtrap Creek and the prototype study area is seen to run through a glacial meltwater channel that extends out to the North Thompson river in the lower right-hand corner of the map.

In August 2003 the McClure forest fire, a high intensity crown fire, burned through 62 % (98 km^2) of the watershed, killing almost all of the vegetation on the Fishtrap Creek floodplain up to the edges of the stream channel (Eaton et al., 2010a). Since then, several long term studies have been conducted in a study reach located approximately 5 km up from the mouth of the creek, documenting the changes that have ensued since the fire.

The study reach, established in 2004 and shown in Figure 2.2, is located just upstream of a Water Survey of Canada stream gauge (station no. 08LB024) that has been monitoring streamflow almost continuously since 1971. Initially the study reach spanned a length of approximately 130 m and encompassed 11 cross-sections (1-11) (Figure 2.3), however in 2006 the study reach was expanded on either side in order to better accommodate a gravel tracer displacement study (Eaton et al., 2010c). Cross-sections A-H were added on the downstream end and cross-sections 12-19 were added to the upstream end, resulting in a total study reach of 440 m (along the thalweg).

As reported in Eaton et al. (2010a), the study reach itself is relatively steep, with a gradient varying from 1.5-2.0%. With a D_{50} of 55 mm, the surface of the bed is quite coarse while the underlying bed material has a finer D_{50} of 35 mm. The average bankfull width of the channel is 10-12 m. According to the WSC records, the mean annual peak flow, which is on average 7.5 m^3/s, occurs during the spring snow melt sometime between April and June.

There have been several studies conducted within the study reach at Fishtrap Creek (see Petticrew et al., 2006; Phillips, 2007; Andrews, 2010; Leach and Moore, 2010). These studies found that Fishtrap Creek had a relatively unusual response to the forest fire, as there was no significant increase in peak flows or suspended sediment loads in the years immediately following the forest fire (Petticrew et al., 2006; Eaton et al., 2010c) in contrast to an increase in suspended sediment that is typically observed post-fire (Keller et al., 1997). Instead, the primary changes have occurred in the channel morphology: there has been a shift from featureless plane-bed morphology to that of a riffle-pool morphology coinciding with an increase in local bed material transport rates (Eaton et al., 2010a,c). Additionally, extensive bank erosion caused some areas of the channel to double in width (Eaton et al., 2010a,c). This morphological change has largely been attributed to changes in the bank strength and stability resulting from a decrease in cohesion as burnt riparian vegetation decays (Eaton, 2008; Eaton and Giles, 2009; Eaton et al., 2010c).

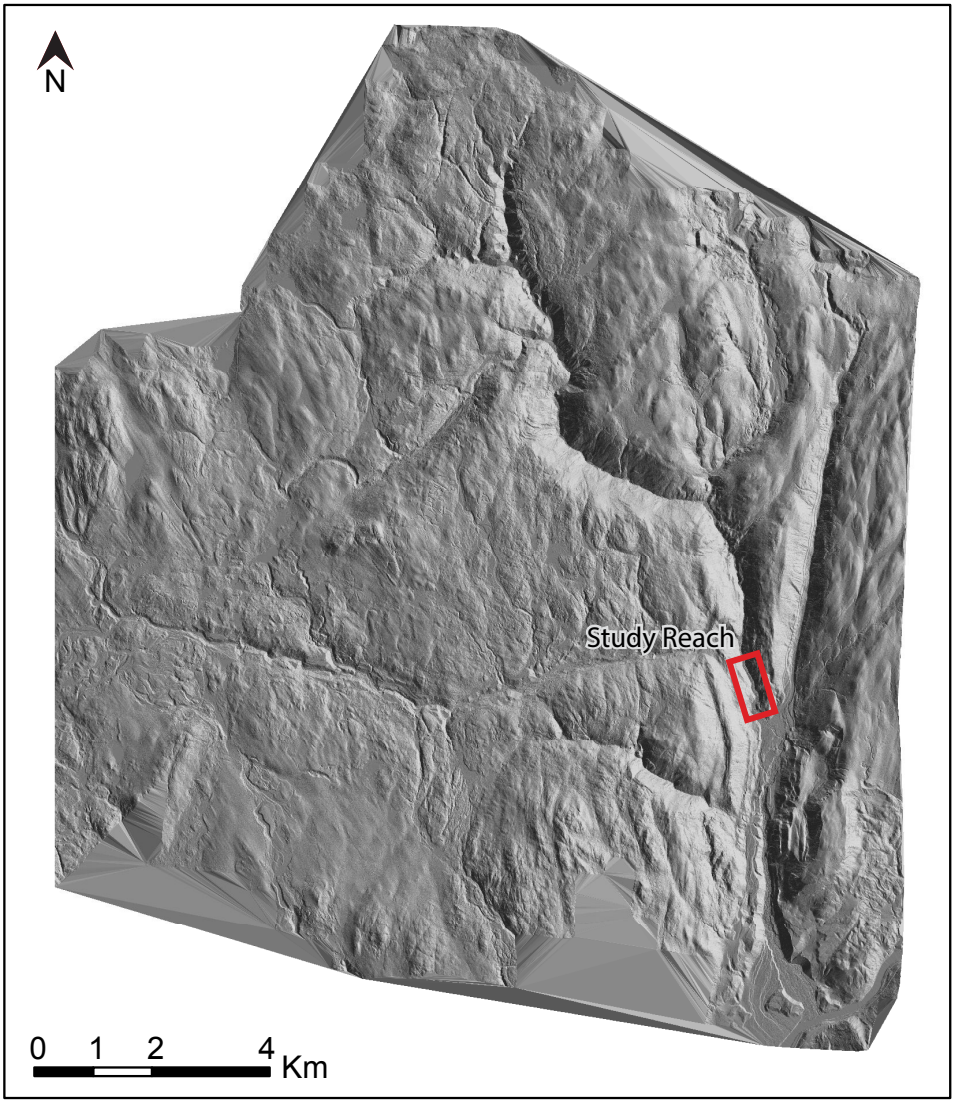

Figure 2.1: LiDAR image of Fishtrap Creek watershed and the surrounding area created from LiDAR data collected in 2007 and visualized using the methods described in Appendix I.

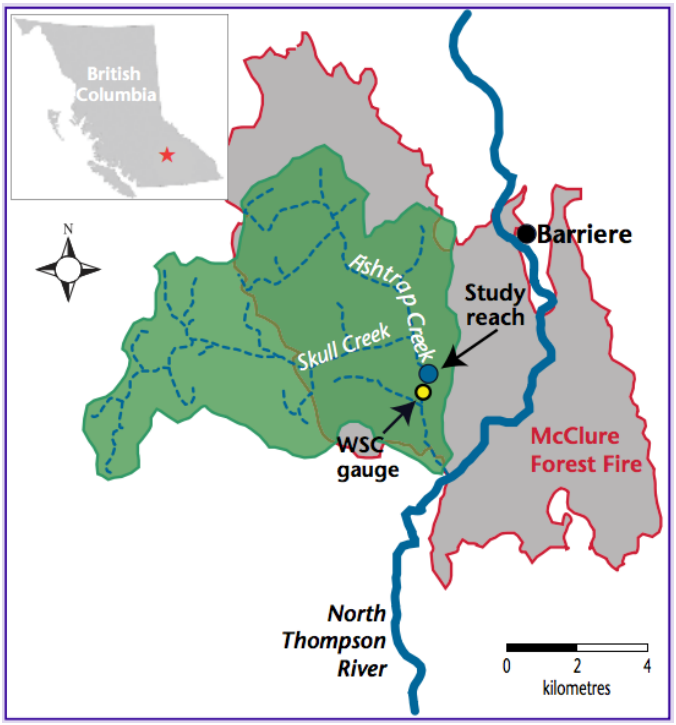

Figure 2.2: Location of Fishtrap Creek and the study reach (Figure taken from Eaton et al., 2010b)

2.3 Model Design

Two fixed-bank, mobile bed, Froude-scaled models of Fishtrap Creek were used to collect the data for this study. The prototype dimensions and parameters used to scale the two models were modeled after actual measurements made of Fishtrap Creek (Figure 2.4) in 2008 and 2009 by Christie Andrews (see Andrews, 2010). Model 1 represents a large portion of the lower half of Fishtrap Creek and encompasses both a relatively straight reach as well as two meander bends. Model 2 is comparatively straighter overall and represents a shorter section of the stream channel.

The experiments presented for Model 1 were conducted in 2011 and 2012. The apparatus used for Model 1 measured 9 m long and 2 m wide, although the channel itself was 8.5 m long and 0.3 m wide. The experiments conducted on Model 2 were done in 2010 and 2011(Davidson, 2011; Davidson and Eaton, 2012). The Model 2 apparatus measured 5 m by 0.85 m. The channel itself spanned 4.5 m in length and was on average 0.35 m wide. The width of the channel was varied for Model 2 but not for Model 1, in order to better isolate the effects of LW in Model 1 as changes to channel width result in slightly variable sediment transport rates (due to variable discharge) along the length of the channel.

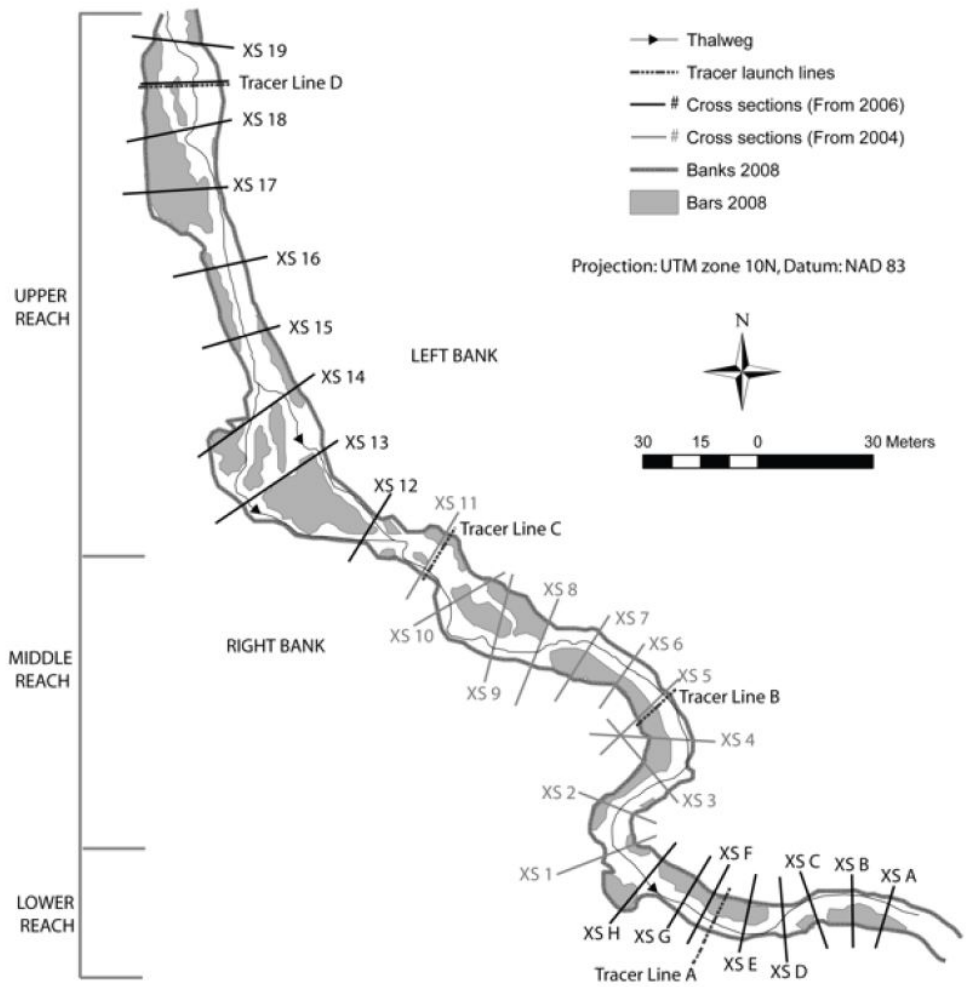

Figure 2.3: Study reach at Fishtrap Creek in 2008 (Figure taken from Eaton et al., 2010a)

Model 1 was run with a single grain size representative of the median subsurface grain size (D_{50}) of Fishtrap Creek. Model 2 was run with a modeled subsurface grain size distribution (GSD) measured in Fishtrap Creek in 2006 (Figure 2.6) The low end of the distribution is truncated in order to avoid the issues of entrainment noted above. The difference in the resulting bed texture of the two models is exemplified in Figure 2.7.

The width, depth, and bed material grain size (W_f, d_f, and D_f) of both models were scaled using a characteristic length scale (L_r) of 1:30. Discharge (Q_f) and time (T_f) were scaled in both models according to the following equations:

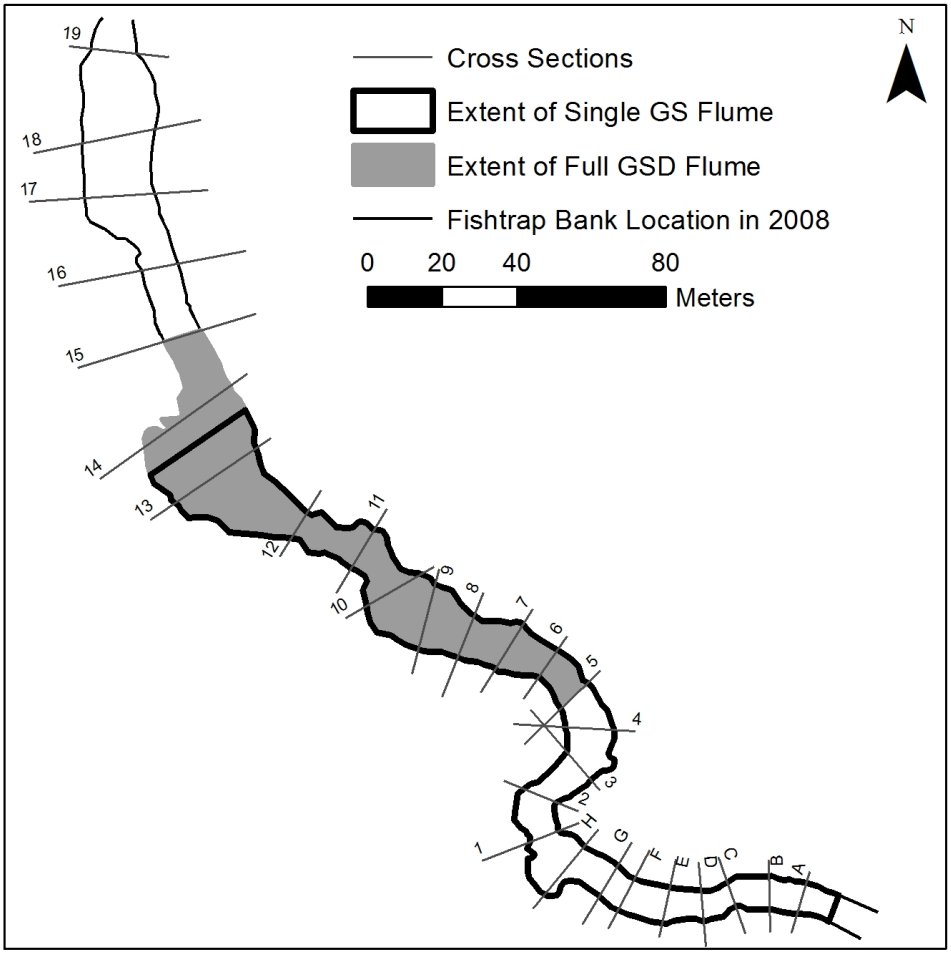

Figure 2.4: The approximate area of Fishtrap Creek represented by the two models

$$T_f = L_r^{0.5} \tag{2.9}$$

$$Q_f = L_r^{2.5} \tag{2.10}$$

Given the difference in composition of the bed material in the two models manifests in the lack of ability for a surface armour to develop in Model 1, it was necessary for the two models to have different slopes in order to maintain a similar $Q_b : Q$ ratio. Maintaining similar sediment

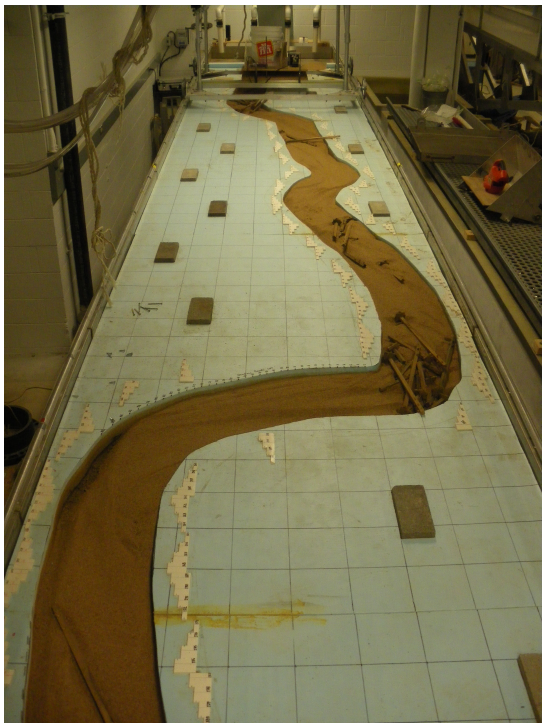

(a) Model 1

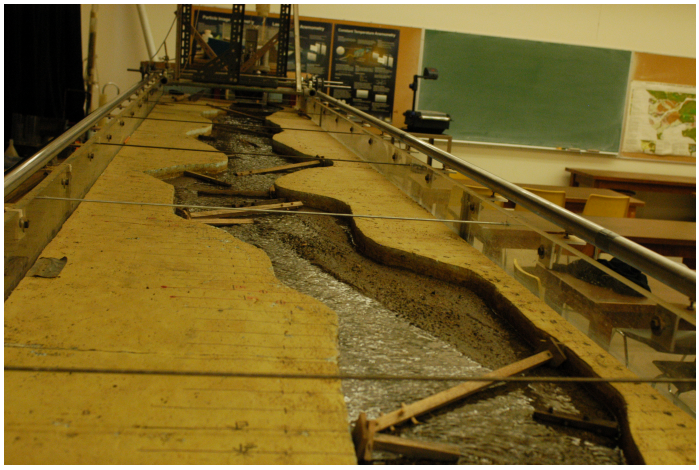

(b) Model 2

Figure 2.5: The two models used to conduct the experiments for this study

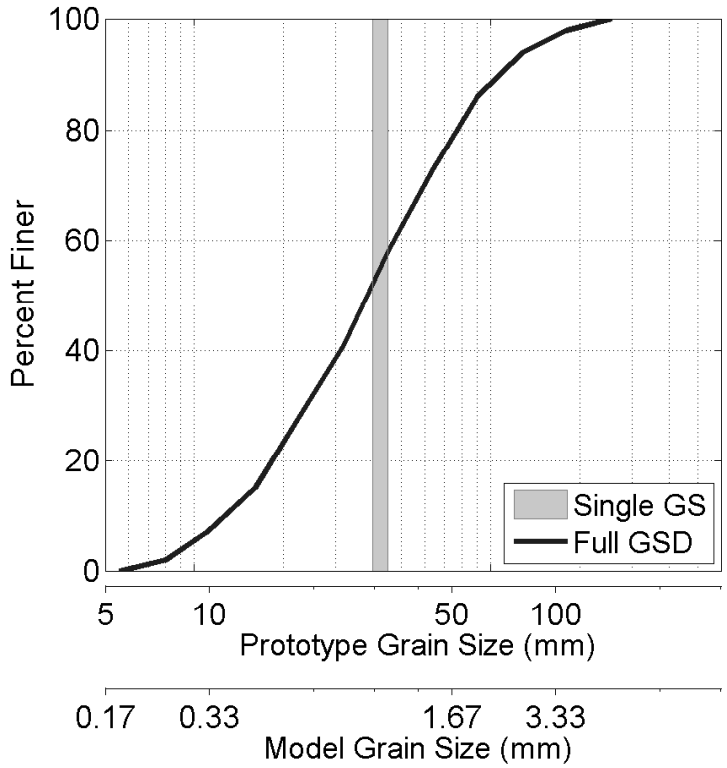

Figure 2.6: Cumulative distribution functions showing the GSD of Model 2 and the grain size used in Model 1.

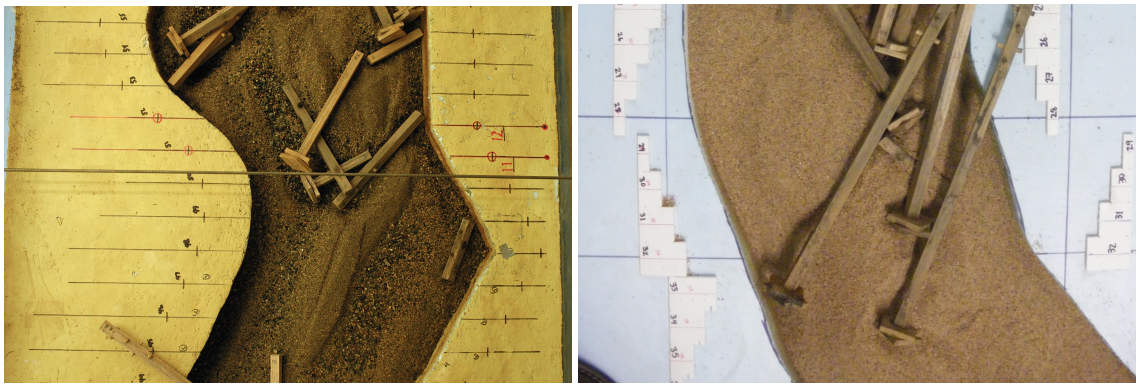

(a) Bed texture from Model 1 **(b)** Bed texture from Model 2

Figure 2.7: Examples of surface bed texture from the two models shown in order to compare the difference in bed texture between the model with a GSD and the one with a single grain size.

Table 2.1: Model and Prototype Parameters

Parameter	Prototype	Models
Width	10-12 mm	0.34 mm
D_{50}	35 mm	1.14 mm
Peak Discharge	7.5 m^3/s	1.6 l/s
Time	27 hours	5 hours

Table 2.2: Comparison between the length classes and frequencies of LW in the prototype stream and those used in the experiments.

Prototype	Prototype	Model	Model Frequency (%)			
Piece Length (m)	Frequency (%)	Piece Length (m)	Exp. 1	Exp. 2	Exp. 3	Exp. 4
2-4	27	0.1	32	33	33	34
4-8	36	0.2	35	33	38	37
8-16	35	0.4	32	33	29	28
16-32	2	–	–	–	–	–

concentrations between the two models is important when comparing rates of geomorphic change. The slope of the full GSD model (Model 2) was given a slope that approximated that of Fishtrap Creek (0.018 m/m or 1.8%) while it was necessary to lower the slope of the single grain size model (Model 1) to 0.008 m/m or 0.8%.

Six different forms of wood pieces (Figure 2.8) were used to represent the range of size classes and wood piece characteristics found in Fishtrap Creek by Eaton et al. (2010a). Characteristics of wood pieces used in the experiments are based on a set of pilot experiments described in (Davidson and Eaton, 2012) which found that pieces made of out of maple with square cross sections were much better at simulating the dynamics of wood pieces in the real stream channel than pieces made out of lighter wood with circular cross sections. Rootwads and branches were added onto many of the pieces as these were found to increase the stability of the pieces and promote interactions between the pieces within the channel.

The three size classes of wood pieces modeled in the two models were scaled geometrically based on length classes and frequencies observed in Fishtrap Creek (Table 2.2). The largest length class observed in the field was omitted from the experiments due to its infrequency within the prototype stream (makes up only 2% of LW surveyed) and because pieces in the 8-16 m size class (the second largest size class observed in the prototype) were considered large enough to function as key members of log jams (Davidson, 2011).

Figure 2.8: Six different model wood piece forms used in the experiments

2.4 Experimental Design and Data Collection

Table 2.3: Summary of the treatments and the run times of all four experiments.

Exp.	**Treatment**		S_f	WL_m	WL_p	T_t	T_w	N_r
	Bed Texture	*Wood Load*	[m/m]	[m^3/m^2]	[m^3/m^2]	[hr]	[hr]	-
1	Single GS	Moderate	$5.4\ x10^{-4}$	0.008	$1.6\ x10^{-2}$	90	35	18
2	Single GS	High	$7.4\ x10^{-4}$	0.008	$2.2\ x10^{-2}$	90	35	18
3	Full GSD	Moderate	$5.4\ x10^{-4}$	0.018	$1.6\ x10^{-2}$	45	15	10
4	Full GSD	High	$7.4\ x10^{-4}$	0.018	$2.2\ x10^{-2}$	55	10	11

S_v = flume slope, WL_m = Scaled wood load (in the model), WL_p = prototype wood load, T_t = total length of the experiment, T_w = time of wood addition, N_r = number of runs

Two experimental treatments were run on each model: moderate wood load and high wood load (Table 2.3). The moderate wood load treatment represents pre-fire wood load conditions at Fishtrap Creek while the high wood load approximates the in-stream wood load five years after the fire as documented by Eaton et al. (2010a). For this study, the two experiments conducted on Model 1 will be referred to as Experiment 1 (moderate wood load) and Experiment 2 (high wood load) while those conducted on Model 2 will be referred to as Experiment 3 (moderate wood load) and Experiment 4 (high wood load).

Each of the experiments were made up of a series of five-hour runs, each meant to simulate one year of morphologic change at Fishtrap Creek. Given that the model is run at the equivalent of peak flow discharge and that peak flows represent the period in which flow is sufficient to mobilize the majority of the bed material (Buffington et al., 2004), these five hour periods were taken to

represent one year of morphologic change.

Throughout all experiments, sediment was input to the flume model at a constant rate of approximately 62 g/min using a rotating feeder. This sediment flux is consistent with values of upstream sediment yield measured at Fishtrap Creek in the period since the fire (Eaton et al., 2010a). Sediment output from the flume was collected from the outlet of the flume at 15 minute intervals. These samples were then dried and weighed in order to determine the sediment output rate. This value of sediment output was also compared to sediment input rate in order to determine when the flume reached steady state. Steady state, or sediment transport equilibrium was defined as a period of five hours or more in which sediment input rate roughly approximated sediment output rate.

The initial bed conditions for each experiment was an imposed flat bed. In each experiment the flume was first run without wood until a steady baseline morphology was reached. Once the flume reached an initial steady state, in which sediment output approximated sediment output for a period of 5 hours, the wood pieces were added all at once while the flume was run at a discharge approximating low flow (1/3*Q_{bf} or 0.4 l/s). The location and orientation at which the wood pieces were introduced were chosen randomly in order to better simulate the natural recruitment of wood into a stream. Following their addition, the location (i.e. the cross section) and the orientation of each wood piece was documented at the end of each five hour run.

Bed morphology data was collected at the end of every five-hour run using a laser profiling system similar to that described by Zimmermann (2009) (Figure 2.9). Following each run the flume was drained of water and images of cross-sections, highlighted by the laser line, were taken at intervals of 38 mm on Model 1 and of 50 mm on Model 2.

Bed facies data was collected by Davidson for the two experiments run on Model 2 (Davidson, 2011). Facies maps, which distinguish between patches of different surface textures, were created by manually mapping the boundaries of each different facies present on the bed. A photo was then taken of a 6” by 8.5” segment of each facies patch in order to later help characterize grain size.

Facies patches were classified according to the grain size categories, developed by Davidson, and presented in Table 2.4. This was done by first conducting Wolman samples on twenty of the facies photos, accomplished by measuring grain sizes in Adobe Illustrator along a super-imposed grid in order to establish representative facies for each of the grain size categories. The remaining facies images were classified visually using the measured facies as reference. Error analysis of the visually classified images revealed a 90% accuracy (Davidson, 2011).

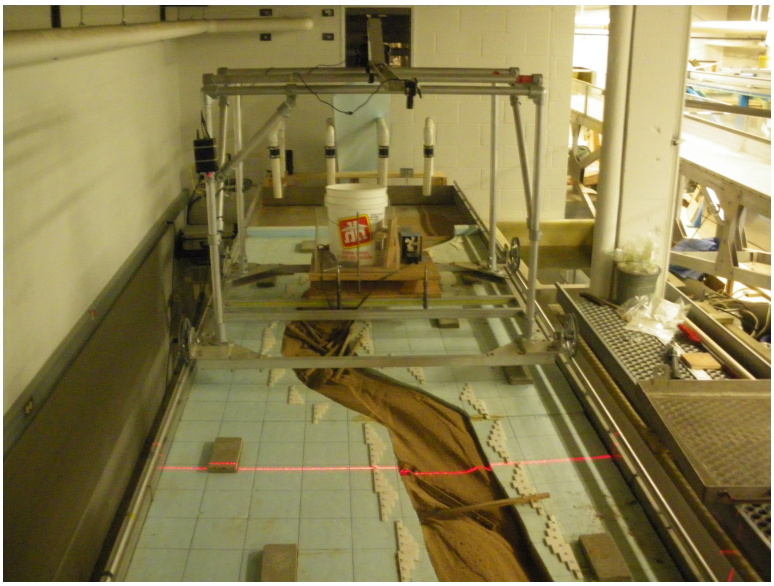

Figure 2.9: Apparatus used to take images of cross-sections in order to create DEMs of the bed surface

Table 2.4: Facies grain size categories used to determine representative grain sizes for each of the facies maps created by Sarah Davidson. Table first presented in Davidson (2011).

Category	Size Range (mm)	Characteristic Size (mm)
Very Fine	0.35-0.50	0.43
Fine	0.50-0.71	0.60
Medium	0.71-1.0	0.85
Coarse	1.0-1.4	1.2
Very Coarse	1.4-2.0	1.7

Chapter 3

Data Analysis

3.1 Bed Elevation

Data extracted from the images of the cross sections were used to determine the bed elevations and create DEMs of the channel bed after each run. Images for each run were digitized using a semi-automated code written in Matlab®. The automated part of the code cycled through each image and first converted it into black and white in order to highlight the laser line in the image and background noise (created through this process) was removed using a patch detector. Next, the cross sections present in the image were converted into a 'skeleton' version where the x and y coordinates (point values) were given for all values along the cross section in which the x values represented the distance across the flume while the y values represented the elevation at each of the points across.

User input was required to georeference the xy coordinate data from the images to the actual elevation values of the flume, which were collected using a total station. Two control points at the corners of the channel, one on the left back and one on the right, were selected on each cross section by the user. If the difference in the relative elevations of control points of the digitized cross section did not match those taken using a total station of the flume, the cross section was tilted to match the actual difference in elevation. All points along the digitized cross section were then assigned actual elevation values based on the known elevations of the control points.

Digital Elevation Models (DEMs) were created from the georeferenced cross sections by interpolation. Although the resolution of the bed elevation points across each cross section are high, the lower resolution in the downstream direction constrains the potential precision of the DEM. In runs where there was no wood present in the flume, linear 1D interpolation was used to up-sample data in the across stream direction after which linear 2D interpolation was used to down-sample

data in the down stream direction. The spatial resolution of the resulting DEMs was approximately half the distance between subsequent cross-sectional images (20 mm in Model 1 and 25 mm in Model 2). This resolution was chosen in order to minimize the error and uncertainty associated with interpolation while maintaining a low enough spatial resolution to identify bed forms such as pools.

Wood pieces were digitized out manually in runs where wood was present. To do this, a code was created to run through each of the cross sections individually and the user must determine whether or not each cross section contains any wood pieces. In the cross sections where wood pieces were present, the user estimated the surface of the bed in the area obscured by the wood. This estimation was facilitated by plotting the same cross section from the previous run and the previous cross section from the current run on top of the cross section to be digitized. The xy coordinates manually generated from the digitization of these wood containing cross section were then interpolated to create a DEM using the same methods described above.

Uncertainty was introduced during several periods of the digitization process. The largest source of error during the creation of DEMs is the presence of shadows in the image of the cross section. Because the image captured of the bed relies on a laser line shot from above, if anything is located between the laser light and the bed, it will be obscured and the image of the cross section will not capture that portion of the bed. The two causes of shadowing are the edges of the bed and the wood pieces of the channel.

Shadowing by the edges of the bed arises due to the fact that the edges of the bed are rigid and oriented at a 90°to the bed. In areas of the channel where the sides of the bed are not perpendicular to the laser line across the bed (i.e. on meander sections), the bed edges shadow a portion of the bed along the side. In order to mitigate for this, measurements of bed elevation (taken as the depth from the top of the bank) were taken along the length of the largest meander in Model 1 where shadowing was prone to occurring. These bed elevation measurements were then employed when digitizing the data in order to fill in the areas where the edges shadowed parts of the bed.

The uncertainty of the bed elevation DEMs must be considered when conducting analysis on the data. The uncertainty in the across stream direction is the same as the resolution of the DEM (20 mm in Model 1 and 25 mm in Model 2) as data was upsampled in this direction. Because data was interpolated in the downstream direction, the uncertainty in this direction is equivalent to the distance between two subsequent cross sections: 38 mm in Model 1 and 50 mm in Model 2.

Additional uncertainty in the elevation values of the DEM is associated with sediment movement between runs and user input error, introduced during the digitization process. Uncertainty associated with user input was estimated to be approximately 1 mm. Because the grid cells of the DEMs are actually averages of several points from the original cross sections, elevation error

Table 3.1: Values used to calculate the standard error (model uncertainty) of the elevation values of the bed elevation DEMs and the resulting standard error values associated with the two flumes

Model	D_{90}	n	$SE_{\bar{x}}$
1	1.4 mm	8	0.5 mm
2	2.8 mm	12	0.8 mm

associated with sediment movement was calculated by determining the standard error of those points using the following equation:

$$SE_{\bar{x}} = \frac{D_{90}}{\sqrt{n}} \tag{3.1}$$

where D_{90} is a representation of the grain size uncertainty and n is the number of original data points used to determine the bed elevation for each cell of the DEM. Values used to in the calculations and the resulting standard error associated with each of the flumes is presented in Table 3.1.

Given the calculated values of standard error and the estimated error associated with digitization, total uncertainty in the elevation values of the bed elevation DEMs was determined to be $\pm$ 1.5 mm for Model 1 and $\pm$ 1.8 mm for Model 2.

DEMs of Difference (DoDs) were created to examine changes in sediment storage between runs. These were made by differencing between two subsequent DEMs of bed elevation. DoDs for all experiments are presented in Appendix C. The DoDs were then used to examine the spatial pattern of erosion and deposition in the flume. For DoDs, the elevation uncertainty is equal to the combined uncertainty of the two DEMs from which it is calculated using the following equation:

$$U_c(x) = \sqrt{(u_1(x))^2 + (u_2(x))^2 + ... + (u_n(x))^2} \tag{3.2}$$

where $u_i(x)$ is the combined uncertainty associated with each of the DEMs used to create a given DoD and $U_c(x)$ is the total uncertainty of the DoD. Using the uncertainty values for the bed elevation DEMs, reported above, the combined error for the DoDs is $\pm$ 2.1 mm for Model 1 and $\pm$ 2.5 mm for Model 2. These uncertainty values are used as the threshold for change detection (i.e. difference in elevation must be $\geq U_c(x)$ to be considered real) when analyzing the DoDs.

3.2 Water Surface Elevation and Water Depth

Water surface elevation profiles were created from measurements taken for all of the runs on Model 2 and for some of the runs for Model 1. Water surface elevations (WSE) were determined by first measuring the distance between the top of the flume and the water surface at regular intervals along the flumes (30 cm intervals on Model 1 and 50 cm intervals on Model 2). Next WSE were calculated at each of those points by subtracting the measured distance from the known flume-top elevation. Once the WSE was found at each of the points along the flume channel, a 1D cubic interpolation was used to find the water surface elevation for all cross sections located between the measured points.

These WSE elevation profiles were then extrapolated to create DEMs containing the values of water surface elevation at each point in the channel. Due to a lack of water surface measurements in the across stream direction, it was necessary to assume that WSE was the same across the channel width.

For Experiment 1, conducted on Model 1, WSE were only measured for the run in which the flume was in equilibrium without wood (Run 8) and the one in which it was in equilibrium with wood present (Run 18). The water surface elevations for the remaining runs were approximated by using the WSE of Run 8 for Runs 1 to 9 (all runs without wood) and the WSE from Run 18 for Runs 10 to 17. For Experiment 2, also on Model 1, although the WSE was taken for each run once wood was added into the flume (Runs 8 to 18), the WSE taken for the flume at equilibrium without wood (Run 7) was used for Runs 1 to 7. WSE was measured for all runs for both Experiment 3 and 4.

DEMs of water depth were created by subtracting the bed surface elevation from the water surface elevation for each of the runs for all experiments. The uncertainty in depths associated with these is determined using Equation 3.2 and therefore have the same uncertainty values as the DoD maps ($\pm$ 2.1 mm for Model 1 and $\pm$ 2.5 mm for Model 2).

The distributions of depths differ between the two flumes (Figure 3.1a). The distributions plotted for the experiments conducted on Model 1 are positively-skewed and have a wide range of depths stretching out to approximately 2.5*$\bar{d}$ (where $\bar{d}$ is the mean depth). On the other hand, the depth distributions shown for Model 2 are more normally distributed around the mean depth and only have maximum depths of approximately 1.75*$\bar{d}$.

It should be noted that although the distributions shown in Figure 3.1a encompass all of the experimental runs conducted on each flume, the depth distributions from individual runs, both with and without wood present, display similar trends as is portrayed by the general population.

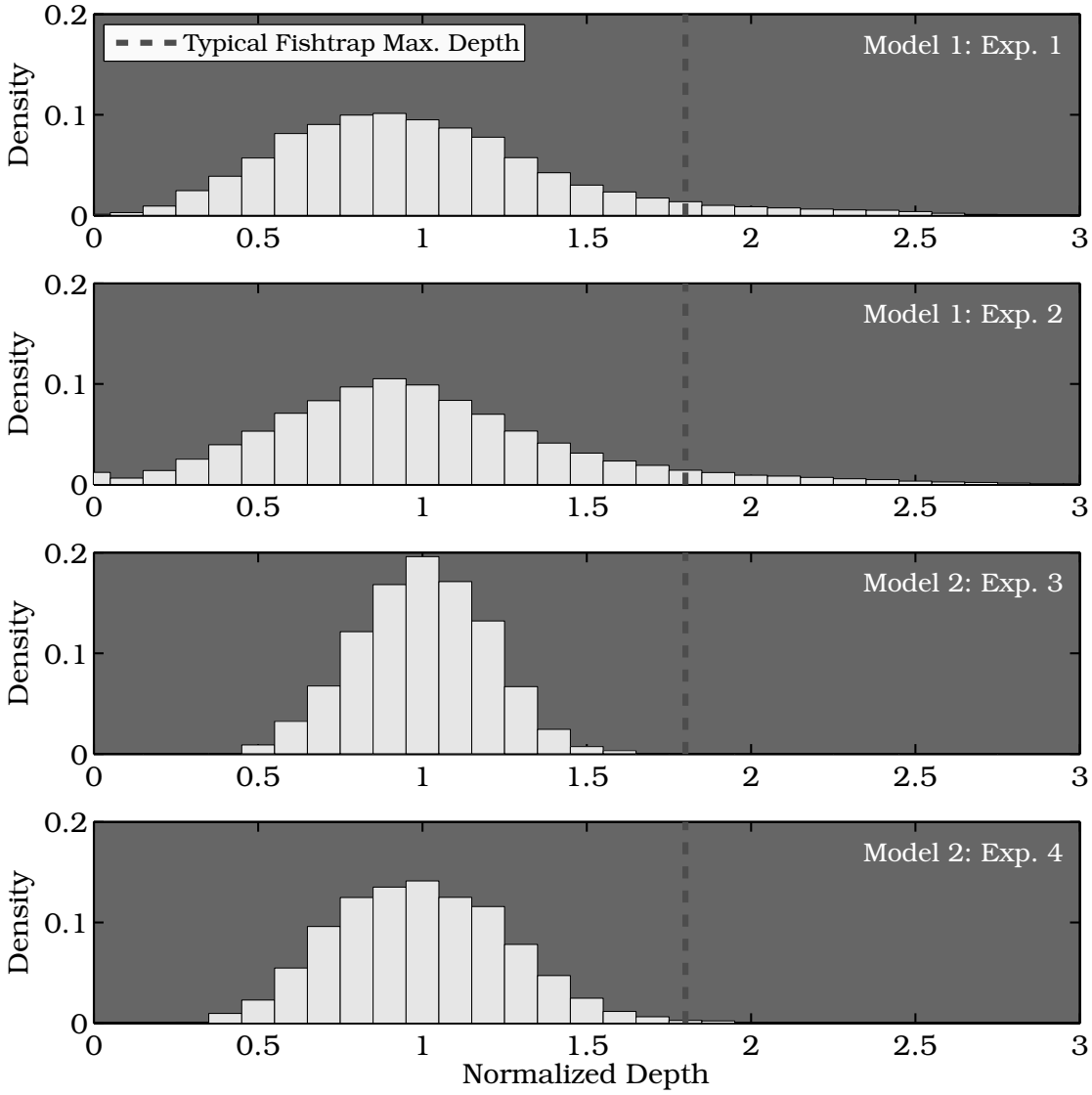

(a) Distributions of depths for all experiments shown as a function of mean depth. The dashed black line represents the typical maximum pool depth at Fishtrap Creek.

Figure 3.1: Depth distributions for each of the experiments. Each distribution is created from depth values gathered off of all runs for that given experiment.

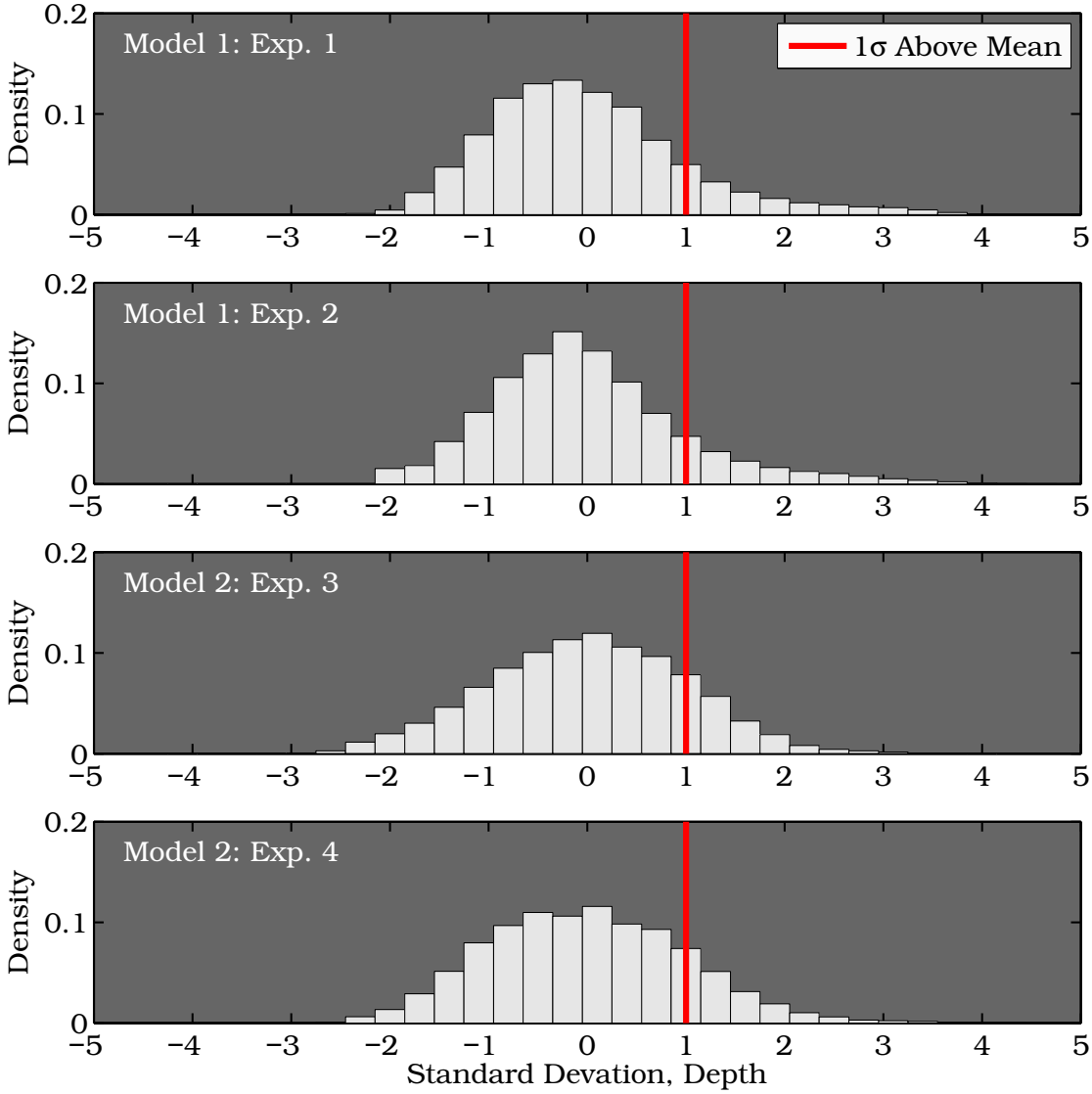

(b) Distributions of depths, normalized by standard deviation above the mean. The red line represents the depth criteria used to identify pool areas.

Figure 3.1: Depth distributions continued

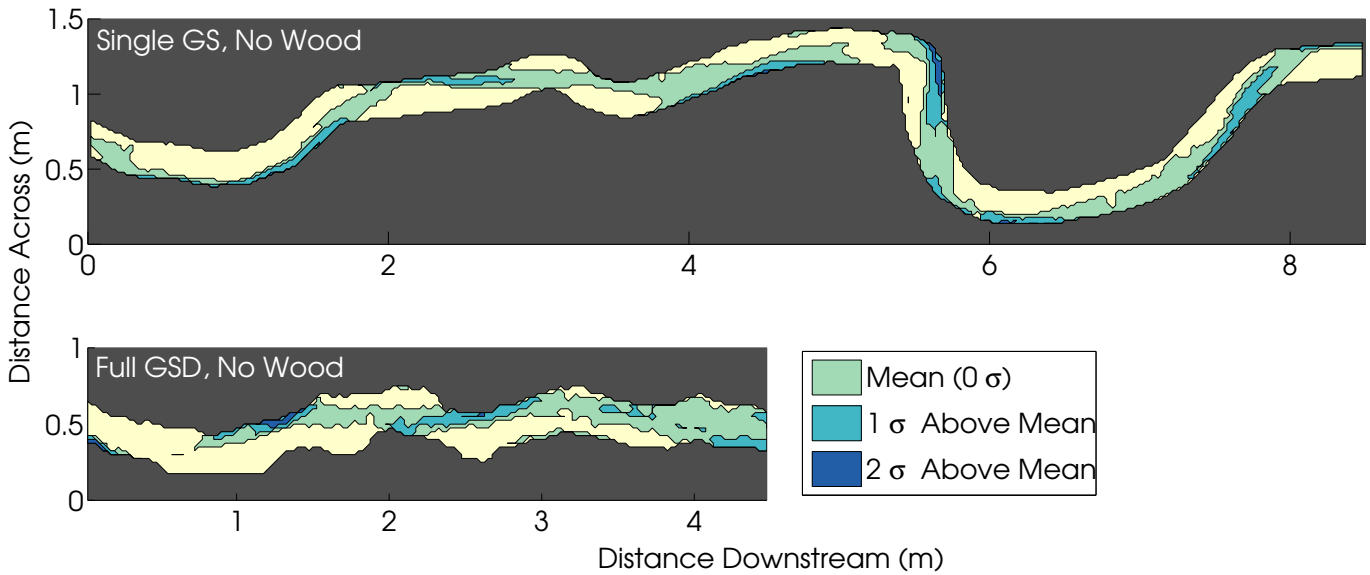

Figure 3.2: Pools areas selected using three different depth criteria shown on an example run from each model.

3.3 Pool Identification

DEMs of water depth were used to identify pool areas. Pools are defined as areas of high flow depths and low flow velocities relative to the rest of the channel (e.g. Whiting and Dietrich, 1993; Abbe and Montgomery, 1996) and, in practice, are most commonly identified from longitudinal bed elevation data using pre-determined criteria (e.g. Lisle, 1987; Montgomery et al., 1995).

The identification of pools from DEMs of water depth allows for a rigorous analysis of the channel morphology as it can account for the fact that more than one pool may be present along any cross section of a stream channel and that pools can vary in form such that the longest axis of the pool may be oriented in any direction relative to the flow, a characteristics that may be overlooked when identifying pools using a longitudinal stream data analysis.

For this study it was established that the criteria used to identify pools should: a) select for areas deeper than the mean depth, b) consistently differentiate between riffle tops and adjacent pools, and c) be applicable to different populations of depth data.

Standard deviation above the mean was used as criteria with which to select pool area from the depth data. As seen in Figure 3.1a, the depth distributions are more comparable between models when normalized by standard deviation. Both visual assessments and sensitivity testing was used to help determine exactly which standard deviation to use as the depth criteria for pools.

Visual assessments of the pools delineated on the DEMs are useful as they reveal how changes to the depth criteria affected the location and areas selected as pools. As shown in Figure 3.2, it was observed that when the mean of the sample was used (i.e. 0 σ), riffle tops were selected as part of the pools. On the other hand, when a high standard deviation (i.e. 3 σ) was used criteria, the resulting pool areas encompassed only the very deepest points of bed depressions.

For the sensitivity testing, the depth criteria threshold was varied between the 0 to 3 standard deviations above the mean (Figure 3.3). A line, representing a pool area of $1/3*W_b^2$ (where W_b is the bankfull width) is shown as a dashed pink line on Figure 3.3. This pool size is consistent with relative pool sizes that have been reported in previous studies (e.g. Bilby and Ward, 1991).

Mean pool area varied over several orders of magnitude depending on the depth criteria employed. As with the results of the visual assessments, when low percentiles closer to the mean of the depth distribution are employed as criteria, the average pool size was found to be too large, whereas the mean pool size was small when the upper percentiles were used. Comparing the results to the representative pool size of $1/3*W_b^2$, it was seen that mean pool size for all experiments coincide approximately with this value when depth criteria is around 1σ above the mean.

Based on the results of the visual assessments and the sensitivity testing, 1σ above the mean was chosen as the depth criteria for isolating pool area. This criteria is a simple measure that is

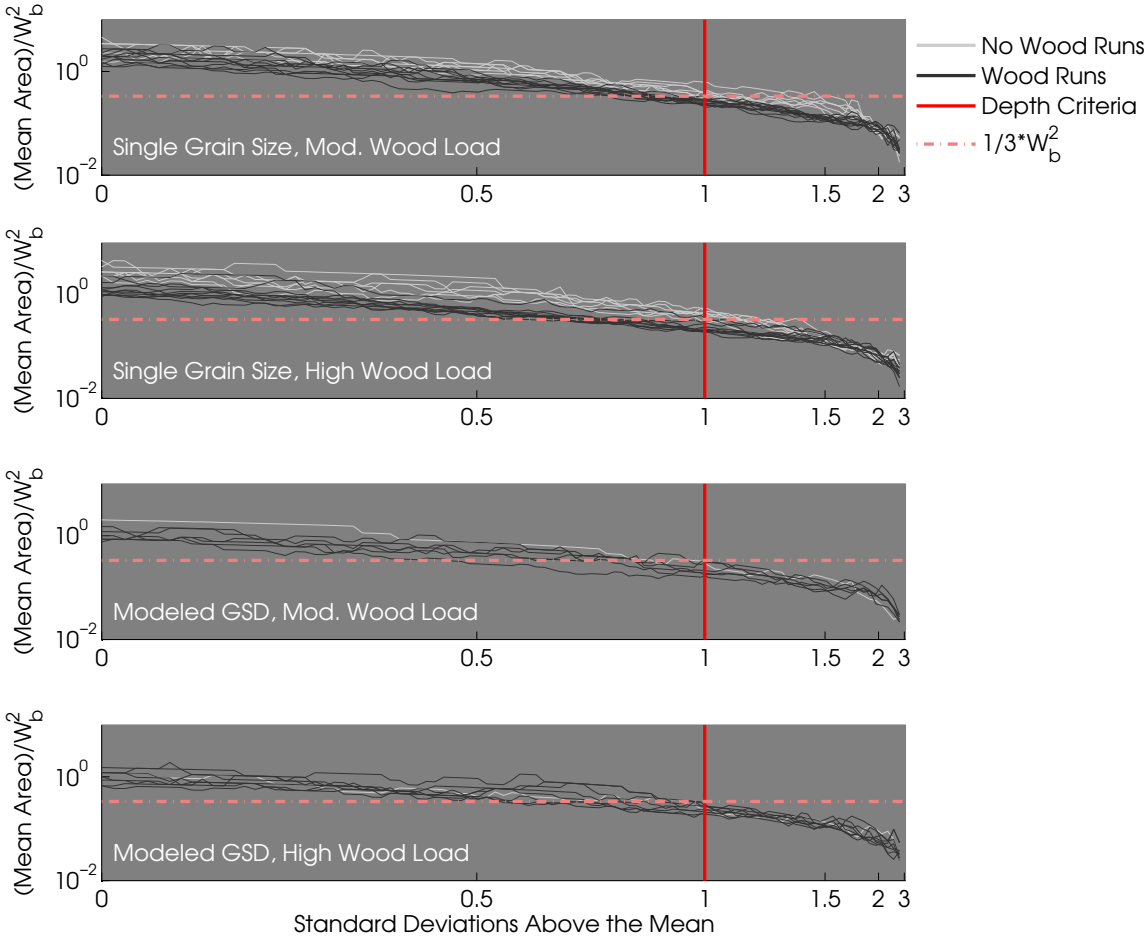

Figure 3.3: Mean pool area, normalized by a representative unit area of W_b^2, is shown for a range of depth criteria for pool selection. The depth criteria value shown at the base of the graph is the standard deviation from the mean. The red horizontal line represents the depth criteria eventually used in the analysis of the data. The dashed red line indicates a pool size of $1/3*W_b^2$.

applicable to different depth distributions and is able to consistently isolate pool areas from other low lying bed forms within the stream channel.

When applying this criteria, it is also necessary to consider the uncertainty of the DEMs. For this study it was determined that any areas selected as pools should be over three pixels in size, which is equivalent to areas of approximately 12 cm^2 in Model 1 and 19 cm^2 in Model 2. Setting this minimum pool size limit helps to assure that all pools are larger than the uncertainty associated with the interpolation used in this study.

The facies maps in Davidson (2011) and the pool areas determined from the depth DEMs were used to find the approximate median grain size found within each pool areas. This was done by georeferencing the facies maps and the delineated pools to each other in ArcGIS®. First the extents of the facies patches and pool areas were then digitized. Next, each facies patch was assigned a characteristic grain size according the methods described in Chapter 2. The extents of the pools were then used to select parts of the bed found within the pool area. The median grain size located in each pool was determined using a weighted average calculated using the facies area found within the pool and its characteristic grain size. In order to compare the characteristic surface grain size of the pool to the rest of the bed surface, weighted averages surface grain size were calculated using the relative facies area and the characteristic grain size for each patch for the whole bed.

3.4 Wood Location Data

The location and the orientation of each wood piece in the flume was recorded at the end of each run. Location was recorded as the cross section at which the upstream-most point of the wood piece was located and orientation was recorded as the direction of the wood piece relative to the channel. This data was later used to plot the location of individual wood pieces and jams along the stream channel.

Chapter 4

Results

The following chapter reviews the results of a set of four comparable experiments conducted in two different fixed-bank, mobile-bed, Froude-scaled prototype flume models of Fishtrap Creek. The main difference between the two models was the grain size distributions of the bed material: Model 1 contained only a single grain size representative of the D_{50} of the prototype stream while Model 2 contained a scaled grain size distribution of that found in the prototype stream.

Two experiments were conducted on each model, one in which a moderate wood load was introduced to the channel at sediment transport equilibrium and another one in which a high wood load was added. Discharge, sediment input, and slope was held constant throughout the length of all experiments.

Table 4.1: Difference in reach-averaged sediment storage (ΔSS) and reach-averaged bed slope (ΔS_b) between equilibrium with and without wood for all experiments

Exp.	ΔSS [cm^3/m^3]	ΔS_b [m/m]
1	4148	0.001
2	5378	0.003
3	3433	0.002
4	7163	0.003

4.1 Experiment 1: Single Grain Size Model, Moderate Wood Load

Experiment 1 was conducted in the single grain size model (Model 1) and was treated to the addition of a moderate wood load (5.4 $x10^{-4}$ m^3/m^2).

Figure 4.1 shows the DEMs of the bed surface for four time periods: at the end of the first

Table 4.2: Summary of steady state morphology with and without wood.

Exp.	No Wood				Wood			
	T_e [hr]	S_b [m/m]	D_{50} [mm]	N_{facies}	T_e [hr]	S_b [m/m]	D_{50} [mm]	N_{facies}
1	35	0.007	1.14	–	50	0.008	1.14	–
2	35	0.007	1.14	–	50	0.010	1.14	–
3	15	0.013	1.04	16	30	0.015	1.00	27
4	10	0.014	1.10	14	50	0.017	1.03	26

T_e = time to equilibrium, S_b = reach-averaged bed gradient, D_{50} = reach-averaged median grain size of bed surface, N_{facies} = number of distinct facies (from the facies maps of the bed)

five hours of run time (i.e. the first run), at equilibrium without wood present, five hours after the addition of wood, and equilibrium with wood present. Similar figures are presented for Experiments 2, 3, and 4 (Figures 4.3, 4.4, and 4.5). The small black lines displayed on the DEMs with wood present represent the approximate locations of LW pieces derived from the LW location data collected at the end of each run (described in Section 3.4).

Pools and riffles were observed to develop from the initial flat-bed surface that was imposed in the flume at the beginning of the experiment during the first hour of run time. By the end of the first run (Figure 4.1a), a pool-riffle pattern had developed that would remain relatively stable until the addition of LW. The DEMs in Figure 4.1 show that there was very little difference in channel morphology after five hours of run time (Figure 4.1a) and after 35 hours of run time (Figure 4.1b)). The location of pools and bars that developed in the absence of wood corresponded to the alignment of the fixed banks, with pools forming in the areas of high scour and flow convergence, for example on the outside of the large meander bend at approximately 5.5 m downstream.

The DEMs of difference created from the DEMs of Experiment 1 (Appendix C) show that although the general morphology of the channel remained stable after the first hour of the experiment, differences in elevation between consecutive runs indicate that sediment continued to move down the length of the flume throughout the first 35 hours of the experiment.

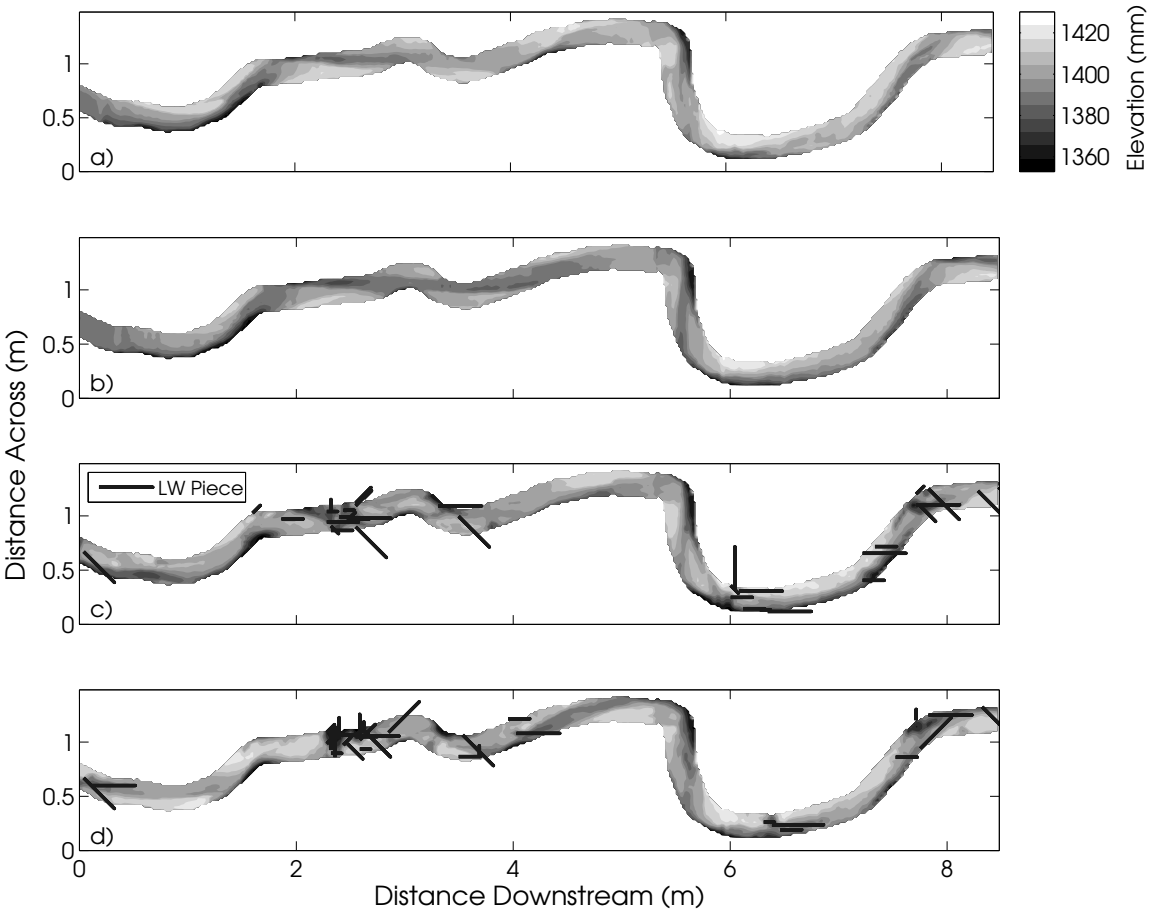

Figure 4.1: DEMs from Experiment 1: a) After the first five hours of run time, b) Equilibrium with wood (35 hours in), c) Five hours after the addition of LW (40 hours in), and d) Equilibrium with LW present (90 hours in)

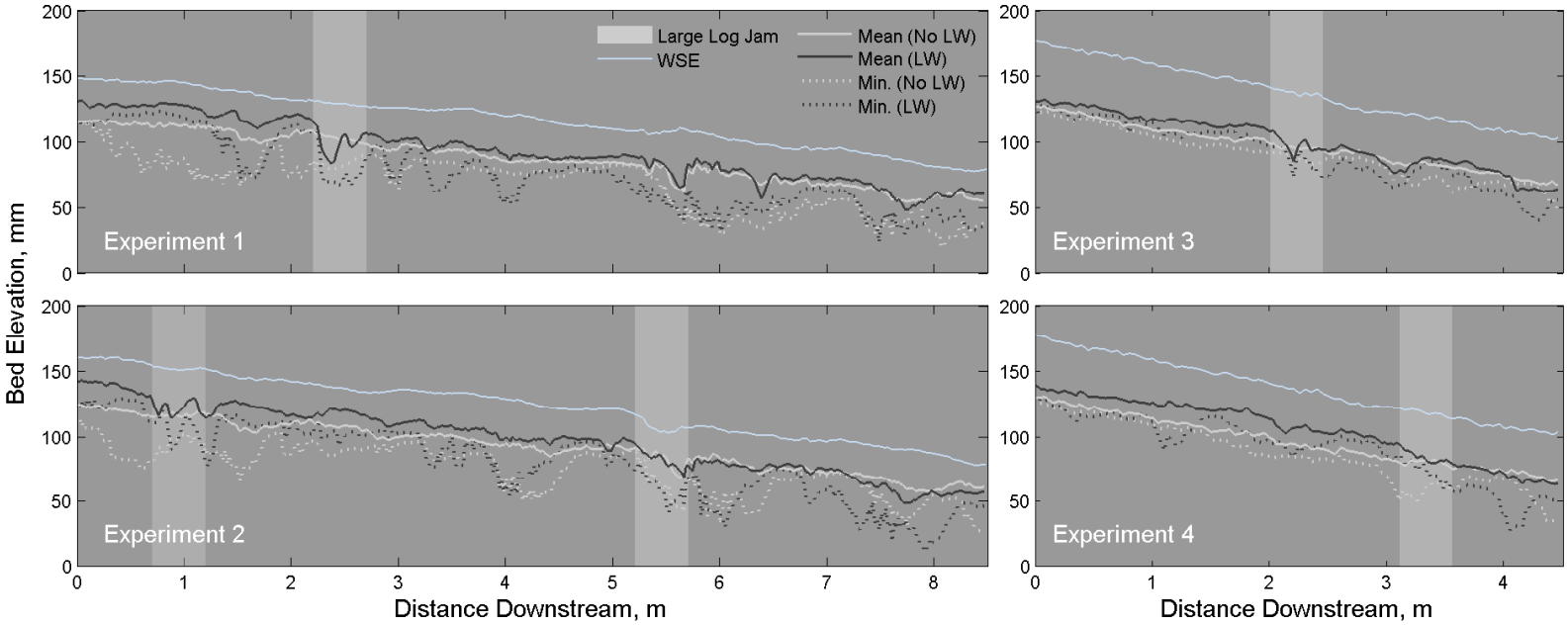

Figure 4.2: Longitudinal profiles of mean and minimum bed elevation shown for equilibrium runs without wood present and with wood present. The water surface elevation (WSE) is shown for the equilibrium run with wood present. The shaded rectangles represent the location of log jams made up of 10 pieces or more.

Without wood present, equilibrium was reached after a total of 35 hours. Scaling this back up to the prototype, this equals to approximately 7 years of morphologic change. Figure 4.2 shows the longitudinal profiles of minimum and mean bed elevation at equilibrium with and without wood present for all experiments. Considering the profiles from Experiment 1 prior to the addition of LW, the profile of mean bed elevation (No LW) is quite uniform and does not show any pronounced pools or bars except for at approximately 5.5 m downstream, which coincides with the location of the model's large meander bend. The equilibrium bed slope without wood present was calculated to be 0.007 m/m. The pool and riffle morphology is apparent on the longitudinal profile of minimum bed elevation (Figure 4.2) with pools characterized as locations where the minimum bed elevation is lower than the mean elevation and riffles characterized by areas where the mean and minimum elevations are similar.

The addition of wood caused local alterations to the background morphology established prior to wood addition. While the location of many of the pools and bars remained constant, once wood was added, new pools and bars developed in proximity to LW pieces, especially where several wood pieces interacted to form jams (Figure 4.1b and Figure 4.1d). Likewise to areas of more intense scour, many of the bars grew in area and in elevation following the addition of LW, indicative of an increase in sediment storage.

A new state of equilibrium was achieved with wood present after 50 hours, which is equivalent to approximately a decade of change in the prototype. Changes to the longitudinal profile of the mean bed elevation reveal that the distribution of sediment storage was not equal throughout the length of the flume as most storage occurred in the area upstream of the largest log jam which occurred at about 2.5 m downstream (Figure 4.2). The equilibrium bed slope with wood present was 0.008 m/m, which is 13% steeper than that of the equilibrium slope without wood. The presence of wood resulted in the creation of a more complex and variable bed surface as evidenced by more pools visible in both the mean and minimum bed elevation profiles (Figure 4.2).

4.2 Experiment 2: Single Grain Size Model, High Wood Load

Experiment 2 was conducted in the single grain size model (Model 1) and was treated to the addition of a high wood load ($7.4\,x10^{-4}$ m^3/m^2). As in Experiment 1, the development of a fairly stable channel morphology occurred within the first hour of run time (Figure 4.1a). Pools and bars developed in similar locations as what was observed in Experiment 1, as areas of erosion and deposition were driven by flow patterns dictated alignment of the fixed flume banks.

The time to equilibrium without wood present (35 hours) and the reach-averaged equilibrium slope (0.007 m/m) were the same for both Experiment 1 and 2. The longitudinal profile of equi-

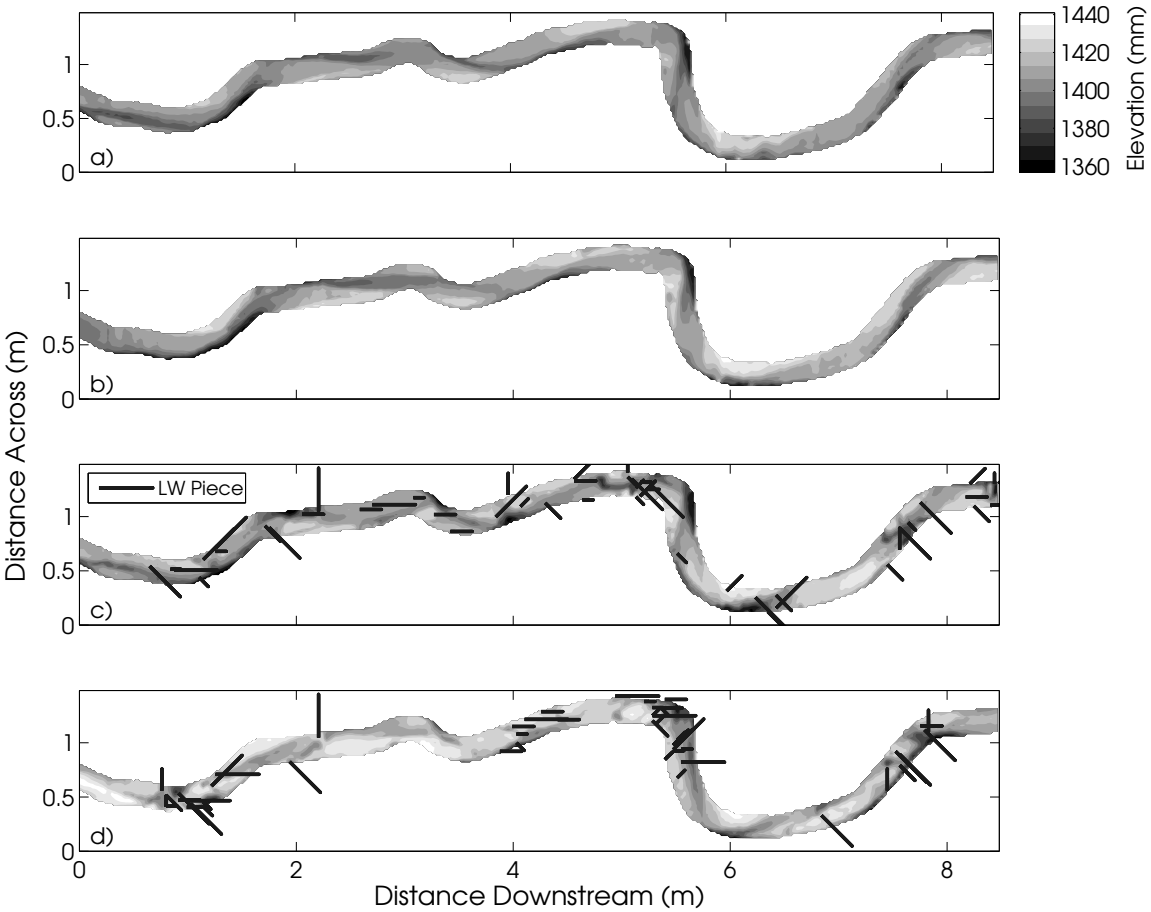

Figure 4.3: DEMs from Experiment 2: a) After the first five hours of run time, b) Equilibrium with wood (35 hours in), c) Five hours after the addition of LW (40 hours in), and d) Equilibrium with LW present (90 hours in)

librium mean bed elevation was also similar between the two experiments (Figure 4.2), however Experiment 1 did not exhibit as pronounced a drop near the large meander bend at 5.5 m downstream.

Like what was observed in Experiment 1, the addition of wood caused new pools and bars to be overlaid onto the pre-existing channel morphology (Figure 4.3c). Two large log jams developed in Experiment 2, one at about 1 m and the other at about 5.5 m downstream. As evidenced by both the DEMs and the longitudinal profiles of bed elevations (Figure 4.2), new scour pools formed in areas around log jams while new bars developed in areas upstream of log jams. Net sediment

storage occurred upstream of both jams, as seen by a rise in the mean bed elevation, while the last 3 m of the model (i.e. below the two log jams) experienced areas of net erosion as a result of upstream sediment trapping by the jams (Figure 4.2).

It took the same amount of time (50 hours) for the model to reach equilibrium with wood present in Experiment 2 as it did in Experiment 1. The combination of deposition in the upstream part and degradation in the lower part of the flume resulted in a equilibrium reached-averaged slope of 0.010 m/m with wood present, a 35% increase over the equilibrium slope without wood. This change in slope was greater than what was observed in Experiment 1 following the addition of a lower

4.3 Experiment 3: Full Grain Size Distribution Model, Moderate Wood Load

Experiment 3 was conducted in the full grain size distribution model (Model 2) and was treated to the addition of a moderate wood load (5.4 $x10^{-4}$ m^3/m^2).

In Experiment 3, a persistent channel morphology developed within the first hour (Figure 4.4a) that was in large part controlled by the alignment of the channel banks. While the rapid development of a stable channel morphology is consistent with the experiments conducted on Model 1, the resulting channel morphology differed in that pools tended to form along the center of the channel while bars formed in the bends along the edges of the flume, resulting in less of a pool-riffle morphology than had been seen in Model 1. This difference can be attributed to lack of large meanders present in Model 2 relative to Model 1.

At 15 hours (prototype equivalent of 3 years), the establishment of equilibrium took less than twice the amount of time in Experiment 3 than it did for the two experiments conducted on Model 1. The equilibrium reach-averaged channel slope was 0.013 m/m which is approximately twice the slope observed in Experiment 1 and 2. This discrepancy is due to the difference in the imposed slope of the two models (Table 2.3).

At equilibrium, the longitudinal profiles of the minimum and mean bed elevation were similar in the upper half of the flume which suggests a plane-bed channel morphology. The profile of the minimum bed elevation deviated from that of the mean bed elevation at about 3 m downstream, suggesting the presence of a large pool. The D_{50} of the equilibrium bed surface without wood was calculated to be 1.04 mm based on the facies maps created by Davidson, with pool areas 15% coarser in than the rest of the average bed surface (Table 4.3).

The flume experienced changes to bed surface texture following the addition of wood (Table 4.2). The number of facies present increased to 27 and median bed surface texture fined by ap-

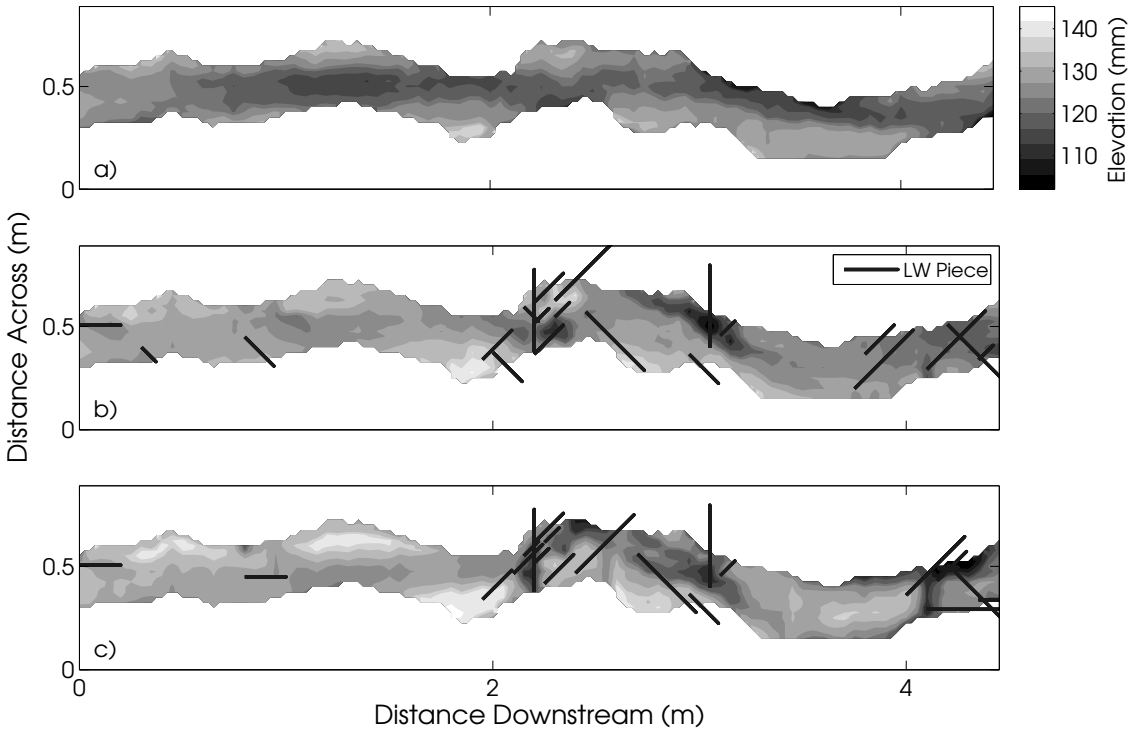

Figure 4.4: DEMs from Experiment 3: a) After the first five hours of run time, b) Equilibrium with wood (15 hours in), c) Five hours after the addition of LW (20 hours in), and d) Equilibrium with LW present (50 hours in)

proximately 5%. Pool areas remained coarser relative to the bed surface with wood present. As seen by the longitudinal profile of minimum bed elevation, most of the pools formed in the lower half of the flume as there are very few differences between the equilibrium minimum bed profiles in the upper half (Figure 4.2).

The reach-averaged slope increased by 14% following the addition of wood, resulting in an equilibrium slope of 0.015 m/m. This was slightly higher than what was observed in Experiment 1, which was conducted with the same wood load, but lower than what was seen in Experiment 2, which had a higher wood load. The longitudinal profile of mean bed elevation (Figure 4.2), shows that most sediment accumulated in the area upstream of the large log that developed at about 2 m downstream. However, unlike what was seen in Model 1, the area of accumulation was more restricted to the area immediately (i.e. one meter) upstream of the jam.

Table 4.3: A comparison between the reach-scale median grain size and the median grain size found within pool areas. The average median grain size of the bed surface and the median grain size for pool areas are given for the two experiments conducted in the full GSD flume for the runs at equilibrium without and with wood present.

	Experiment 3		**Experiment 4**	
	No Wood	*Wood*	*No Wood*	*Wood*
Bed D_{50} (mm)	1.04	1.00	1.10	1.03
Pool D_{50} (mm)	1.20	1.25	1.28	1.21
% Coarser	15 %	25 %	16 %	17 %

4.4 Experiment 4: Full Grain Size Distribution Model, High Wood Load

Experiment 4 was conducted in the full grain size distribution model (Model 2) and was treated to the addition of a high wood load (5.4 $x10^{-4}$ m^3/m^2).

At 10 hours (or the equivalent of two years in the prototype), the development of an equilibrium channel morphology in Experiment 4 was three times shorter than what was observed in Model 1 (Exp. 1 and 2) and five hours shorter than Experiment 3, which conducted in the same model. The longitudinal profile of mean bed elevation was uniform and the profile of the minimum bed elevation suggests that the upper half of the flume was dominated by a plane-bed morphology while the lower half contained some pools and riffles. The equilibrium reach-averaged bed slope without wood was 0.014 m/m, which is slightly higher than what was observed in Experiment 3. Like in Experiment 3.

It took 20 hours longer for equilibrium to establish in the presence of LW in Experiment 4 than in Experiment 3 (Table 4.2). This is equivalent to a difference of 4 years in the prototype channel. The addition of LW resulted in an 19% increase in the equilibrium reach-averaged bed slope (up to 17.2 %). This increase was higher than what was observed in Experiment 3 but was lower than what was observed in Experiment 2 which was conducted with a similar wood load.

Experiment 4 exhibited comparable responses in bed texture to Experiment 3 in response to the addition of LW. The number of facies present at the bed surface increased from 14 to 26, the reach-averaged bed surface D_{50} decreased from 1.10 mm to 1.03 mm, and the surface texture of pool areas remained coarse relative to the averaged bed texture in the presence of LW (Table 4.2 and 4.3).

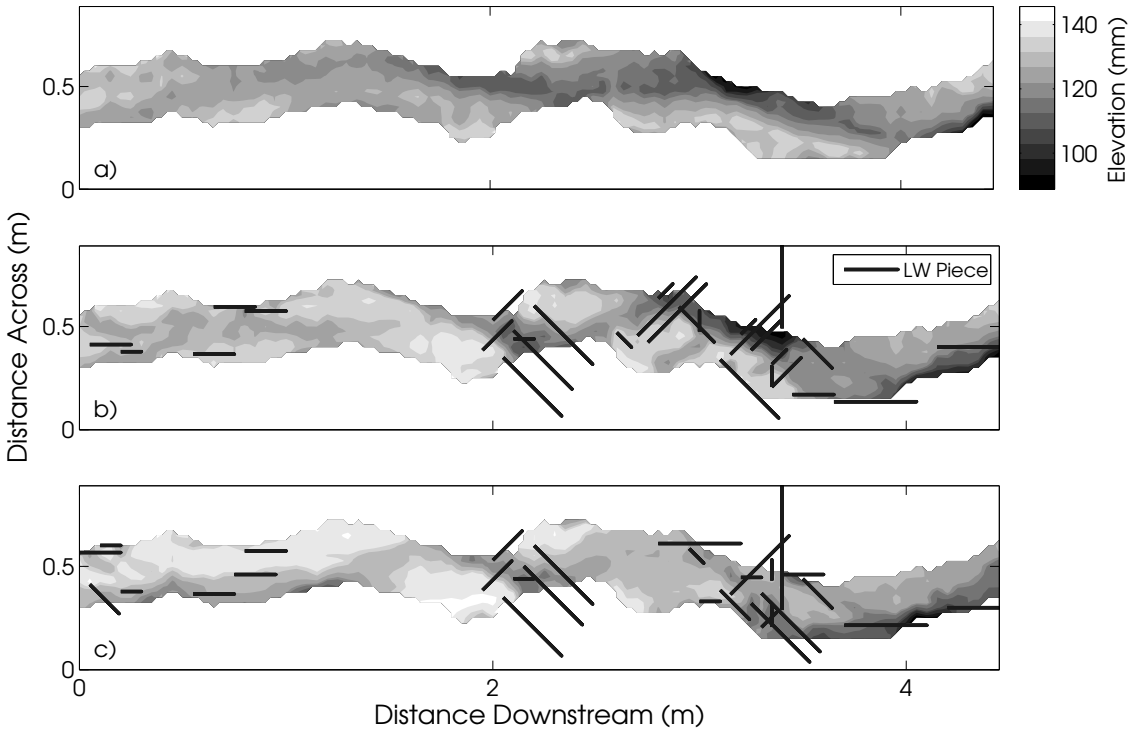

Figure 4.5: DEMs from Experiment 4: a) After the first five hours of run time, b) Equilibrium with wood (10 hours in), c) Five hours after the addition of LW (15 hours in), and d) Equilibrium with LW present (55 hours in)

4.5 Synthesis of Results

Channel morphology was visibly influenced by the addition wood in both models. This can easily seen by contrasting the DEMs of bed surface prior to and following the addition of large wood in all of the experiments. The DEMs of difference shown in Figure 4.6 were created by subtracting the equilibrium DEMs (two with and two without wood) of experiments conducted in the same model from one another. The DoDs in Figure 4.6a show the variability in equilibrium runs conducted on Model 1 (Experiments 1 and 2) while the DoDs given below in Figure 4.6b show the variability between the equilibrium runs on Model 2 (Experiments 3 and 4). In both figures, the upper DoD shows the difference between the equilibrium channel morphologies without wood present, meaning that the bed grain size distribution and model is constant between the two DEMs. The lower DoDs show the difference between the equilibrium morphologies with LW present, meaning that while the bed grain size distribution and models are constant, the wood loads of the two equilibrium DEMs is different.

For both models the differences in elevation between the equilibrium morphologies without wood were relatively small in magnitude, indicating that the general morphology of the channel (i.e. the location of pools and bars) was comparable between the two experiments and that the alignment of the fixed model banks play a important role in dictating channel morphology. The DEMs of difference show a great deal more variability between the two DEMs of the bed at equilibrium with wood present than was seen prior to wood addition. The differences in equilibrium bed elevation (with wood present) occurred in localized areas and elevational differences between the two equilibrium DEMs were as large as 30 mm. Such areas occurred primarily in proximity to the location of the large log jams that developed during the experiments (see Figure 4.2 for locations) which suggests that the larger magnitude of differences in elevation are indicative of local areas of deposition of material and scour caused by the presence of wood at that location.

As seen qualitatively on the DEMs, the addition of wood led to an increase in sediment storage in all experiments (Figure 4.7). Total sediment storage was higher in the high wood load experiments (Experiments 2 and 4) than for the moderate wood load experiments (Experiments 1 and 3) (Table 4.2). These results indicate that wood load, rather than bed texture governs reach-averaged sediment storage.

The storage rate of sediment suggest a two-phase pattern following the addition of wood. The first phase represents a period of a high rate of sediment accumulation immediately following the addition of sediment and can be seen for Experiments 1, 2, and 4 (Figure 4.7). In Experiment 3 this increase in sediment storage does not begin until about five to ten hours into the experiment.

The length of this first phase is influenced by the amount of wood present in the channel as sediment storage rates remain higher for longer when there is more wood present in the channel. In the two experiments containing high wood loads (Exp. 2 and 4), the rate of storage remains high for about 35 hours, while in the two moderate wood load experiments (Exp. 1 and 3), the rate of storage begins to taper out at around 20 hours (Figure 4.7).

The second observed phase of sediment storage occurs when the rate of sediment storage slows down and/or drops to zero as the system comes into a new equilibrium with the wood present. Although periods of low to moderate accumulation followed by sediment release persist throughout this phase, reach-averaged sediment storage remains relatively constant for all experiments during this phase (Figure 4.7).

Coinciding with the increase in sediment storage, an increase in reach-averaged bed slope was observed in all experiments (Table 4.1). The total change in slope was found to be related to wood load, as the increase in reach-averaged bed slope was greater in the experiments run with a higher wood load.

Pools were identified for each of the runs by selecting all areas that are deeper than one stan-

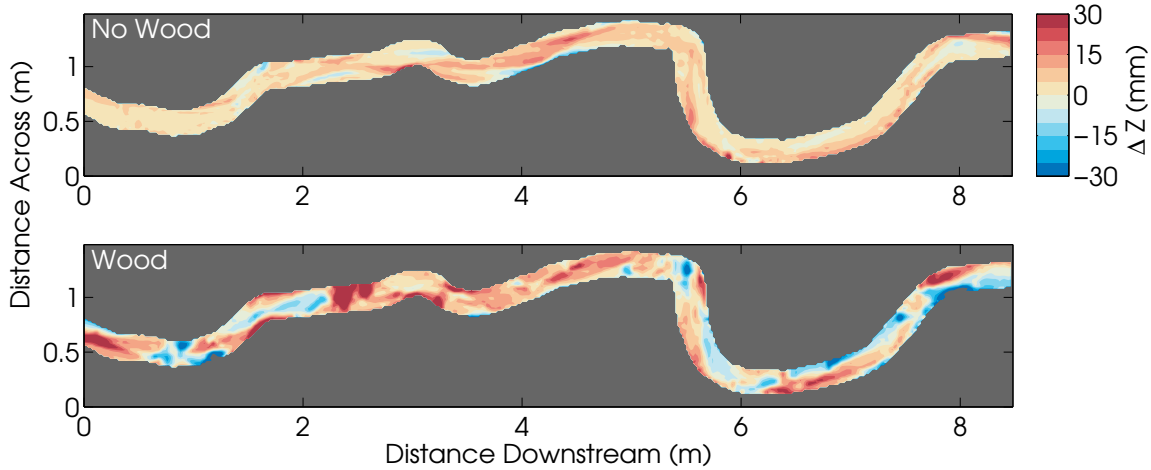

(a) The upper DEM of difference (DoD) shows the difference in channel morphology between the flume runs in equilibrium without wood present from Experiment 1 and Experiment 2, both conducted on Model 1. The lower DoD shows the difference between the channel morphologies of the flume once equilibrium is reached with wood present.

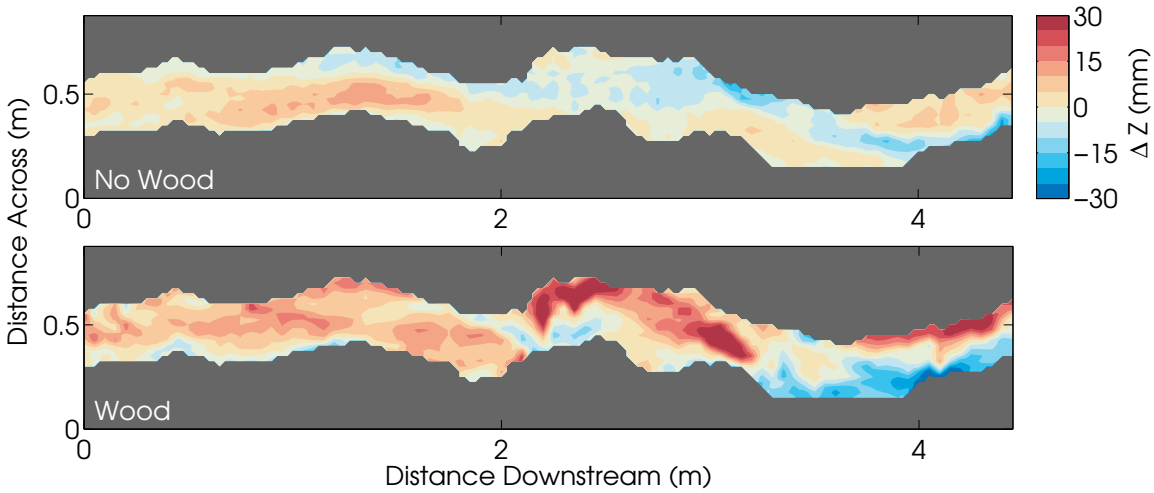

(b) The upper DEM of difference (DoD) shows the difference in channel morphology between the flume runs in equilibrium without wood present from Experiment 3 and Experiment 4, both conducted on Model 2. The lower DoD shows the difference between the channel morphologies of the flume once equilibrium is reached with wood present.

Figure 4.6: DoDs of equilibrium morphologies with and without wood on the two models.

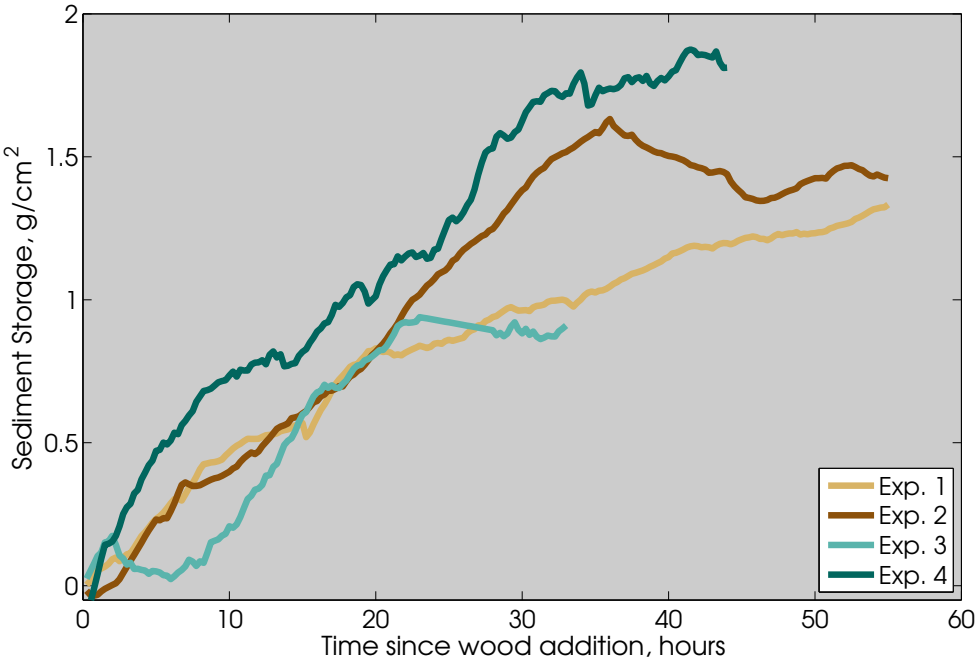

Figure 4.7: Cumulative amount of sediment stored in the flume following the addition of wood for each experiment.

dard deviation above the mean and greater than at least three cells in area (see Chapter 3). Figure 4.8 shows the pool spacing, calculated using the method presented in Montgomery et al. (1995), for each of the runs. Pool spacing is of the same order for all experiments which suggests that the grain size distribution of the bed does not play a role in constraining the number of pools that form in the presence of LW (Figure 4.8).

There was slight decrease in pool spacing, from around 3-4 W_b to 1-2 W_b (where W_b is the bankfull width), following the addition of wood for the experiments conducted in Model 1. Additionally, the variability in pool spacing is higher prior to the addition of wood, while following the addition of wood pool spacing remains relatively constant. There is not enough data prior to wood addition to make similar Experiments 3 and 4, although the results post-wood addition are comparable. These results indicate that it is the presence of wood rather than the wood load that dictates pool spacing and that bed texture does not play a distinguishable role in pool spacing.

The presence of wood in the flume influences the range of pool morphologies present in the stream channel (Figure 4.9). For this study, pool morphology is represented by pool area and maximum pool depth. Pool area is normalized by W_b^2, which represents a unit area of the stream

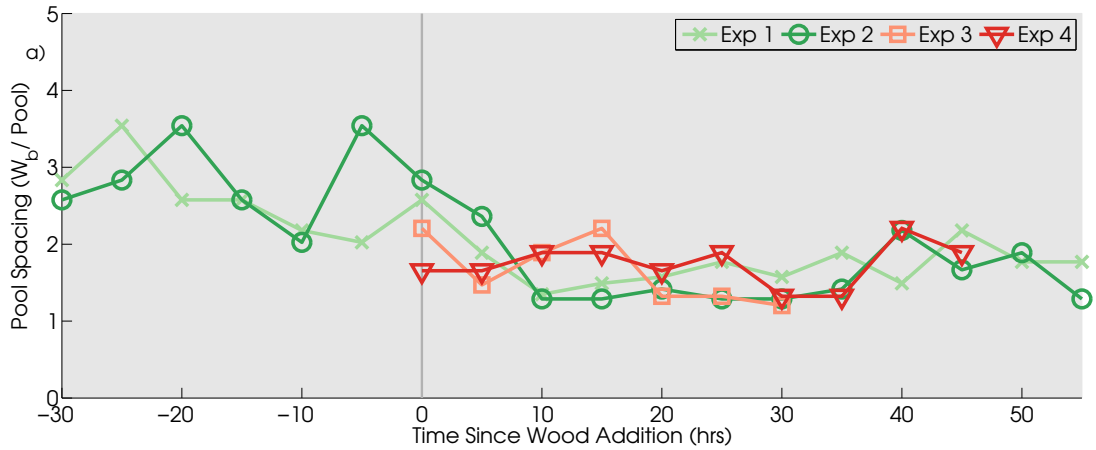

Figure 4.8: Pool spacing, calculated using the method presented in Montgomery et al. (1995), shown through time for all four experiments. The points along the vertical grey line represent the pool spacing in channel equilibrium prior to the addition of LW

channel. The absolute value of maximum pool depth is not given due to the uncertainty associated with digitization, instead, maximum pool depth is approximated by a value representing the depth associated with two standard deviations above the mean depth of the pool ($\mu_p + 2\sigma$). This value is then normalized by mean depth (μ_{tot})for that given run. Data is only shown for Model 1 as there is not enough "No Wood" data to present from Model 2.

Shown only for Experiments 1 and 2 (not enough pre-wood data for Model 2), median pool size decreased in the presence of wood in both experiments (Figure 4.9). The increased number of small pools exhibited a large range of maximum pool depths than pools of similar size that formed prior to wood addition. Very large pools (i.e. $>1 * W_b^2$) occurred less frequently and pools greater than $1.5 * W_b^2$ were not observed. Maximum pool depths remained close to $3 * \mu_{tot}$ regardless of the presence of wood. The range of pool morphologies measured for the high and low wood loads were very similar. All together these results indicate that the presence of wood acts to increase the frequency of smaller, deeper pools while limiting the size of the largest pools regardless of wood load.

Bed texture also played a role in constraining the range of pool depths that were observed in the flumes with wood present in the stream channel (Figure 4.10). The median of maximum pool depths in the single GSD model was found to be close to $1.5 * \mu_{tot}$, while the median in the single grain size model was just above $2 * \mu_{tot}$. In the full GSD model, the largest maximum pool depths were limited to $2 * \mu_{tot}$, with a single outlier at just below $2.5 * \mu_{tot}$, whereas the largest maximum pool depths were found to be up to $3 * \mu_{tot}$ in the single GS model. This difference in

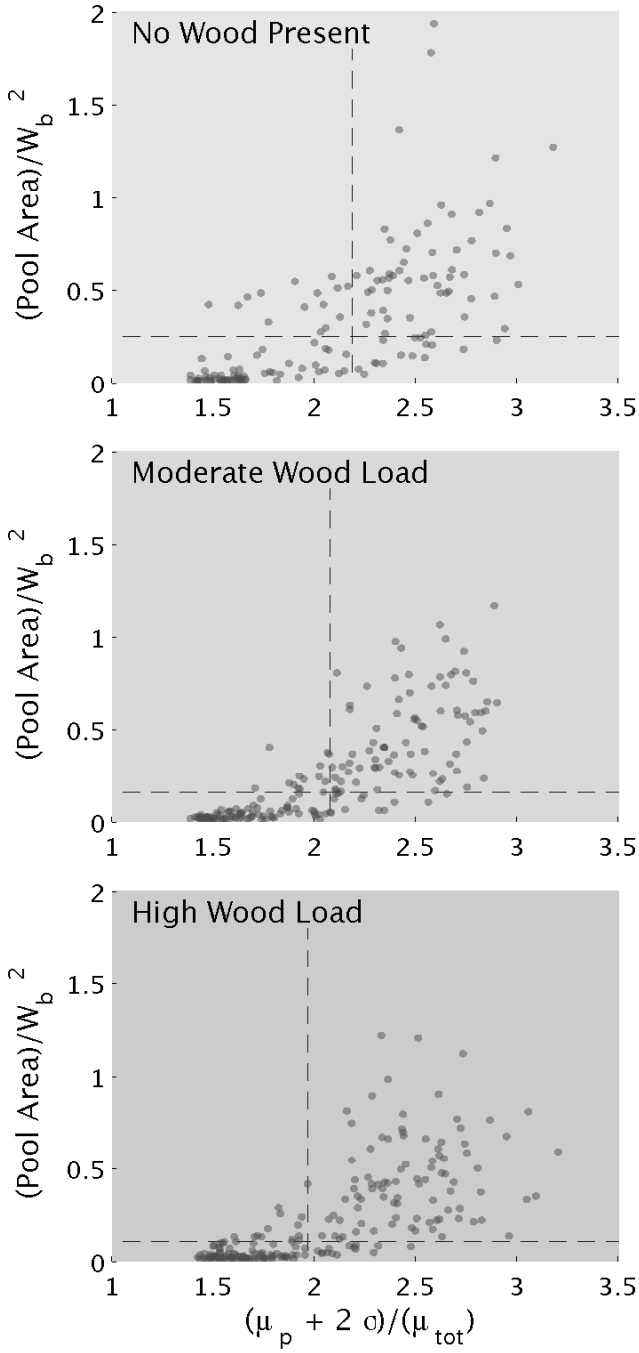

Figure 4.9: The range of pool morphologies found in Model 1 for the given three experimental treatments: no wood, moderate wood load, and high wood load. Each point on the plot represents a pool recorded in the stream channel for the given wood load condition. The dashed lines represent the median pool area (horizontal line) and the median pool depth (vertical line).

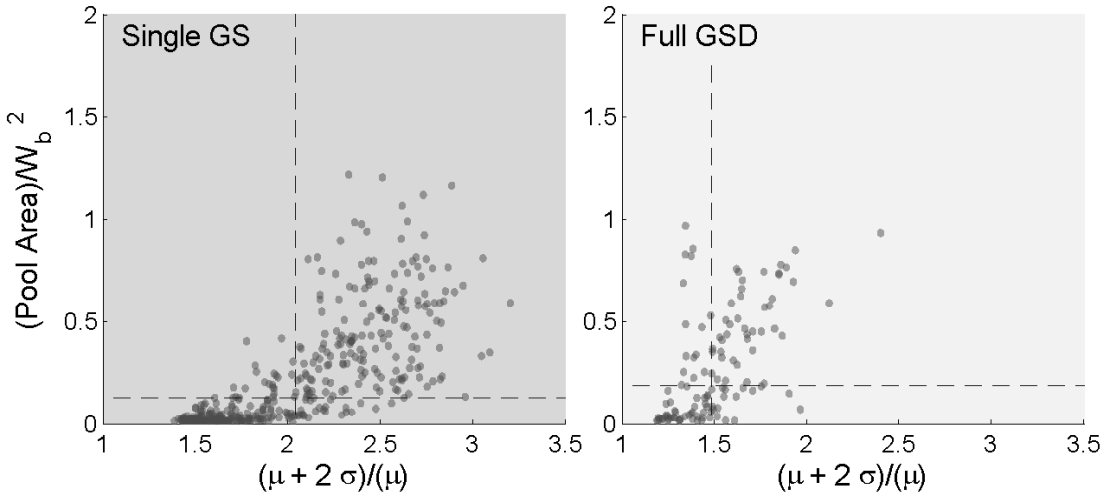

Figure 4.10: Difference in pool morphologies between the two models when wood was present in the stream channel. The results for both the moderate and the high wood load experiments are combined. Each point on the plot represents a pool recorded in the stream channel with wood present on the given model. The dashed lines represent the median pool area (horizontal line) and the median pool depth (vertical line).

the range of pool morphologies mirrors the difference in the depth distributions seen in (Figure 3.1a), where the range of depth values found in Model 1 (single grain size model) had a larger range and maximum depth values than those found in Model 2 (full GSD model).

Pool areas do not appear to be influenced by bed texture in the same way as maximum pool depths (Figure 3.1a). Consequently, the relationship between pool area and maximum pool depth is different between the two models. In the full GSD model (Model 2) small pools had a tendency to be shallow, whereas small pools in the single grain size model (Model 1) varied over a much wider range of maximum pool depths. Conversely, where in Model 2 large pools were found to have maximum depths ranging across the entire observed spectrum, the largest pools in Model 1 were all also quite deep.

Chapter 5

Discussion

The results of the experiments presented Chapter 4 show that both large wood and the particles that make up bed surface texture play a role in dictating equilibrium channel morphology. This is evidenced by the fact that fundamental differences channel morphology between the two models persist even in the presence of large wood.

5.1 Equilibrium Without Wood

Without wood present in the channel, it is possible to see the role that armouring plays in controlling the depth of scour in the flume by comparing the range of depth values observed in each of the two models (Figures 3.1a and 3.1b). In Model 1, with the single grain size bed material, the maximum depth value is about 2.5 times the mean depth. Conversely, in Model 2, where there is a mixture of particle sizes present, maximum depth values are about 1.5 times the mean depth, and are more similar to those found in Fishtrap Creek, the prototype stream, where maximum depths are approximately 1.75 times the mean depth. This similarity between the prototype and Model 2 almost certainly arises due to the presence of armouring of the surface in response to the discharge that they experience.

Without the ability to armour, different processes are needed in order to achieve equilibrium in Model 1. Eaton and Church (2009) proposed that a channel can adjust to imposed conditions by either a) adjusting its bed state, for example through the formation of an armour surface or other bed structures, or by b) reach scale adjustments, such as through changes to channel gradient. Considering the development of steady state morphology prior to the addition of LW, it can be reasoned that the greater range in depths that occur in the single grain size model play a role in stabilizing the channel morphology. When there are no larger particles present, Buffington and Montgomery (1999a) found that flow resistance can be augmented by increasing the amplitude of

the pools and bars present in the channel, thereby increasing the stability of the channel. In this study, the presence of high amplitude bed forms, as indicated by the wide range of depths found in Model 1 suggests that such a process plays a role in stabilizing the bed in this study (Figures 4.1 and 4.3). By comparing the minimum bed elevations (Figure 4.2) as well as the pool spacing (Figure 4.8) between Models 1 and 2 at equilibrium pre-wood, we see that pools occur much more frequently in Model 1. This is further indicative of the stabilizing role that the pool-riffle pattern plays in the single grain size model.

The response time of the two models, characterized by the amount of time it took each of them to come into equilibrium, is highly dependent on the composition of the bed material. It took more than twice the amount of time, or the equivalent of seven years, for the single grain size model to come into equilibrium compared to the equivalent of two to three years in the full GSD model (Table 5.1). This most likely has to do with the lack of armouring capabilities in Model 1 as the development of a armour layer as well as the structures that form from interactions between the larger particles play an important role in the progression towards a stable morphology (Parker and Klingeman, 1982; Dietrich et al., 1989; Church et al., 1998). This difference in time to equilibrium may also stem from discrepancy in reach length between the two models as stream length has been linked to the response time of systems (Howard, 1988). Because the length of Model 1 is almost twice that of Model 2, it is possible that the difference in time to equilibrium between the two models may not actually reflect the differences in bed texture.

The equilibrium morphologies that developed in the absence of wood are similar between the two experiments conducted on each model (Figure 4.6). This is consistent with the main premise of regime theory which suggests that channel will optimize its geometry in response to given any set of imposed governing variables (Eaton and Church, 2004). If the experiments had not been conducted in a fixed-bank flume it is probable that the morphology or pattern of the channel may not have been so similar the imposed channel pattern may have been responsible for the development of similar equilibrium channel configurations.

It has been proposed that the surface grain size can be used to infer the approximate values of the sediment supply and the magnitude of discharge (Dietrich et al., 1989; Lisle et al., 1993; Buffington and Montgomery, 1999a,b). This arises from the premise that where Q is high relative to Q_B, the surface grain size will be coarser than that of the subsurface, and vice versa. It follows that comparing the size of particles found at the surface to those within the subsurface should be indicative of the Q:Q_b ratio. This logic does not extend itself to the results of Model 1, as the system has no ability to modify the surface texture in relation to the imposed governing variables. This shows that the use of such relations to lend an understanding of sediment supply and discharge may be more difficult in implementing in practice as this relation is highly dependent on a non-

uniform size distribution of material.

5.2 The Addition of Large Wood

The mobility of wood pieces simulates how large wood interacts in unregulated forested channels rather than pre-engineered log jams. The majority of wood movement occurred during the first two runs after the addition of wood (Figure 5.1) as individual wood pieces coalesced to form more stable log jams. Most wood pieces remained stable following this period of adjustment although individual pieces were observed to move between subsequent jams. Given that the wood movement slows well before before the models come to equilibrium, it is likely that, while the stability of wood pieces is a prerequisite to the establishment of equilibrium, it is the development of bedforms around the stable LW that largely influence the equilibrium channel morphology.

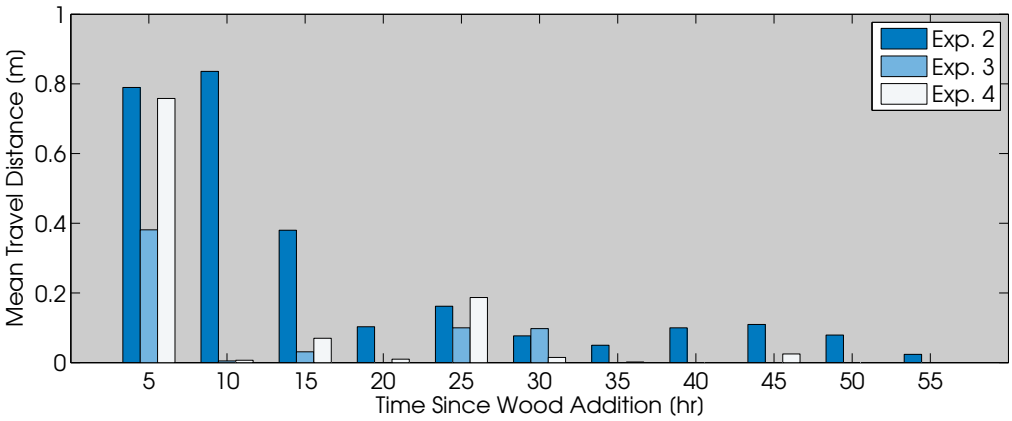

Figure 5.1: The average travel distance of each wood piece following the addition of LW. Experiment 1 is not shown due to some errors in the collection of data.

The morphologic effects of the addition of large wood are visible at two scales: the local scale around LW pieces and at a reach scale. This indicates that the development of an equilibrium morphology is dependent on the interplay between these two scales of forcing. Local scale effects include the formation of scour pools around wood pieces (e.g. Figure 4.1) while at the reach scale effects are manifested as an increase in reach-average slope (Figure 4.2).

Changes to local patterns of erosion and deposition were observed immediately following the addition of LW and are manifested in changes to the characteristics and frequency of pools. With wood present, pools spacing decreased and pools were deeper relative to their areal extent (Figures 4.9 and 4.8), which is consistent with the characteristics of scour pools around obstructions in other studies (e.g. Raudkivi and Ettema, 1985; Abbe and Montgomery, 1996; Kuhnle et al., 2002). It

can be seen from the DEM images that most of the scour pools and bars occur in proximity to LW pieces (e.g. Figure 4.1), and are controlled by altered patterns of flow convergence and divergence around these roughness elements (Cherry and Beschta, 1989; Keller and Swanson, 1979; Abbe and Montgomery, 1996; Wallerstein et al., 2001).

Reach-average sediment transport capacity decreased following the addition of wood as seen in the increase in sediment storage increased following the addition of the LW in almost all experiments (Figure 4.7). Sediment transport capacity responds to changes in channel roughness due to the presence of LW both decreases reach-averaged flow velocity (Davidson and Eaton, 2012) and increases the total shear stress that is required to initiate the movement of material (Assani and Petit, 1995). This change in sediment transport capacity due to wood addition puts the system out of equilibrium, without changing any of the governing variables (Q, Q_b, S_V, or bank strength). In order to regain equilibrium, it is necessary that the system alter its reach-averaged resistance and/or its bed state resistance (Eaton and Church, 2004).

In real stream channels with erodible banks the addition of wood alters bank stability by both increasing bank erosion due to a loss of cohesion associated with roots (Keller and Swanson, 1979; Zelt and Wohl, 2004) as well as by stabilizing banks by lining channel edges and preventing further erosion (Montgomery and Buffington, 1997). At Fishtrap Creek, the 2003 forest fire has led to a significant loss in bank stability as a result of the fallen and standing dead trees (Eaton et al., 2010c). This loss of cohesion has facilitated the creation of new side channels and led to channel widening (Eaton et al., 2010a). Consequently, the progression of Fishtrap Creek towards a new equilibrium form is quite different than what was observed in the model runs.

Changes to sediment supply often accompany changes to bank stability as increased rates of bank erosion provide additional sediment to the system (Wondzell and King, 2003). However, in this study, the sediment input rate remained constant throughout the length of the experiments. While constant input rate is consistent with response of the prototype stream in the years since the fire (Eaton et al., 2010a), it could be expected that if sediment input was increased following wood addition, more aggradation would have occurred, as the ratio of sediment transport capacity to sediment availability would have been much lower.

5.3 Equilibrium with Wood Present

Reach-averaged equilibrium bed gradient increased in all experiments in response to the decrease in sediment transport capacity caused by the presence of LW (Figure 4.2). Given that the addition of LW results in a lower sediment transport capacity than without wood present, it would be expected that the system should adjust by increasing transport capacity in order to re-attain sediment

transport equilibrium with the input rate. However, the results from this study are inconsistent with those of Eaton and Church (2009) which predict that in a fixed-bank flume, the fluvial system should adjust to changes in the governing conditions primarily through changes to its bed state while maintaining a comparable bed gradient and morphology for a range of conditions. Bed state adjustments in the form of surface armouring does not appear to contribute substantially to the development of an equilibrium morphology in this study as equilibrium is still attained even when the bed is composed of a single grain size.

Differences in equilibrium bed morphology with and without wood present can be attributed to local changes in erosion and deposition induced by the presence of LW. This is supported by the fact that the location of scour pools and bars coincide with the location of LW (e.g Figure 4.1). The DEMs of difference (Figure 4.6) show that the equilibrium morphologies are highly variable with wood present, which suggests that LW ultimately governs the location and size of bedforms.

The net aggradation of material in response to the addition of wood was not uniform along the length of the flume. In all experiments most aggradation occurred in the area upstream of largest log jam(s) that developed (Figure 4.2). In contrast, the areas downstream of the largest jams experienced degredation as a result of a low ratio of sediment supply to sediment transport. Both the aggradation in the upper half and the degradation in the lower half contributed to the increase in channel gradient.

The locations of sediment storage occur in relation to the location of large log jams ($\geq$ 10 pieces) observed in the flume. This occurs due to the fact that as large log jams form through piece accretion (Bocchiola et al., 2008), they function as barriers, decreasing sediment transport immediately upstream of the jam (Assani and Petit, 1995; Keller and Swanson, 1979). This deposition of sediment acts in conjunction with the log jam barrier to further decrease sediment transport capacity by further lowering the channel gradient (May and Gresswell, 2003; Webb and Erskine, 2003). The long term of effects of this, as the channel approaches a new equilibrium morphology with wood present, is an increase the mean bed elevation in areas upstream of the log jams, while adjusting to downstream sediment starvation by maintaining the pre-wood mean bed elevation and affording local areas of degradation (Figure 4.2).

Net sediment storage in the flume was proportional to the amount of wood present, as more sediment was stored for experiments with higher wood loads (Figure 4.7). Following the addition of wood, all experiments exhibited a similar rate of sediment storage during the first 20 hours (although Experiment 3 did experience a short period of net loss). This net accumulation continued until which point a threshold was reached and the rate of storage decreased to approximately zero. The time at which this threshold was reached appears to be related to the wood load present in the channel, with lower wood load experiments reaching the threshold sooner.

This threshold may either represent the reach-averaged storage capacity of the flume which can be thought of as the sum of the sediment storage capacities of all the wood barriers present in the channel. Following wood addition, areas behind these jams start to fill up with sediment in response to the decrease in local sediment transport. Sediment storage rate levels off once a jam becomes "filled" Megahan (1982). The threshold at which sediment storage rate decreases to zero may be when all or most of the jams within the flume have reached their sediment storage capacity.

Alternatively, the threshold may represent the point at which net aggradation within the flume has created a new gradient that has allowed the flume to come into sediment transport equilibrium given the governing variables. If this is the case, it would be expected that the total amount of sediment storage should be less for a lower sediment input given the same wood load, discharge, and slope.

In reality, this threshold is likely related to both of these processes in that individual log jams store the sediment needed to alter the channel gradient in response to wood addition, however it is the total wood load of the reach that dictates how much sediment must aggregate in order to allow for a sediment transport equilibrium. Given this scenario, it would be expected that the same log jam would store more or less sediment depending on the amount of other wood pieces present in the surrounding area.

These results suggest that while predicting an exact equilibrium form in the presence of mobile wood pieces is difficult due to the variability in the interactions and spacing between individual wood pieces and log jams, it may be possible to predict reach-averaged responses to different wood loads. Further experimentation in which channel morphodynamics were explored by comparing runs with mobile wood pieces and runs in which log jams were engineered in place could help to further our understanding of the role that LW plays in local and reach-averaged channel morphology.

5.4 The Role of a GSD

When considering the importance of LW pieces compared to particles found on the bed, it would be expected that, given the large discrepancy in the size between these two roughness elements, properties of the grain size distribution should play a only relatively small part in dictating channel morphology (Manga and Kirchner, 2000; Wilcox and Wohl, 2006). The results of this study show that, while the presence of LW does increase the complexity of the bed morphology in both models, there is a consistent difference in the distribution of depths measured in two models, regardless of the presence of LW. Although a study conducted by Gill (1972) found that equilibrium scour

depth is governed by the grain size of bed material in uniform sand beds, it is important to note that the difference in scour depth observed in this study did not occur due to a difference in median grain size, as the bed material of both models have the same median grain size. Consequently it can proposed that the difference in depth distributions between the two models arises in large part due to the absence or presence of a range of grain sizes.

A bed composed of a non-uniform mixture of sediment sizes can act to limit scour: this self-stabilization process occurs as smaller particles, transported by the imposed flow conditions, are moved out of the system, while larger particles remain in place and eventually make up the bed surface (Parker and Klingeman, 1982; Gomez, 1983; Dietrich et al., 1989). Two lines of evidence show the role that armouring plays a role in limiting the depth of scour and stabilizing the bed. First of all, in Model 2, the median grain size of pool areas were all over 15% coarser than the average median surface grain size of the entire bed. This suggests that pools depths are limited by the creation of an armour layer, which is consistent with previous studies (e.g. Borah, 1989; Kassem and Chaudhry, 2005). Second, median pool depths from the single grain size flume were deeper then those found in the full GSD flume. This suggests that deeper scouring is more likely to occur when the system does not have the ability to armour.

Aside from the ability of the full GSD model to form an armour surface there are other processes or characteristics that may have contributed to the difference in depths between the two models. It is possible that the difference in the channel form imposed by the fixed-banks may have contributed to the disparity between the channel morphologies given that single grain size model contained a large meander bend, however it was observed that the distribution of depths for Model 1 remained wide even when the data from the meander bend was excluded. Discrepancies in the Reynolds number and turbulent structures present in the channel, due to the differences in bed surface texture between the two models, may have also contributed to the two alternate morphologies, although this was not measured in any of the experiments.

In previous experiments, it has been observed that when the bed material is composed of a range of grain sizes, changes to the governing variables can be compensated for through adjustments of the bed texture (Eaton and Church, 2009). These changes, either towards a coarser or a finer bed surface, can help to increase or decrease flow resistance within the reach in order to establish a new stable form. That there was a shorter response time (i.e. time to equilibrium) in the experiments conducted in the full grain size distribution model is consistent with these previous findings, although it is important to consider that part of this discrepancy may arise as a result of the differences in the imposed shape and length of the two models.

Table 5.1: Summary of the Effects of Wood Addition, Wood Load, and GSD

		Presence of Wood	**Wood Load**	**GSD**
Time to Equilibrium		Longer time to equilibrium with wood present	No discernible effect	Longer time to equilibrium with a single grain size
Sediment Storage		More sediment stored in the presence of wood	More sediment stored with higher wood load	No discernible effect
Channel slope	*Mean Bed Elevation*	Increased mean bed elevation in the upper half of the flume with wood present	No discernible effect	No discernible effect
	Min. Bed Elevation	More variability in the minimum bed elevation with wood present	No discernible effect	Less variability in the minimum bed elevation with a full GSD
	Reach-averaged Slope	Higher reach-averaged channel slope with wood present	Higher reach-averaged channel slope with a higher wood load	No discernible effect
Number of Facies		Increased number of facies with wood present	No discernible effect	–
Surface D_{50}		Higher surface D_{50} without wood present	Slightly higher surface D_{50} with a higher wood load	–
Distribution of Depths		No discernible effect	No discernible effect	Wider range of depths with a single grain size

Table 5.1 Continued

		Presence of Wood	**Wood Load**	**GSD**
Pool Spacing		Decrease in pool spacing following the addition of wood	No discernible effect	No discernible effect
Pool Morphology	*Area*	Larger pool areas with wood present	No discernible effect	No discernible effect
	Max. Depth	No discernible effect	No discernible effect	Deeper pool depths with a single grain size
	Dimensions	More small, deep pools and fewer small, shallow pools with wood present	No discernible effect	More small, deep pools and fewer small, shallow pools with a single grain size

Chapter 6

Conclusions

The morphology of stream channels is dictated by the interactions between discharge, sediment flux and size distribution, and the characteristics of the surrounding environment. While fluvial systems can accommodate minor adjustments to these governing variables without significant morphologic change (Montgomery and Buffington, 1997; Eaton and Church, 2009), sudden or sustained large scale alterations to these conditions forces the morphology of the channel to adjust in order to re-establish a new equilibrium morphology (Howard, 1982). Analytic regime theory has been developed in order to help guide our understanding of how fluvial systems adjusts to such changes by advancing a physically-based understanding of the processes that drive channel morphodynamics. The results from this study help to further this knowledge by isolating the effects that two different roughness elements, bed texture and large wood, have on channel form. The findings of this study show that bed texture plays a large role in shaping channel morphology regardless of whether it is the dominant roughness element in a stream channel. This highlights the necessity of considering the full grain size distribution when modelling channel response to changes in governing variables.

6.1 Grain Size Distribution

The role that bed grain size distribution plays in channel morphology is independent of the effects of large wood as indicated by the fact that the range of depths recorded in the channel remained higher in the single grain size flume than in the full GSD flume regardless of the presence of LW in the channel. Maximum depths as much as 2.5 times the mean depth of the channel were found using a uniform sediment size, whereas maximum depths were limited to approximately 1.5 times the mean depth in the full GSD model. Furthermore, pools were deeper relative to pool area in the single grain size model.

The results of this study suggests that armouring played a role in limiting the range of depths in the full GSD model. Armouring occurs as finer particles are transported away while larger particles remain, eventually creating a coarse surface layer in areas of local flow convergence, thereby limiting the local depth of scour (Borah, 1989; Parker and Klingeman, 1982). This process is apparent in the full GSD model as the median surface grain size in pools was found to be higher than the reach-averaged D_{50}.

It was proposed that range of particle sizes also facilitated the development of an equilibrium channel form, as the response time of the single grain size flume to wood addition was almost twice as long as it was for the full GSD flume. This discrepancy can also be linked to the availability of a range of particles sizes, as previous studies have found that changes to bed texture help stabilize channel morphology (Parker and Klingeman, 1982; Eaton and Church, 2009). These results suggest that, in addition to the sediment supply and sediment transport capacity (Howard, 1982; Montgomery and Buffington, 1997), the grain size distribution of sediment present in a stream channel plays a significant role in the response time of the system.

6.2 The Presence of Large Wood

Morphologic changes occurred at both a reach-scale and bed-form scale in response to the addition of wood into the flume. At a reach scale, the presence of LW increased flow resistance and decreased the sediment transport capacity within the channel. Individual wood pieces and log jams influenced local channel hydraulics, leading to changes in the pattern of erosion and deposition within the flume.

Sediment storage increased following LW addition in response to the decrease in sediment transport capacity. Sediment storage occurred disproportionally in the areas upstream of the largest log jam(s) in the flume, with some reaches below the log jams experiencing net degradation. This increase in sediment storage coincided with a increase in bed slope following wood addition. In the full grain size model, median grain size decreased following the addition of wood, due to the fact that the wood pieces impounded a greater amount of finer material in the flume.

Prior to the addition of wood, the location of pools and bars was dictated by the alignment of the non-erodible flume walls. The introduction of LW into the channel caused new areas of scour and deposition to be imposed onto the pre-established background form. In the full GSD flume, the number of distinct facies almost doubled with wood present due to the increased heterogeneity of flow patterns. Local flow convergence around LW pieces induced additional areas of scour, as seen by a decrease in pool spacing from three to four channel widths to about two channel widths. Both pool area and maximum pool depth were found to decrease as a result of this change in

channel hydraulics.

6.3 Wood Load

While wood load was found to influence the total sediment stored in the flume and the magnitude of change in reach-averaged bed slope, it was found to have little effect on channel morphology at a bed-form scale, as characteristics such as pool spacing and pool morphology were similar regardless of wood load. As such, it can be concluded that the system re-equilibrates its morphology to an imposed wood load by altering its reach scale resistance as opposed to its bed form resistance.

Instead of being driven by the wood load of the channel, pool characteristics were driven instead by local flow patterns around LW, either as individual pieces or amalgamated as log jams (Abbe and Montgomery, 1996). The results from this study suggest that at a local scale, the total amount of wood present in the surrounding reach has little effect on the patterns of scour and deposition that are imposed by individual wood pieces.

Wood load was found to dictate the total amount of reach-scale change that must occur in order for a new equilibrium form to be attained. More sediment storage, and consequently a steeper equilibrium slope was observed under the conditions of a high wood load.

6.4 Applications of this Study

All methods of modelling require the reduction of a complex system. This can mean that components of the system are omitted or certain relationships or variables are simplified. An example of this is the use of a single grain size or a highly distorted grain size distribution to represent the range of grain sizes found in a real channel (e.g. Wallerstein et al., 2001; Malverti et al., 2008). While this application is necessary in order to isolate relationships between individual variables or, in the case of numerical modelling, to reduce the computation power required, it runs the risk that processes are not accurately portrayed.

The results of this study show that it is important to consider the full range of sediment sizes when attempting to model equilibrium channel morphodynamics. The capacity of a stream channel to armour and to limit the depth of scour plays a key role in dictating the response time of a system to changes in the governing variables, both with and without wood present. The studies that disregard or oversimplify a modelled grain size distribution may poorly predict the proper range of depths that occur in a channel, in particular the depth of scour.

This study also presented a novel method of identifying pool areas from DEMs of depth. While previous studies used other methods of selecting pool areas (e.g. Montgomery and Buff-

ington, 1998), these methods have a tendency to be somewhat subjective as they often require the researcher to qualitatively identify and measure morphologic features such as riffle tops or pool depths. By selecting for areas greater than one standard deviation above the mean depth of the reach, this method can be applied to any fluvial system, regardless of the morphology of the channel, as it uses the unique depth distribution of the channel in question.

6.5 Future Work

Physical modelling provides an excellent opportunity to further our understanding of how equilibrium conditions are met in a range of scenarios. While this study has broadened our understanding of the types of variables that are influenced by the addition of wood into the channel, the next step is to further understand the processes that drive the observed outcomes.

While this study examined the effects of mobile wood pieces added to the channel, many stream restoration projects employ engineered log jams (ELJ) which are stable, fixed structures. Consequently, understanding how a channel adjusts to the addition of these ELJ as opposed to the addition of individual mobile wood pieces would prove to be useful when utilizing such methods in rehabilitation projects. Given that, in the absence of LW, this study showed that equilibrium channel form was dictated by the pattern of the stable, non-erodible banks, it could be hypothesized that, like channel banks, the presence of stable log jams should produce comparable channel morphologies between experiments if all other variables were held constant.

Results from this study suggest that the mobility of LW pieces contributes to the time it takes for the channel to come into equilibrium as the small adjustments in wood location that occur throughout the length of the experiment prolong the establishing of a stable channel form. If the location of LW pieces were stable throughout the length of the experiment, it is predicted that the response time of the system would be shorter.

Broadening our understanding of channel response to changes in governing conditions is key to building better regime models in order to better predict how our fluvial systems respond to changes in governing conditions. The results from this study exemplify the contribution that physical modelling can make towards how we understand and model fluvial systems.

Bibliography

Abbe, T. and Montgomery, D. 1996. Large woody debris jams, channel hydraulics and habitat formation in large rivers. *Regulated Rivers Research & Management*, 12(23):201–221. → pages 3, 34, 55, 56, 64

Abbe, T. and Montgomery, D. 2003. Patterns and processes of wood debris accumulation in the Queets River Basin, washington. *Geomorphology*, 51(1):81–107. → pages 2

Andreoli, A., Comiti, F., and Lenzi, M. 2007. Characteristics, distribution and geomorphic role of large woody debris in a mountain stream of the Chilean Andes. *Earth Surface Processes and Landforms*, 32(11):1675–1692. → pages 2

Andrews, C. 2010. A Stream in Transition: Short Term Morphodynamics of Fishtrap Creek Following Wildfire. Master's thesis, University of British Columbia. → pages 16, 18

Ashmore, P. 1991a. Channel morphology and bed load pulses in braided, gravel-bed streams. *Geografiska Annaler. Series A. Physical Geography*, pages 37–52. → pages 4

Ashmore, P. 1991b. How do gravel-bed rivers braid? *Canadian Journal of Earth Sciences*, 28(3):326–341. → pages 7

Ashmore, P. E. 1988. Bed load transport in braided gravel-bed stream models. *Earth Surface Processes and Landforms*, 13(8):677–695. → pages 7

Assani, A. and Petit, F. 1995. Log-jam effects on bed-load mobility from experiments conducted in a small gravel-bed forest ditch. *Catena*, 25(1):117–126. → pages 56, 57

Bennett, R., Welham, K., Ford, A., et al. 2012. A comparison of visualization techniques for models created from airborne laser scanned data. *Archaeological Prospection*, 19(1):41–48. → pages 80, 81

Bilby, R. and Ward, J. 1991. Characteristics and function of large woody debris in streams draining old-growth, clear-cut, and second-growth forests in southwestern washington. *Canadian Journal of Fisheries and Aquatic Sciences*, 48(12):2499–2508. → pages 34

Bocchiola, D. 2011. Hydraulic characteristics and habitat suitability in presence of woody debris: A flume experiment. *Advances in Water Resources*, 34(10):1304–1319. → pages 2, 7, 11, 15

Bocchiola, D., Rulli, M., and Rosso, R. 2008. A flume experiment on the formation of wood jams in rivers. *Water Resources Research*, 44(2). → pages 57

Borah, D. K. 1989. Scour-depth prediction under armoring conditions. *Journal of Hydraulic Engineering*, 115(10):1421–1425. → pages 59, 63

Braudrick, C., Dietrich, W., Leverich, G., and Sklar, L. 2009. Experimental evidence for the conditions necessary to sustain meandering in coarse-bedded rivers. *Proceedings of the National Academy of Sciences*, 106(40):16936–16941. → pages 7, 13

Braudrick, C. A. and Grant, G. E. 2000. When do logs move in rivers? *Water resources research*, 36(2):571–583. → pages 11, 15

Braudrick, C. A. and Grant, G. E. 2001. Transport and deposition of large woody debris in streams: a flume experiment. *Geomorphology*, 41(4):263–283. → pages 6, 15

Braudrick, C. A., Grant, G. E., Ishikawa, Y., and Ikeda, H. 1997. Dynamics of wood transport in streams: a flume experiment. *Earth Surface Processes and Landforms*, 22(7):669–683. → pages 15

Brummer, C., Abbe, T., Sampson, J., and Montgomery, D. 2006. Influence of vertical channel change associated with wood accumulations on delineating channel migration zones, Washington, USA. *Geomorphology*, 80(3):295–309. → pages 2

Bruun, P. 1966. Model geology: prototype and laboratory streams. *Geological Society of America Bulletin*, 77(9):959–974. → pages 7

Buckingham, E. 1915. *Model experiments and the forms of empirical equations*. → pages 7

Buffington, J. M., Lisle, T. E., Woodsmith, R. D., and Hilton, S. 2002. Controls on the size and occurrence of pools in coarse-grained forest rivers. *River Research and Applications*, 18(6):507–531. → pages 3

Buffington, J. M. and Montgomery, D. R. 1999a. Effects of hydraulic roughness on surface textures of gravel-bed rivers. *Water Resources Research*, 35(11):3507–3521. → pages 2, 53, 54

Buffington, J. M. and Montgomery, D. R. 1999b. Effects of sediment supply on surface textures of gravel-bed rivers. *Water Resources Research*, 35(11):3523–3530. → pages 2, 54

Buffington, J. M., Montgomery, D. R., and Greenberg, H. M. 2004. Basin-scale availability of salmonid spawning gravel as influenced by channel type and hydraulic roughness in mountain catchments. *Canadian Journal of Fisheries and Aquatic Sciences*, 61(11):2085–2096. → pages 24

Chang, H. H. 1979. Minimum stream power and river channel patterns. *Journal of Hydrology*, 41(3):303–327. → pages 4, 5

Cherry, J. and Beschta, R. 1989. Coarse woody debris and channel morphology: A flume study. *JAWRA Journal of the American Water Resources Association*, 25(5):1031–1036. → pages 7, 56

Church, M., Hassan, M. A., and Wolcott, J. F. 1998. Stabilizing self-organized structures in gravel-bed stream channels: Field and experimental observations. *Water Resources Research*, 34(11):3169–3179. → pages 2, 4, 54

Clark, C. D. 1997. Reconstructing the evolutionary dynamics of former ice sheets using multi-temporal evidence, remote sensing and gis. *Quaternary Science Reviews*, 16(9):1067–1092. → pages 77

Clarke, R. 2007. Hydrological prediction in a non-stationary world. *Hydrology and Earth System Sciences*, 11(1):408–414. → pages 4

Davidson, S. 2011. Modeling channel morphodynamics associated with large wood in an intermediate-sized stream. Master's thesis, University of British Columbia. → pages 8, 9, 15, 18, 23, 25, 26, 36

Davidson, S. L. and Eaton, B. C. 2012. Modeling channel morphodynamic response to variations in large wood: Implications for stream rehabilitation in degraded watersheds. *Geomorphology*. → pages 2, 18, 23, 56

Davies, T. and Lee, A. 1988. Physical hydraulic modelling of width reduction and bed level change in braided rivers. *Journal of hydrology. New Zealand*, 27(2):113–127. → pages 7

Davies, T., McSaveney, M., and Clarkson, P. 2003. Anthropic aggradation of the Waiho River, Westland, New Zealand: microscale modelling. *Earth Surface Processes and Landforms*, 28(2):209–218. → pages 14

Davies, T. R. and Sutherland, A. J. 1983. Extremal hypotheses for river behavior. *Water Resources Research*, 19(1):141–148. → pages 4, 5

Déry, S. J., Stahl, K., Moore, R., Whitfield, P., Menounos, B., and Burford, J. E. 2009. Detection of runoff timing changes in pluvial, nival, and glacial rivers of western Canada. *Water Resources Research*, 45(4). → pages 1

Devereux, B., Amable, G., and Crow, P. 2008. Visualisation of LiDAR terrain models for archaeological feature detection. *Antiquity*, 82(316):470–479. → pages 80, 81

Dey, S. and Raikar, R. V. 2007. Clear-water scour at piers in sand beds with an armor layer of gravels. *Journal of Hydraulic Engineering*, 133(6):703–711. → pages 7

Dietrich, W. E., Kirchner, J. W., Ikeda, H., and Iseya, F. 1989. Sediment supply and the development of the coarse surface layer in gravel-bedded rivers. *Nature*, 340(6230):215–217. → pages 54, 59

Dunne, T. and Leopold, L. B. 1978. *Water in environmental planning*. W.H. Freeman and Company, New York. → pages 1

Eaton, B. 2008. Potential Channel Changes Following Wildfire: Applying the UBC Regime Model to Fishtrap Creek, British Columbia. *Streamline Water Management Bulletin*, 12(1):28–33. → pages 16

Eaton, B., Andrews, C., Giles, T., and Phillips, J. 2010a. Wildfire, morphologic change and bed material transport at Fishtrap Creek, British Columbia. *Geomorphology*, 118(3):409–424. → pages 15, 16, 19, 23, 24, 25, 56

Eaton, B. and Church, M. 2004. A graded stream response relation for bed load–dominated streams. *Journal of geophysical research*, 109(F3):F03011. → pages 1, 2, 4, 7, 8, 9, 13, 54, 56

Eaton, B. and Church, M. 2009. Channel stability in bed load-dominated streams with non-erodible banks: Inferences from experiments in a sinous flume. *Journal of Geophysical Research*, 114:F01024, doi:10.1029/2007JF000902. → pages 8, 9, 13, 53, 57, 59, 62, 63

Eaton, B., Giles, T., Heise, B., Moore, R. D., Owens, P., and Petticrew, E. 2010b. Fishtrap Creek watershed project. *Streamline Water Management Bulletin*, 14:12–13. → pages 18

Eaton, B., Moore, R., and Giles, T. 2010c. Forest Fire, bank strength, and channel instability: The ”unusual” response of Fishtrap Creek, British Columbia. *Earth Surface Processes and Landforms*, 35(10):1167–1183. → pages 16, 56

Eaton, B. C., Church, M., and Millar, R. G. 2004. Rational regime model of alluvial channel morphology and response. *Earth Surface Processes and Landforms*, 29(4):511–529. → pages 4, 5, 7

Eaton, B. C. and Giles, T. R. 2009. Assessing the effect of vegetation-related bank strength on channel morphology and stability in gravel-bed streams using numerical models. *Earth Surface Processes and Landforms*, 34(5):712–724. → pages 2, 16

Eaton, B. C. and Millar, R. G. 2004. Optimal alluvial channel width under a bank stability constraint. *Geomorphology*, 62(1):35–45. → pages 2

Gaines, R. and Maynord, S. 2001. Microscale loose-bed hydraulic models. *Journal of Hydraulic Engineering*, 127(5):335–338. → pages 13

Gantenbein, C. 2012. Creating shaded relief for geologic mapping using multiple light sources. In *Digital Mapping Techniques ’10 - Workshop Proceedings*. → pages 78, 79

Garcia, M. 1993. Hydraulic jumps in sediment-driven bottom currents. *Journal of Hydraulic Engineering*, 119(10):1094–1117. → pages 13

Gilbert, G. K. and Murphy, E. C. 1914. *The transportation of debris by running water*, volume 86. US Government Printing Office. → pages 7

Gill, M. A. 1972. Erosion of sand beds around spur dikes. *Journal of the Hydraulics Division*, 98(hy9). → pages 58

Glenn, N. F., Streutker, D. R., Chadwick, D. J., Thackray, G. D., and Dorsch, S. J. 2006. Analysis of LiDAR-derived topographic information for characterizing and differentiating landslide morphology and activity. *Geomorphology*, 73(1):131–148. → pages 77

Gomez, B. 1983. Temporal variations in the particle size distribution of surficial bed material: The effect of progressive bed armouring. *Geografiska annaler. Series A. Physical geography*, 65(3-4):183–192. → pages 59

Gomi, T., Sidle, R. C., Bryant, M. D., and Woodsmith, R. D. 2001. The characteristics of woody debris and sediment distribution in headwater streams, southeastern Alaska. *Canadian Journal of Forest Research*, 31(8):1386–1399. → pages 2

Hassan, M. A., Hogan, D. L., Bird, S. A., May, C. L., Gomi, T., and Campbell, D. 2005. Spatial and Temporal Dynamics of Wood in Headwater Streams of the Pacific Northwest. *JAWRA Journal of the American Water Resources Association*, 41(4):899–919. → pages 2

Haugerud, R. A., Harding, D. J., Johnson, S. Y., Harless, J. L., Weaver, C. S., and Sherrod, B. L. 2003. High-resolution lidar topography of the Puget Lowland, Washington. *GSA Today*, 13(6):4–10. → pages 77

Hebertson, J. G. 1969. Scaling procedures for mobile bed hydraulic models in terms of similitude theory. *Journal of Hydraulic Research*, 7(3):315–353. → pages 7

Hobbs, F. 1995. The rendering of relief images from digital contour data. *Cartographic Journal, The*, 32(2):111–116. → pages 79, 80

Hobbs, K. F. 1999. An investigation of RGB multi-band shading for relief visualisation. *International Journal of applied earth observation and geoinformation*, 1(3):181–186. → pages 79, 80

Hooke, R. 1968. Model geology: prototype and laboratory streams: discussion. *Geological Society of America Bulletin*, 79(3):391–394. → pages 6, 7, 14

Howard, A. 1988. Equilibrium models in geomorphology. *Modelling Geomorphological Systems*, pages 49–72. → pages 3, 54

Howard, A. D. 1982. Equilibrium and time scales in geomorphology: Application to sand-bed alluvial streams. *Earth Surface Processes and Landforms*, 7(4):303–325. → pages 3, 62, 63

Jencso, K. G., McGlynn, B. L., Gooseff, M. N., Wondzell, S. M., Bencala, K. E., and Marshall, L. A. 2009. Hydrologic connectivity between landscapes and streams: Transferring reach-and plot-scale understanding to the catchment scale. *Water Resources Research*, 45(4). → pages 1

Jenny, B. and Hurni, L. 2006. Swiss-style colour relief shading modulated by elevationand by exposure to illumination. *Cartographic Journal, The*, 43(3):198–207. → pages 80

Jones, A. F., Brewer, P. A., Johnstone, E., and Macklin, M. G. 2007. High-resolution interpretative geomorphological mapping of river valley environments using airborne LiDAR data. *Earth Surface Processes and Landforms*, 32(10):1574–1592. → pages 77

Kassem, A. and Chaudhry, M. H. 2005. Effect of bed armoring on bed topography of channel bends. *Journal of hydraulic engineering*, 131(12):1136–1140. → pages 59

Keller, E. and Swanson, F. 1979. Effects of large organic material on channel form and fluvial processes. *Earth surface processes*, 4(4):361–380. → pages 56, 57

Keller, E. A., Valentine, D. W., and Gibbs, D. R. 1997. Hydrological response of small watersheds following the Southern California Painted Cave Fire of June 1990. *Hydrological Processes*, 11(4):401–414. → pages 16

Kennelly, P. J. 2008. Terrain maps displaying hill-shading with curvature. *Geomorphology*, 102(3):567–577. → pages 77, 80

Kennelly, P. J. and Kimerling, A. J. 2004. Hillshading of terrain using layer tints with aspect-variant luminosity. *Cartography and Geographic Information Science*, 31(2):67–77. → pages 80

Kirkby, M. 1977. *Maximum sediment efficiency as a criterion for alluvial channels*. University of Leeds, School of Geography. → pages 4, 5

Koss, J., Ethridge, F., and Schumm, S. 1994. An experimental study of the effects of base-level change on fluvial, coastal plain and shelf systems. *Journal of Sedimentary Research*, 64(2). → pages 14

Kuhnle, R. A., Alonso, C. V., and Shields Jr, F. D. 2002. Local scour associated with angled spur dikes. *Journal of Hydraulic Engineering*, 128(12):1087–1093. → pages 7, 55

Lajeunesse, E., Malverti, L., Lancien, P., Armstrong, L., Métivier, F., Coleman, S., Smith, C., Davies, T., Cantelli, A., and Parker, G. 2009. Fluvial and submarine morphodynamics of laminar and near-laminar flows: A synthesis. *Sedimentology*, 57(1):1–26. → pages 14

Lancaster, S. T., Hayes, S. K., and Grant, G. E. 2001. Modeling sediment and wood storage and dynamics in small mountainous watersheds. *Water Science and Application*, 4:85–102. → pages 3

Lane, E. W. 1955. Design of stable channels. *Transactions of the American Society of Civil Engineers*, 120(1):1234–1260. → pages 3

Lane, E. W. 1957. *A study of the shape of channels formed by natural streams flowing in erodible material*. US Army Engineer Division, Missouri River. → pages 1

Lasaponara, R. and Masini, N. 2011. On the processing of aerial LiDAR data for supporting enhancement, interpretation and mapping of archaeological features. In *Computational Science and Its Applications-ICCSA 2011*, pages 392–406. Springer. → pages 80, 81

Leach, J. and Moore, R. 2010. Above-stream microclimate and stream surface energy exchanges in a wildfire-disturbed riparian zone. *Hydrological Processes*, 24(17):2369–2381. → pages 16

Lidmar-Bergström, K., Elvhage, C., and Ringberg, B. 1991. Landforms in Skåne, South Sweden. *Geografiska Annaler. Series A. Physical Geography*, pages 61–91. → pages 77, 79

Lisle, T. 1987. Using" residual depths" to monitor pool depths independently of discharge. → pages 34

Lisle, T. E. 1986. Stabilization of a gravel channel by large streamside obstructions and bedrock bends, Jacoby Creek, northwestern California. *Geological Society of America Bulletin*, 97(8):999–1011. → pages 3

Lisle, T. E., Iseya, F., and Ikeda, H. 1993. Response of a channel with alternate bars to a decrease in supply of mixed-size bed load: A flume experiment. *Water Resources Research*, 29(11):3623–3629. → pages 54

Loisios, D., Tzelepis, N., and Nakos, B. 2007. A methodology for creating analytical hill-shading by combining different lighting directions. In *Proceedings of 23rd International Cartographic Conference, Moscow*. → pages 78, 79, 80, 88

Lukas, K. and Weibel, R. 1995. Assessment and improvement of methods for analytical hillshading. In *Proc. 17 th Internat. Cartogr. Conf., Barcelona*, volume 2, pages 2231–2240. → pages 78, 79, 80

Mackin, J. H. 1948. Concept of the graded river. *Geological Society of America Bulletin*, 59(5):463–512. → pages 1

Madej, M., Sutherland, D., Lisle, T., and Pryor, B. 2009. Channel responses to varying sediment input: A flume experiment modeled after Redwood Creek, California. *Geomorphology*, 103(4):507–519. → pages 7, 8, 12, 13, 14

Malverti, L., Lajeunesse, E., and Métivier, F. 2008. Small is beautiful: upscaling from microscale laminar to natural turbulent rivers. *Journal of Geophysical Research*, 113(F4):F04004. → pages 12, 13, 14, 64

Manga, M. and Kirchner, J. W. 2000. Stress partitioning in streams by large woody debris. *Water Resources Research*, 36(8):2373–2379. → pages 2, 58

Mark, R. K. 1992. *A multidirectional, oblique-weighted, shaded-relief image of the island of Hawaii*. US Department of the Interior, US Geological Survey. → pages 79, 80, 81, 84, 88

May, C. L. and Gresswell, R. E. 2003. Processes and rates of sediment and wood accumulation in headwater streams of the Oregon Coast Range, USA. *Earth Surface Processes and Landforms*, 28(4):409–424. → pages 2, 57

Megahan, W. F. 1982. Channel sediment storage behind obstructions in forested drainage basins draining the granitic bedrock of the Idaho batholith. *Sediment budgets and routing in forested drainage basins*, pages 114–121. → pages 2, 58

Millar, R. G. 2005. Theoretical regime equations for mobile gravel-bed rivers with stable banks. *Geomorphology*, 64(3):207–220. → pages 2, 3, 5

Millar, R. G. and Quick, M. C. 1993. Effect of bank stability on geometry of gravel rivers. *Journal of Hydraulic Engineering*, 119(12):1343–1363. → pages 1, 4, 5

Montgomery, D., Buffington, J., Smith, R., Schmidt, K., and Pess, G. 1995. Pool spacing in forest channels. *Water Resources Research*, 31(4):1097–1105. → pages 34, 49, 50

Montgomery, D., Collins, B., Buffington, J., and T.B., A. 2003. Geomorphic effects of wood in rivers. In *American Fisheries Society Symposium*. American Fisheries Society. → pages 3

Montgomery, D. R. and Buffington, J. M. 1997. Channel-reach morphology in mountain drainage basins. *Geological Society of America Bulletin*, 109(5):596–611. → pages 2, 56, 62, 63

Montgomery, D. R. and Buffington, J. M. 1998. Channel processes, classification, and response. *River ecology and management*, 112:1250–1263. → pages 1, 3, 64

Notebaert, B., Verstraeten, G., Govers, G., and Poesen, J. 2009. Qualitative and quantitative applications of LiDAR imagery in fluvial geomorphology. *Earth Surface Processes and Landforms*, 34(2):217–231. → pages 77, 79

Onorati, G., Ventura, R., Poscolieri, M., Chiarini, V., and Crucilla, U. 1992. The digital elevation model of italy for geomorphology and structural geology. *Catena*, 19(2):147–178. → pages 79

Pagliara, S. and Carnacina, I. 2010. Temporal scour evolution at bridge piers: Effect of wood debris roughness and porosity. *Journal of Hydraulic Research*, 48(1):3–13. → pages 7

Parker, G. and Klingeman, P. C. 1982. On why gravel bed streams are paved. *Water Resources Research*, 18(5):1409–1423. → pages 54, 59, 63

Pawley, S. and Atkinson, N. 2010. Application of airbourne LiDAR imagery for surficial geology mapping in densely vegetated (Boreal Zone) terrain, Lesser Slave Lake, Northern Alberta. Poster. → pages 80, 81

Peakall, J., Ashworth, P., and Best, J. 1996. Physical modelling in fluvial geomorphology: principles, applications and unresolved issues. *The Scientific Nature of Geomorphology*, pages 221–253. → pages 11, 14

Petticrew, E. L., Owens, P. N., and Giles, T. R. 2006. Wildfire effects on the quantity and composition of suspended and gravel-stored sediments. In *The Interactions Between Sediments and Water*, pages 283–292. Springer. → pages 16

Phillips, J. 2007. Post-Fire Dynamics of a Gravel Bed Stream: Fishtrap Creek, British Columbia. Master's thesis, University of British Columbia. → pages 16

Podobnikar, T. 2012. Multidirectional visibility index for analytical shading enhancement. *Cartographic Journal, The*, 49(3):195–207. → pages 80

Pohl, C. and Van Genderen, J. 1998. Review article multisensor image fusion in remote sensing: concepts, methods and applications. *International journal of remote sensing*, 19(5):823–854. → pages 80

Pollen, N. and Simon, A. 2006. Geotechnical implications for the use of alfalfa in experimental studies of alluvial-channel morphology and planform. In *AGU Fall Meeting Abstracts*, volume 1, page 1455. → pages 13

Postma, G., Kleinhans, M., Meijer, P., and Eggenhuisen, J. 2008. Sediment transport in analogue flume models compared with real-world sedimentary systems: A new look at scaling evolution of sedimentary systems in a flume. *Sedimentology*, 55(6):1541–1557. → pages 7, 14

Raudkivi, A. J. and Ettema, R. 1985. Scour at cylindrical bridge piers in armored beds. *Journal of Hydraulic Engineering*, 111(4):713–731. → pages 55

Renwick, W. H. 1992. Equilibrium, disequilibrium, and nonequilibrium landforms in the landscape. *Geomorphology*, 5(3):265–276. → pages 3

Ryder, J. M., Fulton, R. J., and Clague, J. J. 1991. The Cordilleran Ice Sheet and the glacial geomorphology of southern and central British Colombia. *Géographie physique et Quaternaire*, 45(3):365–377. → pages 15

Sandford, R. W. 2012. *Cold matters: the state and fate of Canada's fresh water*. Rocky Mountain Books Ltd. → pages 4

Schowengerdt, R. A. 2006. *Remote sensing: models and methods for image processing*. Academic press. → pages 80

Schumm, S. and Khan, H. 1972. Experimental study of channel patterns. *Geological Society of America Bulletin*, 83(6):1755–1770. → pages 7, 12, 13

Schumm, S. A., Mosley, M. P., and Weaver, W. 1987. Experimental fluvial geomorphology. → pages 7

Shook, K. and Pomeroy, J. 2012. Changes in the hydrological character of rainfall on the Canadian prairies. *Hydrological Processes*, 26(12):1752–1766. → pages 4

Smith, M. J. and Clark, C. D. 2005. Methods for the visualization of digital elevation models for landform mapping. *Earth Surface Processes and Landforms*, 30(7):885–900. → pages 78, 79, 80

Smith, M. J. and Wise, S. M. 2007. Problems of bias in mapping linear landforms from satellite imagery. *International Journal of Applied Earth Observation and Geoinformation*, 9(1):65–78. → pages 78

Stromberg, J., Briggs, M., Gourley, C., Scott, M., Shafroth, P., Stevens, L., Baker Jr, M., Ffolliott, P., DeBano, L., and Neary, D. 2004. Human alterations of riparian ecosystems. *Riparian Areas of the Southwestern United States: Hydrology, Ecology, and Management*, pages 101–126. → pages 4

Štular, B., Kokalj, Ž., Oštir, K., and Nuninger, L. 2012. Visualization of LiDAR-derived relief models for detection of archaeological features. *Journal of Archaeological Science*, 39(11):3354–3360. → pages 80

Tal, M., Gran, K., Murray, A. B., Paola, C., and Hicks, D. M. 2004. Riparian vegetation as a primary control on channel characteristics in multi-thread rivers. *Riparian vegetation and fluvial geomorphology*, pages 43–58. → pages 13

Tal, M. and Paola, C. 2007. Dynamic single-thread channels maintained by the interaction of flow and vegetation. *Geology*, 35(4):347–350. → pages 13

Tecle, A., Bojonell, H. A., and King, J. G. 2001. Modeling sediment storage behind obstructions in small headwater streams. *Journal of the Arizona-Nevada Academy of Science*, pages 83–92. → pages 2

Termini, D. 2009. Experimental observations of flow and bed processes in large-amplitude meandering flume. *Journal of Hydraulic Engineering*, 135(7):575–587. → pages 7

Thompson, D. 1995. The effects of large organic debris on sediment processes and stream morphology in Vermont. *Geomorphology*, 11(3):235–244. → pages 2, 3

Van Heijst, M. and Postma, G. 2002. Fluvial response to sea-level changes: a quantitative analogue, experimental approach. *Basin Research*, 13(3):269–292. → pages 14

Van Heijst, M., Postma, G., Meijer, X., Snow, J., and Anderson, J. 2002. Quantitative analogue flume-model study of river–shelf systems: principles and verification exemplified by the Late Quaternary Colorado river–delta evolution. *Basin Research*, 13(3):243–268. → pages 14

Wallerstein, N. P., Alonso, C. V., Bennett, S. J., and Thorne, C. R. 2001. Distorted Froude-scaled flume analysis of large woody debris. *Earth Surface Processes and Landforms*, 26(12):1265–1283. → pages 6, 12, 13, 15, 56, 64

Webb, A. A. and Erskine, W. D. 2003. Distribution, recruitment, and geomorphic significance of large woody debris in an alluvial forest stream: Tonghi Creek, southeastern Australia. *Geomorphology*, 51(1):109–126. → pages 2, 57

White, W.R., B. R. and Paris, E. 1982. An analytical approach to river regime. *Journal of the Hydraulics Division*, 108(10):1179–1193. → pages 5

Whiting, P. and Dietrich, W. 1993. Experimental studies of bed topography and flow patterns in large-amplitude meanders: 1. observations. *Water Resources Research*, 29(11):3605–3614. → pages 7, 12, 13, 34

Wilcox, A. C., Nelson, J. M., and Wohl, E. E. 2006. Flow resistance dynamics in step-pool channels: 2. partitioning between grain, spill, and woody debris resistance. *Water Resources Research*, 42(5). → pages 2, 4

Wilcox, A. C. and Wohl, E. E. 2006. Flow resistance dynamics in step-pool stream channels: 1. large woody debris and controls on total resistance. *Water Resources Research*, 42(5). → pages 58

Wohl, E. 2011. Threshold-induced complex behavior of wood in mountain streams. *Geology*, 39(6):587–590. → pages 3

Wolman, M. G. and Miller, J. P. 1960. Magnitude and frequency of forces in geomorphic processes. *The Journal of Geology*, pages 54–74. → pages 1

Wondzell, S. M. and King, J. G. 2003. Postfire erosional processes in the Pacific Northwest and Rocky Mountain regions. *Forest Ecology and Management*, 178(1):75–87. → pages 56

Yalin, M. S. 1971. *Theory of hydraulic models*, volume 266. Macmillan London. → pages 11

Young, W. and Davies, T. 1991. Bedload transport processes in a braided gravel-bed river model. *Earth Surface Processes and Landforms*, 16(6):499–511. → pages 7

Zelt, R. B. and Wohl, E. E. 2004. Channel and woody debris characteristics in adjacent burned and unburned watersheds a decade after wildfire, Park County, Wyoming. *Geomorphology*, 57(3):217–233. → pages 56

Zimmermann, A. E. 2009. *Experimental investigations of step-pool channel formation and stability*. PhD thesis, University of British Columbia. → pages 25

Appendix A

LiDAR Visualization

A.1 LiDAR: Remotely Sensed Data

LiDAR (Light Detection And Ranging) is a type of remote sensing technology that measures the distance between the source of a light beam and a remote target surface in order to create a digital elevation model (DEM) where the value of each cell in the resulting raster image represents the elevation of the terrain at that point. Airborne LiDAR data, collected using a downward-looking LiDAR system mounted on a plane, is of great importance to terrain mapping and other geomorphological endeavors due to its high spatial resolution and the ability to filter out vegetation during the processing of the data in order to create a "bare earth" model of a land surface.

Many types of geomorphic maps have been created using LiDAR-derived DEM. In glacial applications, DEMs are commonly used to delineate drumlins, eskers, spillways, and other glacial features (e.g. Lidmar-Bergström et al., 1991; Haugerud et al., 2003) whose orientations and that can be used to reconstruct the dynamics of former ice sheets (Clark, 1997). In fluvial applications, DEMs have been used to conduct watershed assessments and determine flood risk (e.g. Jones et al., 2007; Notebaert et al., 2009). LiDAR data has also proven useful for locating mass-wasting events in order to monitor landslide activity (e.g. Glenn et al., 2006).

Because digital elevation models represent the distributions of elevations for a location they can be used to derive other types of data about the landscape (Kennelly, 2008). Slope gradient (the rate of change in elevation) and slope aspect (the compass direction of the steepest slope) are first order derivatives of a DEMs while profile and planimetric curvature (measured across and along the direction of maximum slope) represent second order derivatives. While elevation and first and second order derivatives may be visualized as rasters, these "unbiased" representations of the landscape are often unintuitive to interpret. In order to get a real sense of the landscape it is

often necessary to employ other visualization techniques.

Originally developed as a complex hand-shading process, hill-shading, or analytical shading (when referring specifically to the computational procedure), is a process in which a diffuse reflection illumination model is applied to a digital elevation (or terrain) model to create a raster image. Compared to a DEM and its first and second order derivatives, these ”illuminated,” hill-shaded landscapes more closely resemble what a land surface looks like when lit by the sun. This method is also easy to apply as most GIS programs have a hill-shading function that allows the user to easily create one from an inputted DEM.

Issues arise when a single hill-shaded image (i.e. created from one illumination source) is used in terrain interpretation (Lukas and Weibel, 1995; Loisios et al., 2007; Smith and Wise, 2007). Landforms, especially high ridges, running perpendicular to the direction of illumination experience overexposure of light on one side and improper or lack of lighting on the other. Linear features, such as drumlins, ridges, and stream channels, that run parallel to the light source, blend into to the background as a result of both sides being illuminated equally (Lukas and Weibel, 1995). Additionally, if the light source is projected from a southern or easterly direction, relief inversion may occur in which the viewer perceives that concave landforms (e.g. stream channel) protrude from the landscape and convex landforms (e.g. ridges) appear incised (Lukas and Weibel, 1995; Gantenbein, 2012).

A.1.1 Research Objectives

The illumination bias of single hill-shaded images has been accounted for through various visualization methods (see Smith and Clark, 2005 for a review). Because these different methods range in complexity and their portrayal of the landscape, their applicability depends on the goal of the study for which they are employed. The first half of this paper will discuss the technique of hill-shading and will address issues and methods pertaining to it.

Given that many field-based geomorphic studies now employ DEMs as a tool from which to plan field sites or to get a sense of the landscape prior to field work, it is necessary to maximize the clarity of the DEM visualization without requiring that the user have a large understanding of different visualization methods or take too much time processing the data. The second half of the paper will apply several visualization methods to a dataset in order to determine a simple yet effective method of visualizing a LiDAR-derived DEM for use in glacial and fluvial geomorphological studies. Methods considered in this paper must be relatively quick and easy to do and must not require extensive knowledge of GIS.

A.2 LiDAR Visualization Methods

When creating a hill-shaded image it is necessary to define an azimuth, the altitude and any vertical exaggeration (aka. the z factor). Hill-shaded tools in most GIS applications have default values for each of these variables. The defaults mentioned below pertain to those found in ArcGIS™.

Azimuth is the compass direction, in degrees (i.e. between 0° and 360°), of the light source. The default azimuth is 315°, which represents a light source shining from the north-west. This default azimuth creates a visually appealing landscape (Gantenbein, 2012) but biases against landforms parallel to that direction, as will be shown later. Because of this, knowing something about the direction of linear features within the landscape prior to choosing the azimuth is valuable when producing a single hill-shaded image.

The altitude is the angle of the light source up from the horizon (i.e. between 0° and 90°). If a high altitude is chosen, the terrain will appear "washed out" while the selection of a low altitude will cause more of the landscape to be shadowed. The default altitude is 45°, which is high enough to minimize shadows, but low enough that the surface does not appear expressionless.

Although the default choice is for there to be no vertical exaggeration, choosing a value greater than one may help to accentuate low lying terrain features. However, like with a low altitude, this must be balanced out against the shadowing of terrain due to the increased relief.

Hill-shaded images may be combined either through raster addition or by layering the two and changing the opacity of the overlying images to create a composite image that exhibits less bias than a single hill-shaded image alone. A simple and commonly employed method is to combine two orthogonally oriented hill-shaded images in order to enhance the visibility of linear features (e.g. Lidmar-Bergström et al., 1991; Onorati et al., 1992; Lukas and Weibel, 1995; Notebaert et al., 2009). In theory, the two illumination sources should be parallel and perpendicular to the general trend of linear features within the landscape, however this is not always possible due to either a lack of prior knowledge of the terrain (e.g. Lidmar-Bergström et al., 1991) or the presence of several directional trends within the landscape (e.g. Smith and Clark, 2005).

In order to diminish the necessity of defining a single linear trend within the terrain, other studies have proposed combining three (Hobbs, 1995; Lukas and Weibel, 1995; Hobbs, 1999; Gantenbein, 2012) or four (Mark, 1992; Loisios et al., 2007) hill-shaded images. In these situations the width and direction of the illumination sector (the range and values of the azimuths), the altitude, and the vertical exaggeration is often predefined within these methods in order to minimize the subjectivity in creating the hill-shaded images.

In methods that utilize raster addition, it is necessary to defined the relative weight that each of the input images go into creating the final raster. Some methods predefine the relative weights

of input raster (Lukas and Weibel, 1995) while others weight them depending on distribution of aspect values within a landscape (Mark, 1992; Loisios et al., 2007). In a study building on a method originally proposed by Mark (1992) in which aspect is used to determine weighting, Loisios et al. (2007) highlight the differences between assigning a single global weight to each image added together versus determining the weights of the hill-shaded images on a cell-by-cell basis. While cell-by-cell weighting resulted in a slightly more detailed image, the procedure does require a more rigorous knowledge of GIS programming.

The single largest problem that arises during the addition of hill-shaded images is the creation of a single image with an overall lower contrast than all of the input rasters (Lukas and Weibel, 1995; Devereux et al., 2008; Štular et al., 2012). This is due to the fact many terrain features are replicated in several, if not all of the images, so when they are added to each other the light areas on one image will effectively cancel out the darker areas of a one, resulting in an expressionless image. This is problem can be mediated by weighting each of the rasters independently rather than weighing them all equally as well as making sure the illumination directions of inputted images are never directly opposite of each other (i.e. 315° and 135°).

Hill-shaded images have been visualized in other ways. Colour and shading techniques, such as swiss-style shading (Jenny and Hurni, 2006), aspect variant luminosity (Kennelly and Kimerling, 2004), multidirectional visibility index (Podobnikar, 2012), and RGB layering (Hobbs, 1995, 1999), are often used to emphasize the range of aspects present in a landscape. Hill-shaded images may also be combined with other raster representations of the landscape. Because hill-shading does not indicate terrain elevation, adding a coloured DEM behind a hill-shaded image can help to clarify the elevation trends for the viewer (Kennelly and Kimerling, 2004). Other studies suggest layering hill-shaded images with first or second order derivative maps such as slope or curvature to aid in reducing the illumination bias (Smith and Clark, 2005; Kennelly, 2008). Unfortunately, layering these derivative maps, like adding in many hill-shaded images, tends to reduce the contrast of the resulting image.

One method, namely Principal Component Analysis (PCA), has surfaced that has proven useful in reducing data redundancy and other problems associated with adding several hill-shaded images together (Smith and Clark, 2005; Devereux et al., 2008; Pawley and Atkinson, 2010; Lasaponara and Masini, 2011; Bennett et al., 2012). PCA works by taking a set of inter-correlated variables and transforming them into a new set of uncorrelated variables, or components (Devereux et al., 2008). A more thorough explanation of the principles and methods behind PCA can be found in other sources such as Pohl and Van Genderen (1998) or Schowengerdt (2006). For the purposes of this paper it suffices to understand that, in this context, a PCA takes the variability present in all of the inputted hill-shades and creates a set of components, or images, where the

major portion of the variance of the inputs is represented by the first three components (Devereux et al., 2008). Essentially, the first component represents the areas that are highlighted in all of the inputted hill-shades, the second component shows areas present in all but one of the hill-shades, and so on.

Because most GIS software programs have a PCA function, this procedure is relatively simple. There are, however, certain considerations that must be taken into account when conducting a PCA on a dataset. First of all, the number of hill-shaded images that must be inputted has not been well defined. Although Devereux et al. (2008) report using 16 hill-shaded images with azimuths equally spaced between 0° and 360°, it remains unclear as to whether increasing the number of inputted images affects the results of the PCA. Secondly, like when creating hill-shades for use in a weighted raster addition, the range of illumination sector must be considered, for example, whether it is constrained to a single section (i.e. Mark, 1992) or if hill-shades from all directions should be considered.

When visualizing the resulting PCA components most studies tend to present each of the components separately (e.g. Pawley and Atkinson, 2010; Lasaponara and Masini, 2011; Bennett et al., 2012; see Figure A.1b-e) The first three components may also be viewed as single, false coloured composite image, although this creates an image that is overwhelming to analyze (Devereux et al., 2008; see Figure A.1a). Despite the many advantages that PCA has over raster addition, little effort has been put into examining the range of visualization possibilities that exist for the data.

A.3 Proposed Method of Visualization

The following section describes the steps taken and variables considered to create the visualization of the study area that fulfills the main goal of this study: to be able to easily discern and interpret a range of fluvial and glacial landforms from a LiDAR-derived DEM using a simple and quick method of visualization (Figure A.2). The method described below, which uses a combination of hill-shading and PCA techniques, was deemed to present the clearest representation of the terrain for almost all landforms present in the study area. Although, this study was conducted using ArcGIS™, most GIS software programs have similar tools that can be used to replicate these results, although certain settings may differ slightly.

The first step is to create the hill-shaded images to be used in the PCA. Although Devereux et al. (2008) use 16 hill-shaded images as input to their PCA, this study found no discernible difference between using 16 and 4 images as input to the analysis. When experimenting with the illumination sector of the input hill-shades it was found that using hill-shaded images with azimuths that represent all of the main compass directions (i.e. North, South, East, and West) have

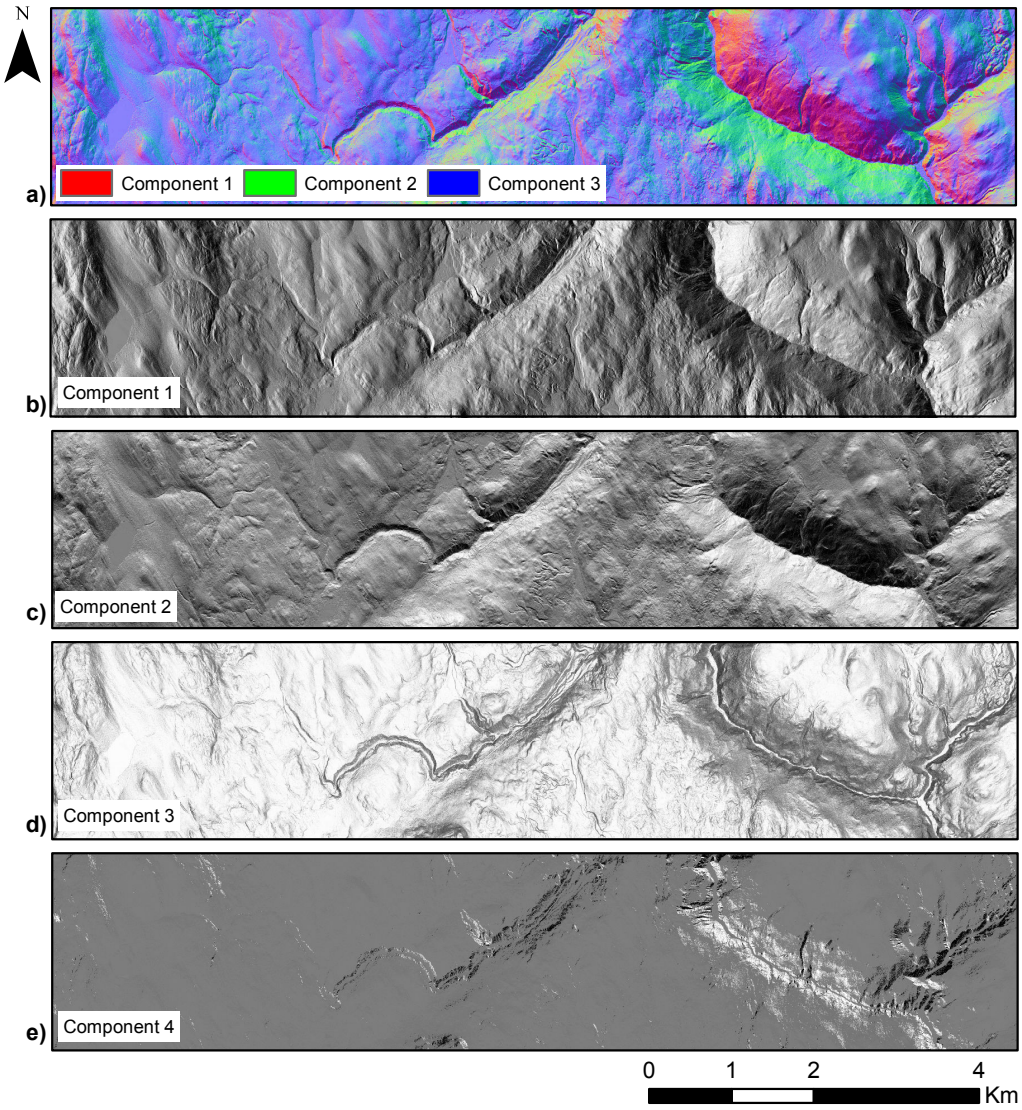

Figure A.1: Components of a PCA

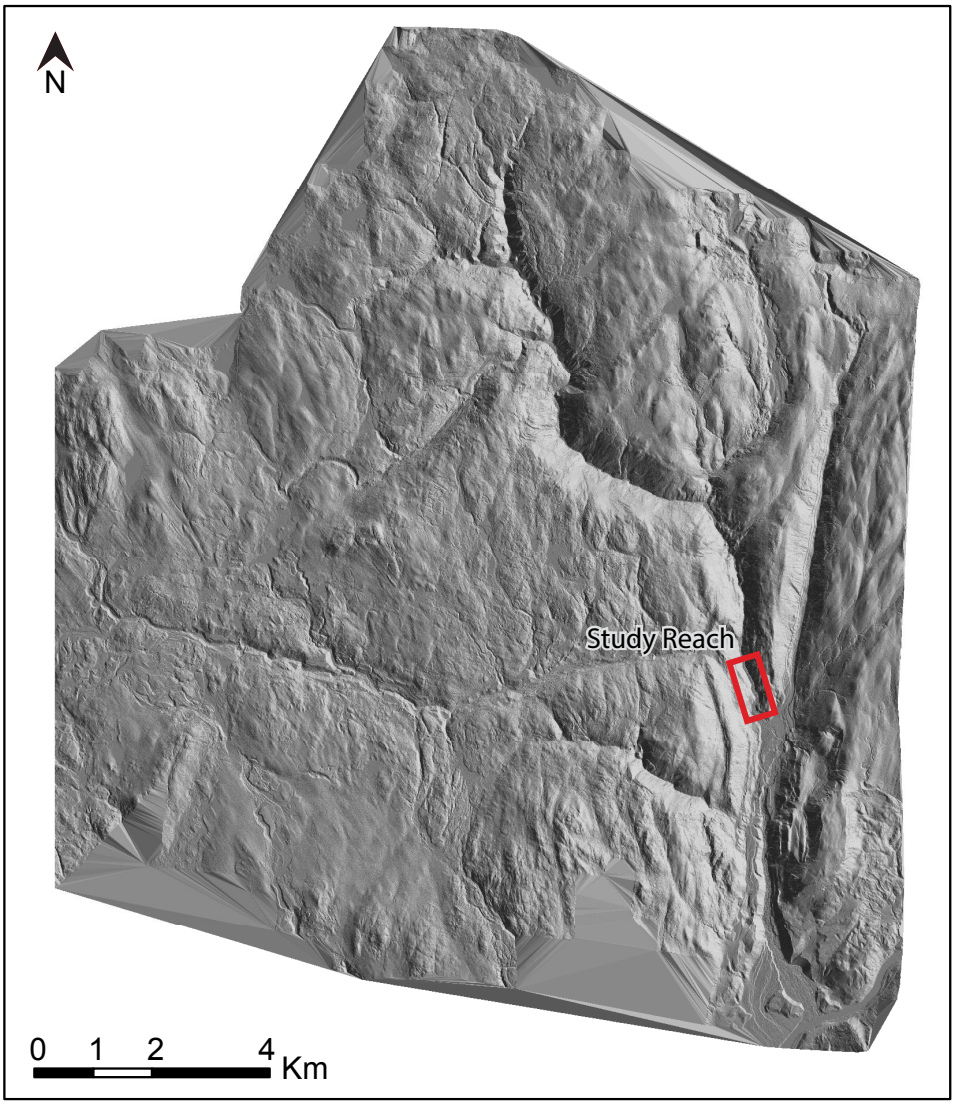

Figure A.2: Visualization of LiDAR-derived DEM of the study area using the method presented in this study.

Table A.1: Percent of variability present in the landscape represented by each of the components of the PCA.

Component	Variation
1	48.5%
2	36.8%
3	14.3%
4	0.3%

better results than if the azimuths of the input images only represent a illumination from a limited spectrum (i.e. the directions used by Mark, 1992). This is evidenced by the fact that when a PCA is conducted on images with azimuths restricted to the north and north-west the resulting PCA components under-represent south-east facing slopes. This study therefore proposes using four hill-shades created with the following azimuths: 360°, 270°, 180°, and 90°.

Choosing the proper altitude and vertical exaggeration for the hill-shades requires finding the right medium between a washed out landscape (i.e. high altitude/low vertical exaggeration) and one in which there are too many dark shadows (i.e. low altitude/high vertical exaggeration). After testing several different values for the two, it was found that an altitude of 45° and a vertical exaggeration of two allows low-lying features to be discerned without casting large areas of the landscape into shadow.

Once the four hill-shaded images are created, the next step is to conduct a PCA using them as input rasters. The PCA conducted on the hill-shaded images of the study area resulted in a set of components in which the first three account for over 99% of the variation of the landscape (see Table A.1).

The next and most important step in the process is the visualization of the PCA components. Several methods of visualization were experimented with (see Figure A.3) in order to determine which one gives the overall best representation of the study area. The largest problem that arises in visualizing PCA components is finding the right degree of contrast such that there are no areas that are over or under exposed but there is still enough contrast to discern as many landforms as possible. When the first three components are added together using equal weights (Figure A.3a), the resulting image is slightly over-exposed in flat areas which causes small scale features and textures in these areas to become indiscernible. The opposite is true (i.e. east facing slopes are quite under-exposed and lack fine detail) for the case when the PCA components, weighted according to the percent of variance that they represent, are added together (Figure A.3b) as well as when only the first component is visualized (Figure A.3c).

Layering of PCA components was experimented with in order to find the medium between the

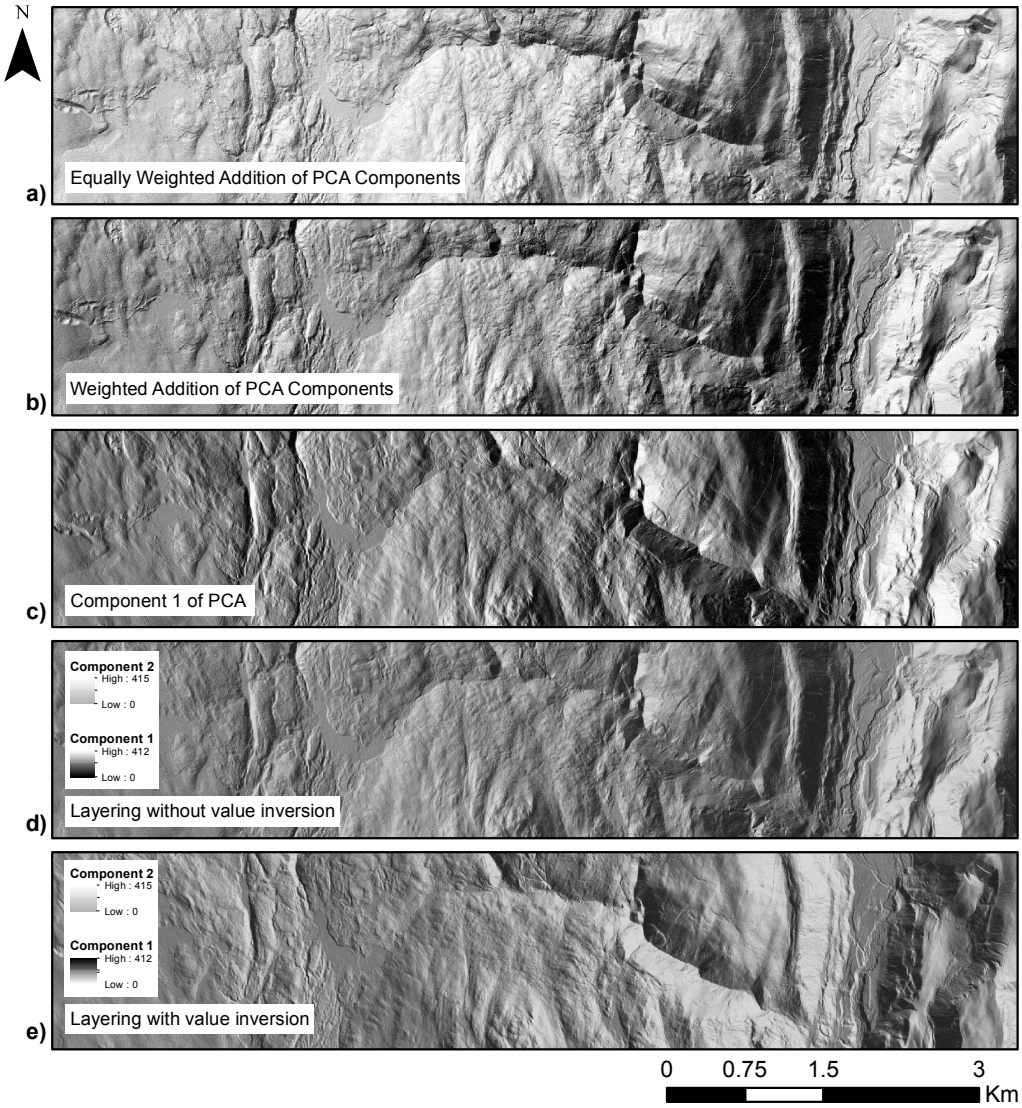

Figure A.3: Several methods of visualizing the PCA results examined for this study. The image shown in e) is the method that is found to best represent the study area.

contrast issues innate in PCA component addition and the under-exposure of the single component. Only the first two components were used as using all through three was found to lower the contrast to the extent that many of the fine details were lost. In experimenting with the transparency of the overlying layer (Component 2) it was found that a transparency level between 60 and 70% lightens the dark areas of component 1 without lowering the overall contrast of the image too much.

Although Figure A.3d does a fairly good job of displaying many details and textures within the study area, it can be noted that there exists an illumination bias against north-west trending objects, as evidenced by the lack of contrast present for the valley in the mid-right side of Figure A.3d. The default for ArcGIS™is to symbolize the PCA components with high values as a light colour and low values as a dark colour (see legend in Figure A.3d), however it was found that if this is inverted for Component 1 (see legend in Figure A.3e), many of the linear features within the landscape become more pronounced.

This simple method, found to create the most detailed and useful visualization of the study area (Figure A.2), is summarized in a flowchart shown in Figure A.4.

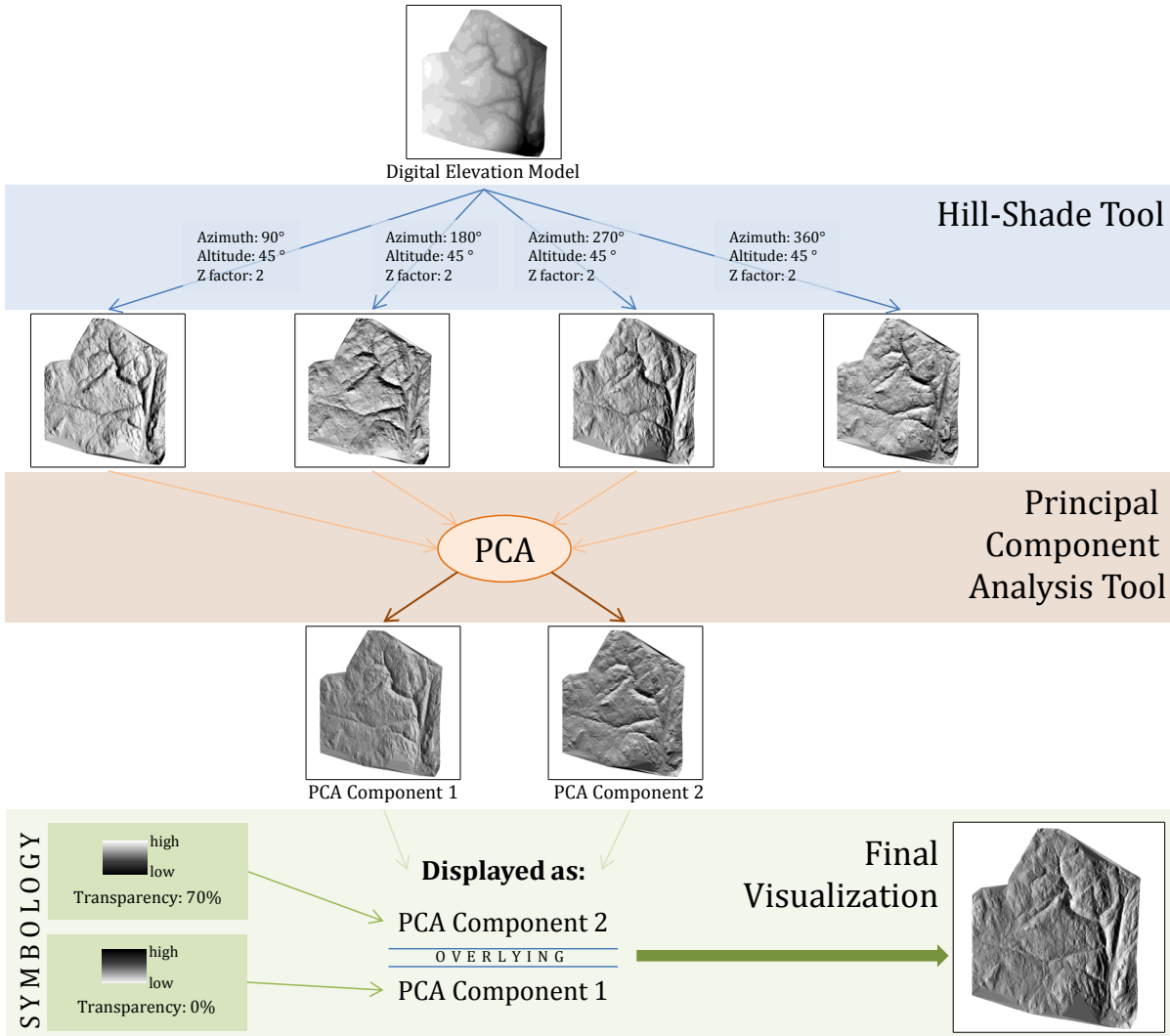

Figure A.4: Flow chart summarizing the LiDAR visualization method proposed in this study

A.3.1 Comparison of Visualization Methods

Although the visualization method presented in this paper allows for the geomorphic interpretation of LiDAR-derived DEMs, there are other simple visualization methods that are commonly used for similar applications. In this section the method proposed in this paper (to be known from now on as the Hill-shade + PCA method) will be compared to three other commonly-used visualization techniques:

1. **Default Hill-shading**: A single hill-shaded image created using the ArcGIS™hillshade tool default settings (i.e. azimuth: 315°; altitude: 45°, z factor: 1)

2. **Equal-weighted Orthogonal Addition**: Two hill-shaded images with orthogonal azimuths added together using equal weights.

3. **Mark, 1992 adapted by Loisios et al., 2007**: Four hill-shaded images with north-westerly azimuths added together and globally weighted according to the relative proportion of the total landscape made up of that aspect.

It is important in areas, such as British Columbia where the geomorphology is dictated by both modern fluvial processes and quaternary glacial deposits, to visualize the terrain in such a way that a range of landform types may be identified. Three locations that highlight landforms associated with different geomorphic processes are shown in Figures A.5 to A.7. Locations 1 and 2 are areas dominated by linear glacial features (drumlins) while Location 3 contains fluvial features like terraces, gullies, abandoned stream channels, and bars.

Comparing it to the rest of the visualization methods, it is clear that the image created using the default hill-shade setting does an overall poor job in highlighting many of the landforms present across the study area (Figures A.5a, A.6a, and A.7a). This is especially true for the drumlin fields shown in Figures A.5 and A.6 which happen to be oriented parallel to the default azimuth. Although not all landscapes will have linear features parallel to the angle of illumination, these figures show how a single hill-shaded image can easily under-represent the range of landforms present.

The number of landforms, especially linear ones, visible in the landscape is greatly increased by simply adding an orthogonally illuminated image to the default hill-shaded image (Figures A.5b, A.6b, and A.7b). This method it does a very good job in visualizing the large-scale features of landscape considering its simplicity. The main shortcoming of this method is that the displayed surface lacks fine textural detail as it appears smoothed compared to the methods shown in c) and d). Given that texture often plays a large role in diagnosing terrain features, certain features may be overlooked or mistakenly identified given this visualization method.

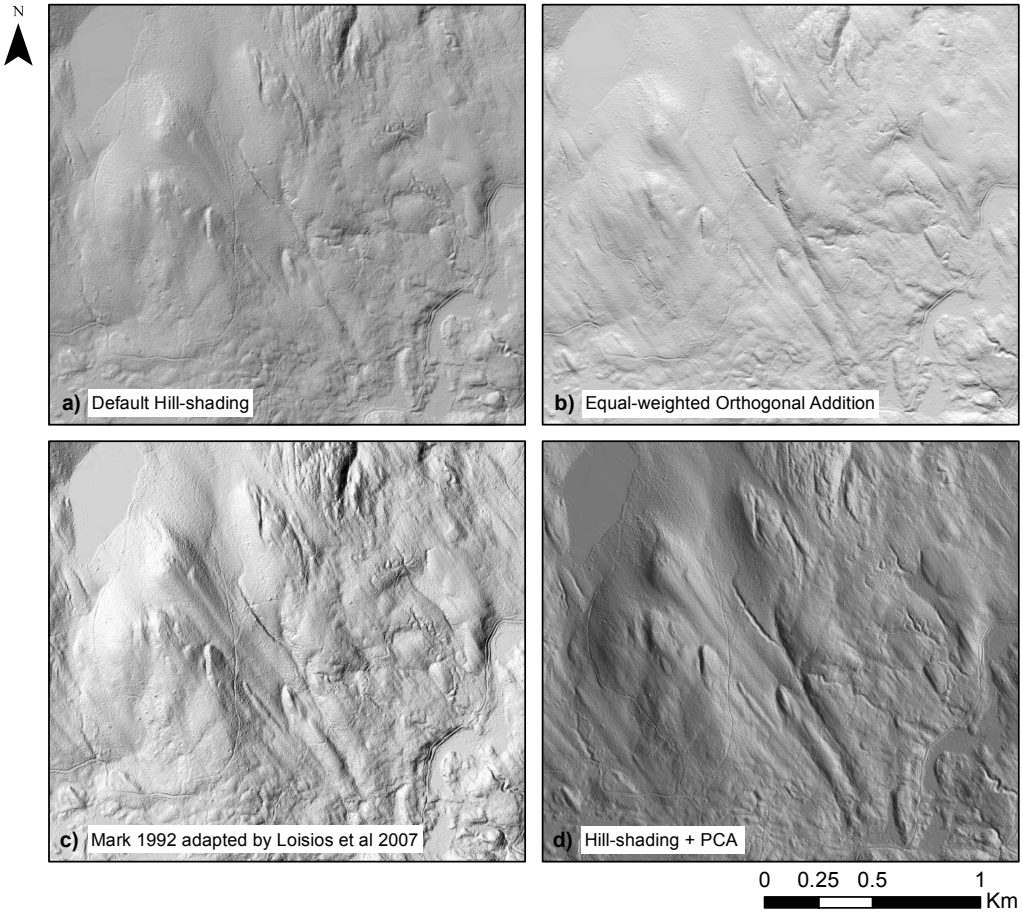

Figure A.5: Visualization methods compared for location 1.

The ability of the weighted raster addition method shown in Figures A.5c, A.6c, and A.7c to represent the landscape is highly inconsistent. This method does a very good job displaying certain parts of the landscape, for example the area shown in Figure A.5c, while completely under-representing others, like the area displayed in Figure A.6c. In comparison, the hill-shade + PCA method defined in this paper consistently highlights both large landforms of all orientations as well as the finer surface texture of the study area (Figures A.5d, A.6d, and A.7d).

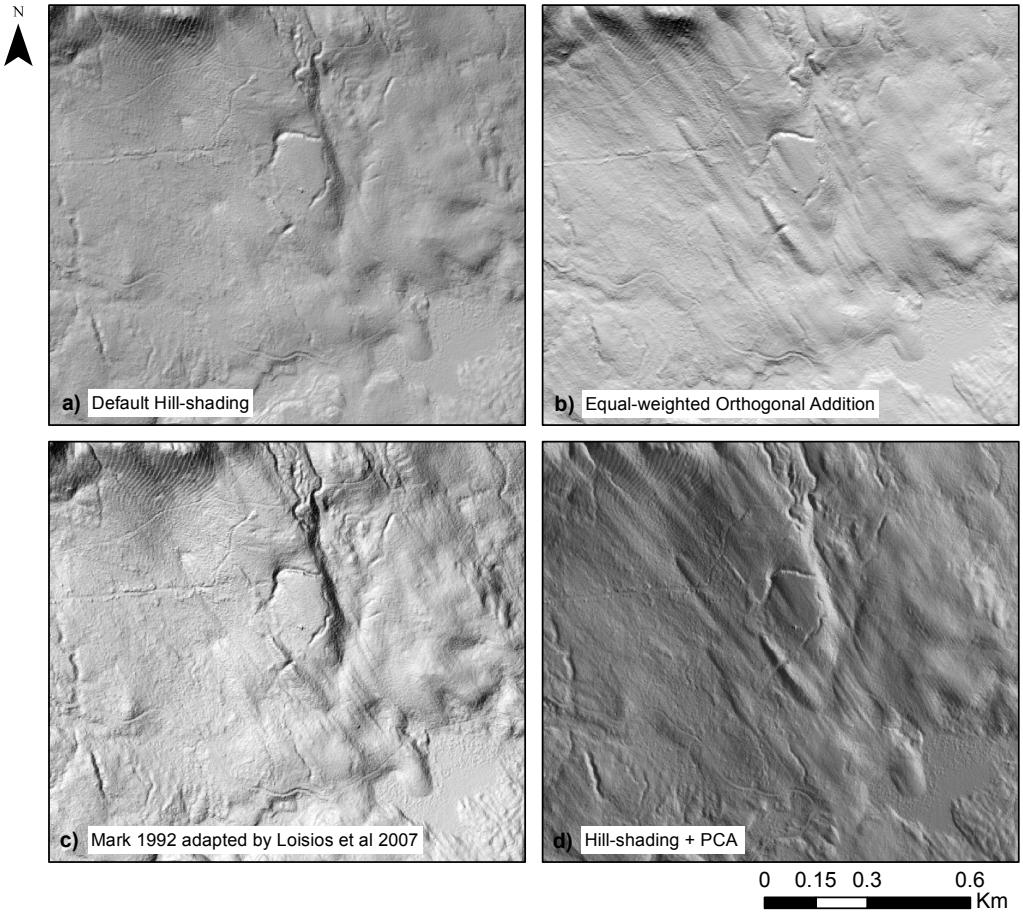

Figure A.6: Visualization methods compared for location 2.

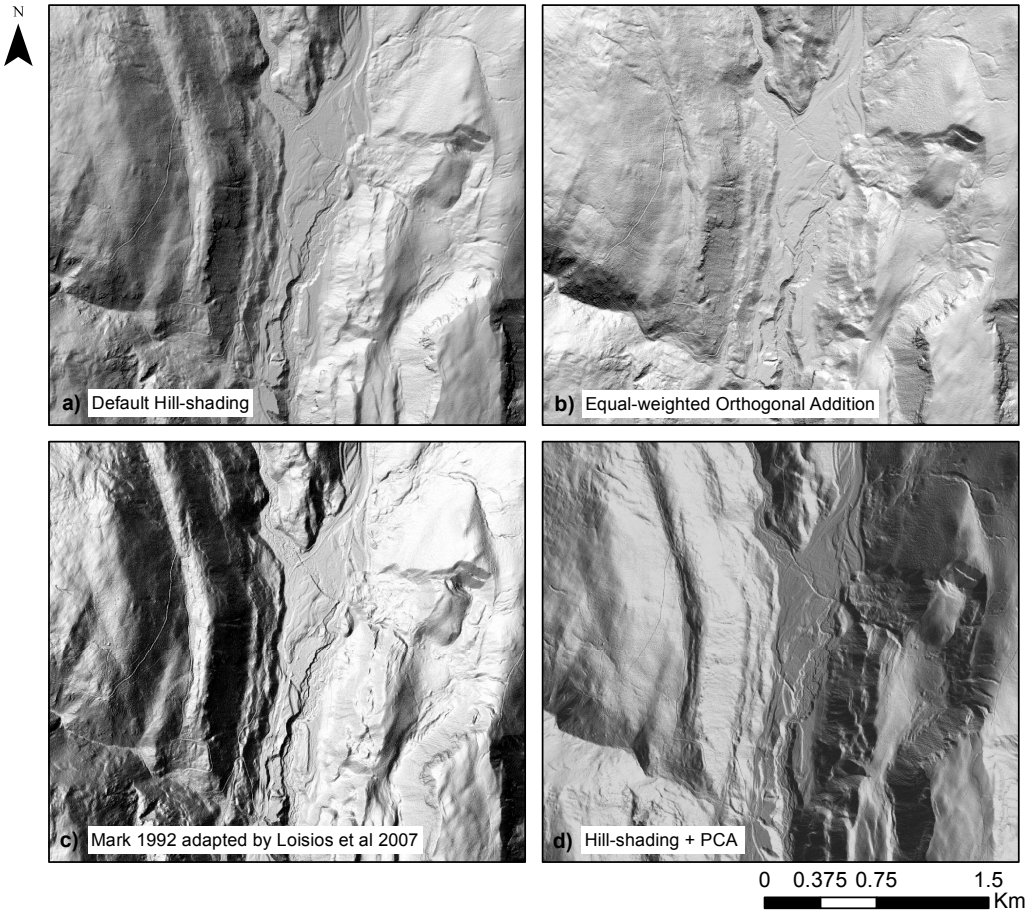

Figure A.7: Visualization methods compared for location 3.

Appendix B

Digital Elevation Models

Digital elevation models were created using the methods described in Section 1 of Chapter 3. The experiments conducted on Model 1 use the legend shown in Figure B.1a while those conducted on Model 2 use the legend shown in Figure B.1b.

(a) DEM legend for Model 1

(b) DEM legend for Model 2

Figure B.1: Legends used for all of the DEMs presented below. Values show elevation in millimeters.

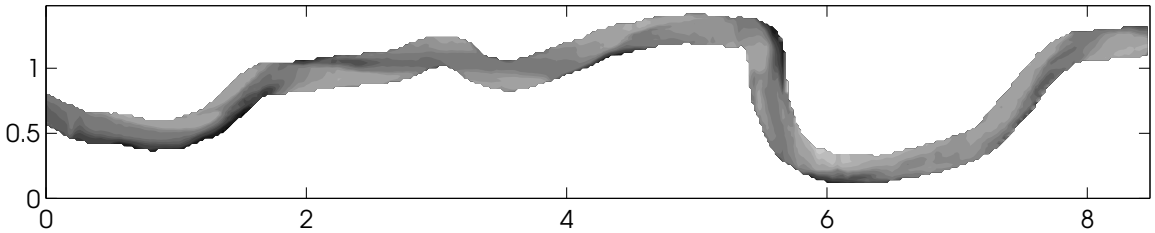

(a) Experiment 1: Hour 5

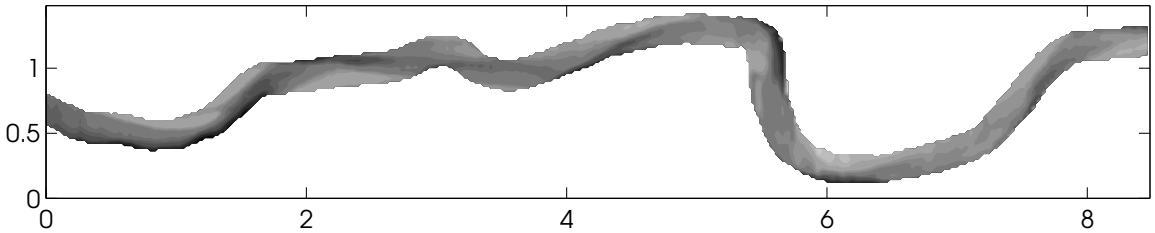

(b) Experiment 1: Hour 10

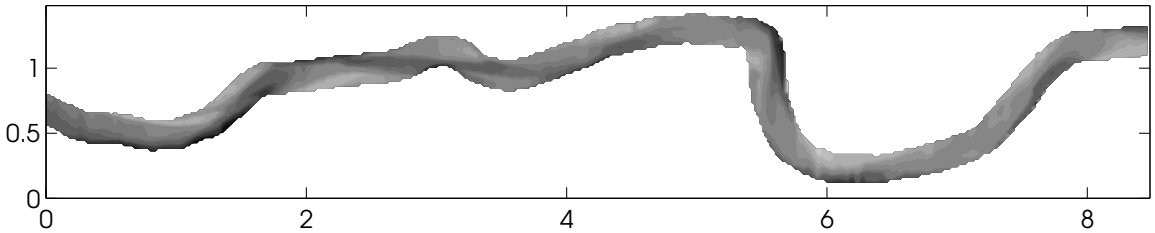

(c) Experiment 1: Hour 15

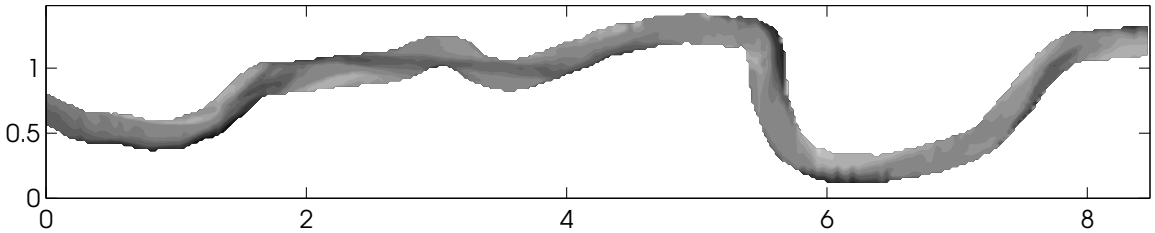

(d) Experiment 1: Hour 20

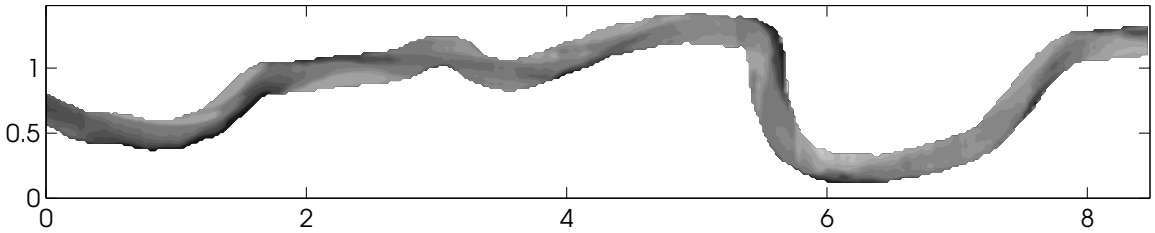

(e) Experiment 1: Hour 25

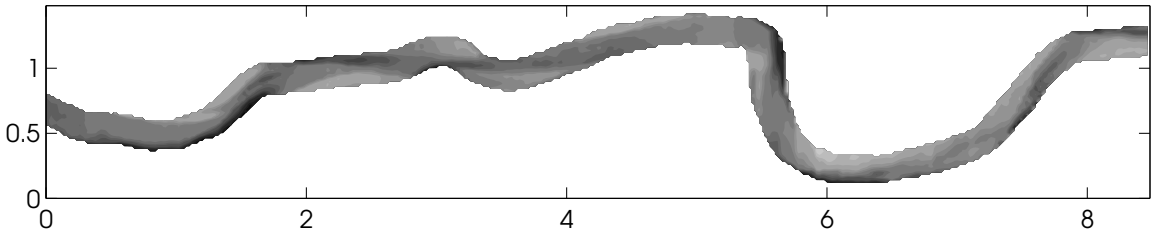

(f) Experiment 1: Hour 30

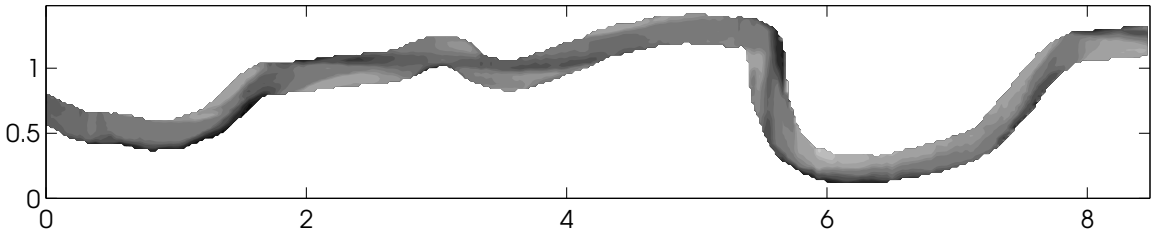

(g) Experiment 1: Hour 35

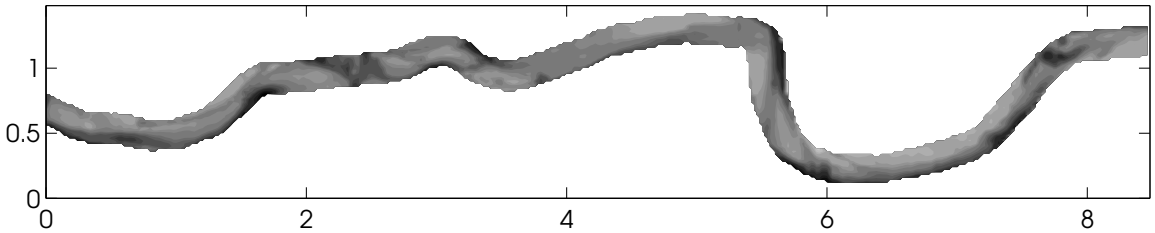

(h) Experiment 1: Hour 40

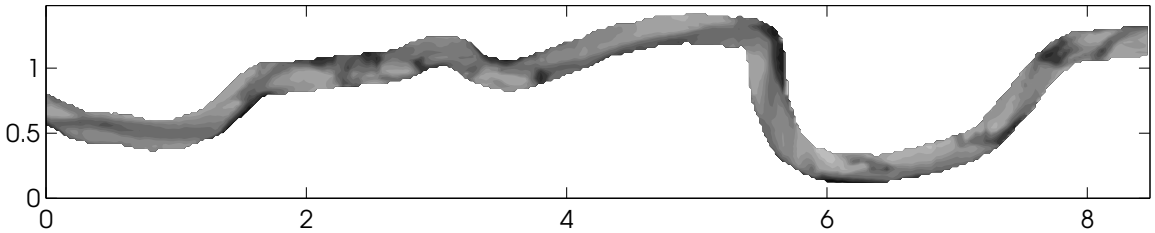

(i) Experiment 1: Hour 45

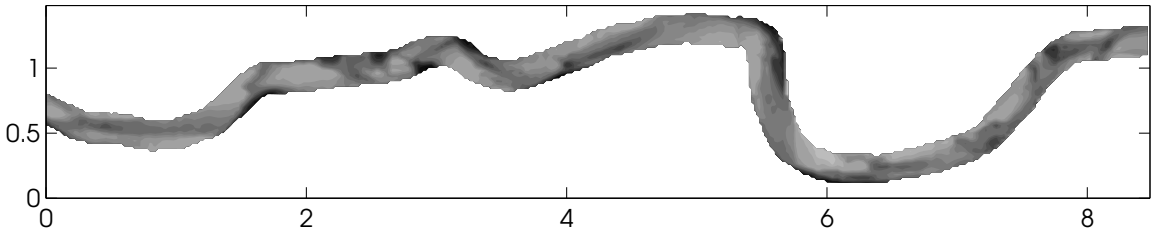

(j) Experiment 1: Hour 50

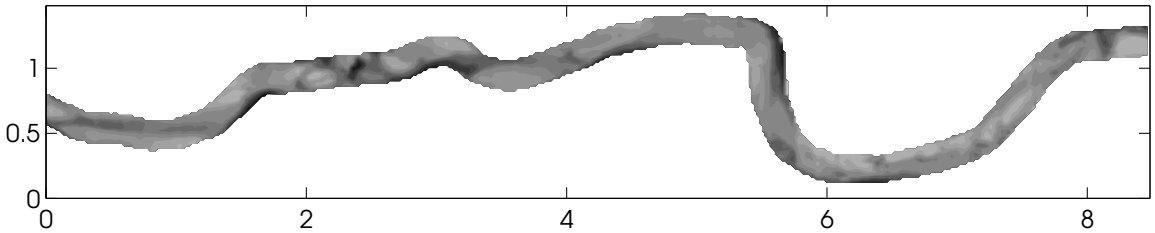

(k) Experiment 1: Hour 55

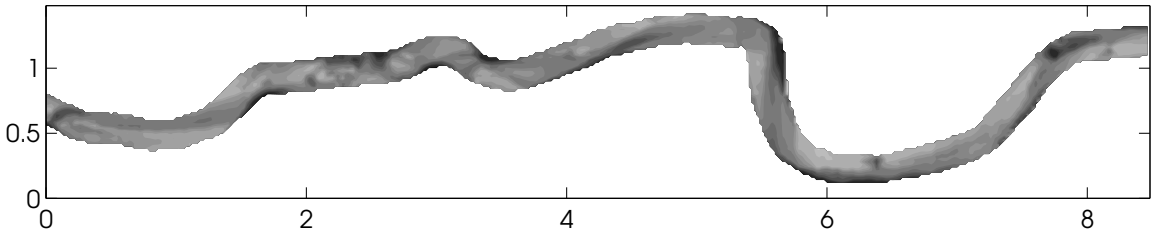

(l) Experiment 1: Hour 60

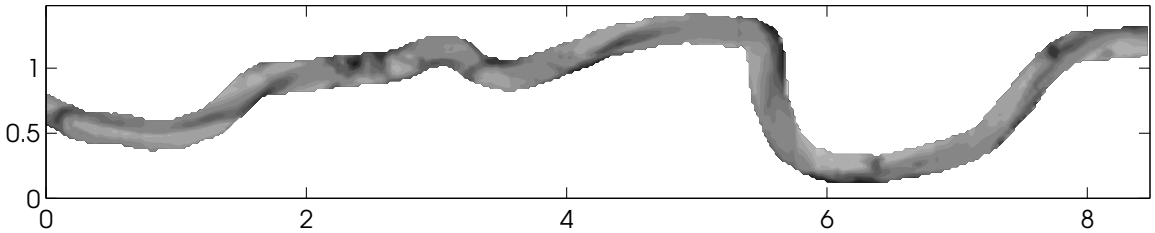

(m) Experiment 1: Hour 65

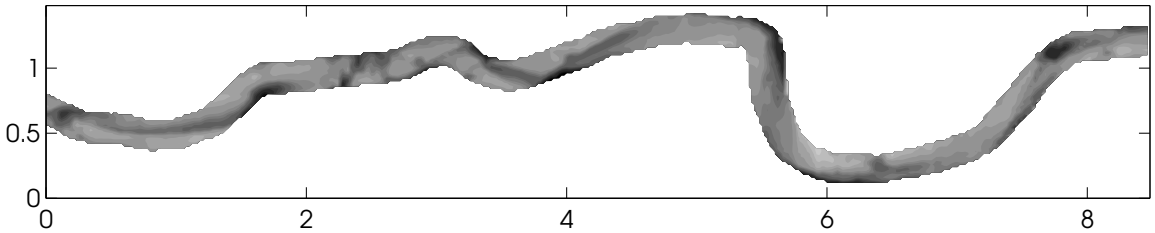

(n) Experiment 1: Hour 70

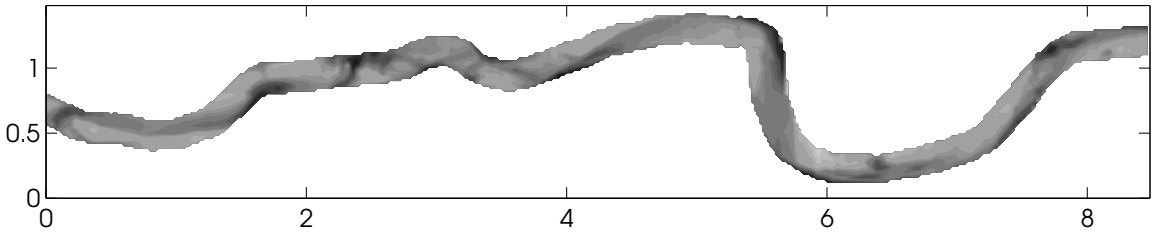

(o) Experiment 1: Hour 75

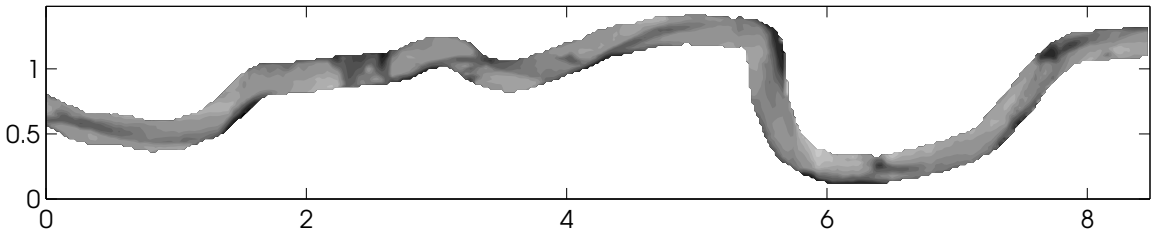

(p) Experiment 1: Hour 80

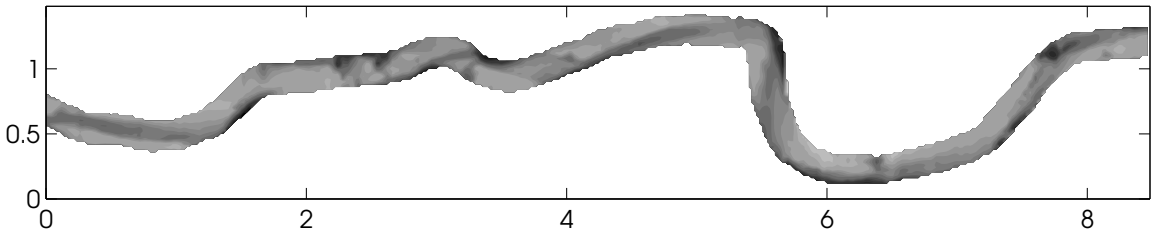

(q) Experiment 1: Hour 85

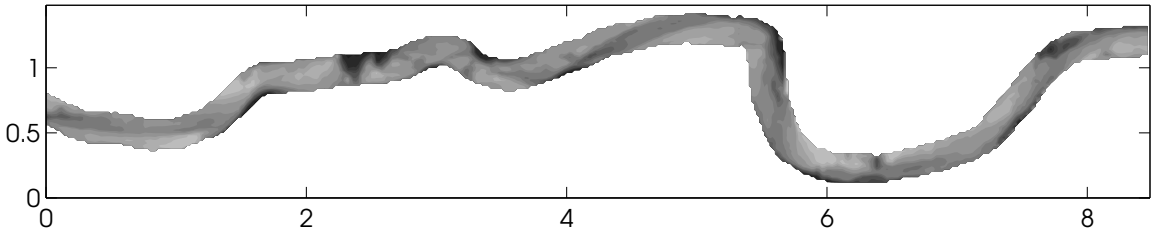

(r) Experiment 1: Hour 90

Figure B.2: Digital Elevation Models for Experiment 1

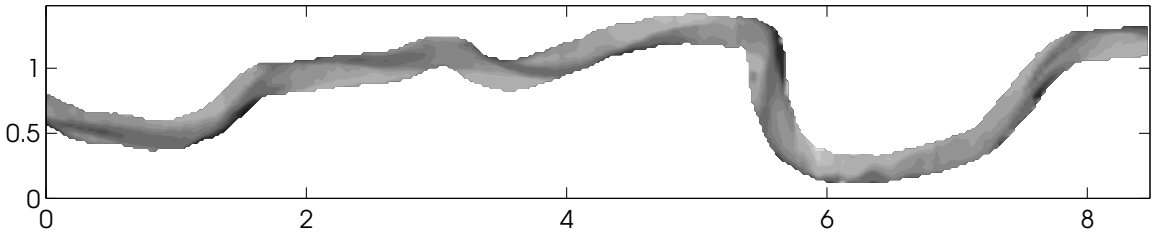

(a) Experiment 2: Hour 5

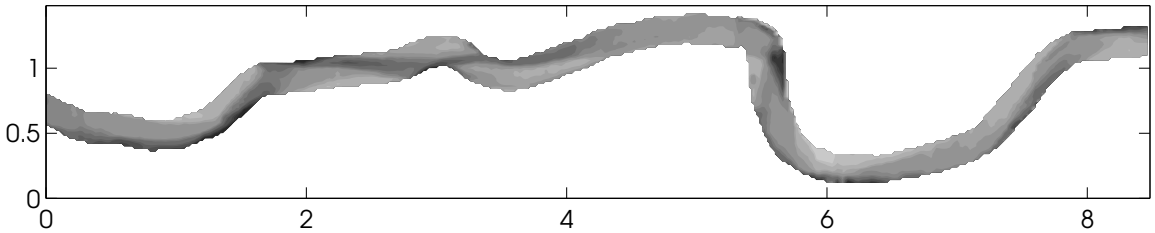

(b) Experiment 2: Hour 10

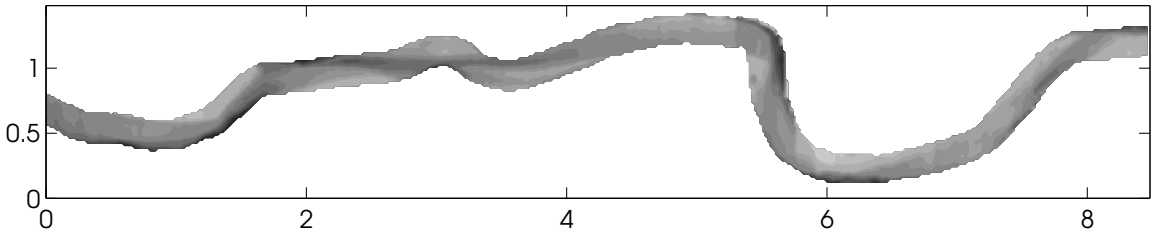

(c) Experiment 2: Hour 15

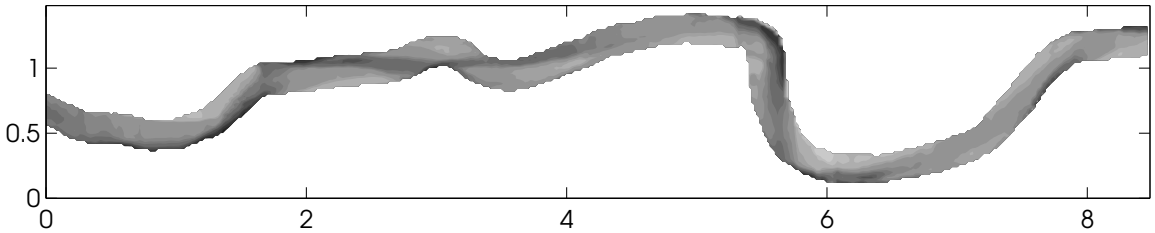

(d) Experiment 2: Hour 20

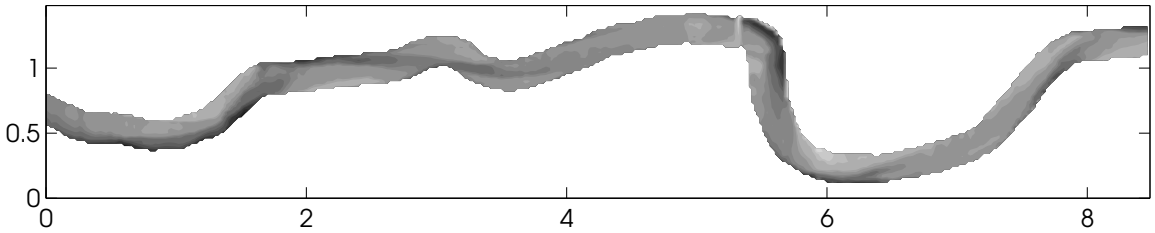

(e) Experiment 2: Hour 25

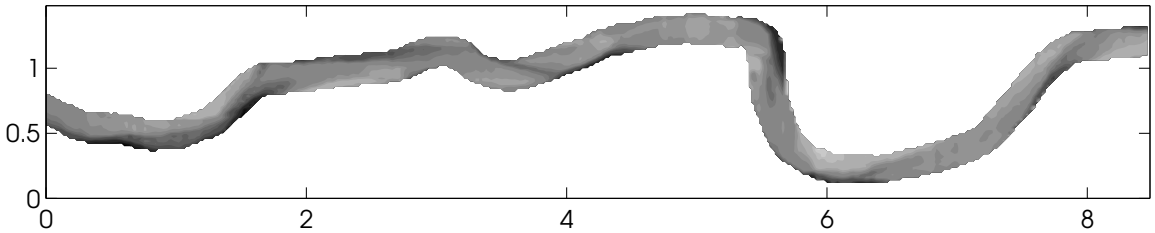

(f) Experiment 2: Hour 30

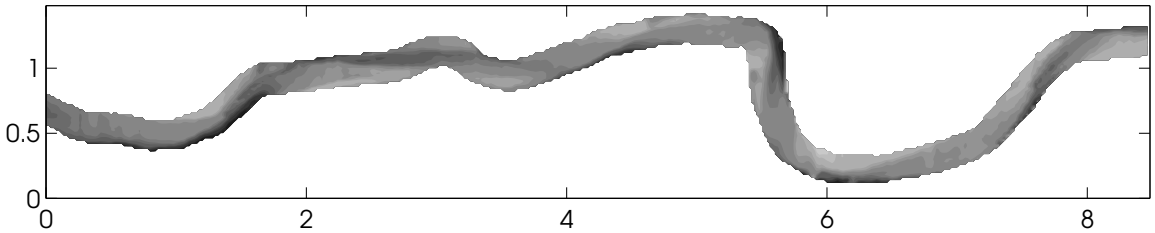

(g) Experiment 2: Hour 35

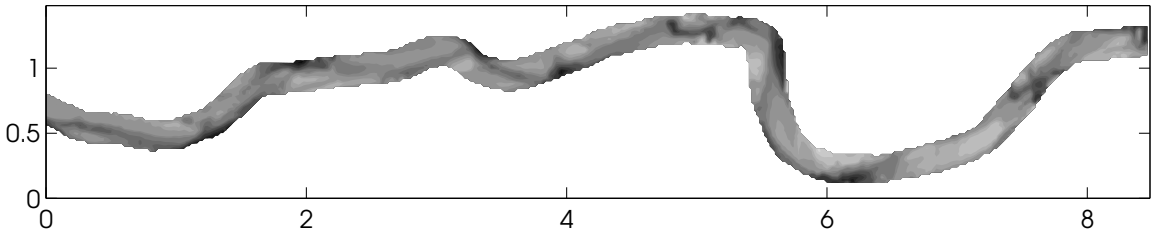

(h) Experiment 2: Hour 40

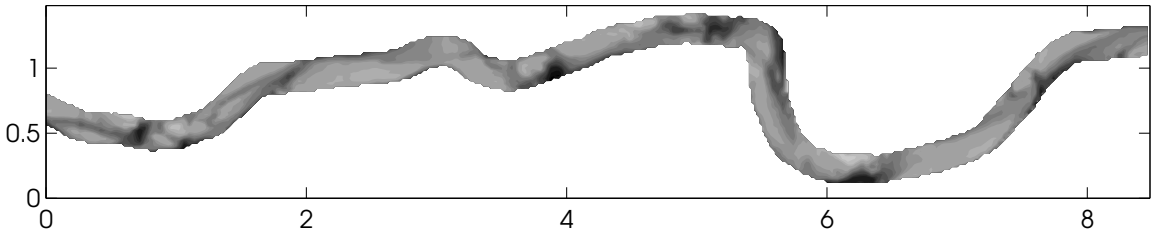

(i) Experiment 2: Hour 45

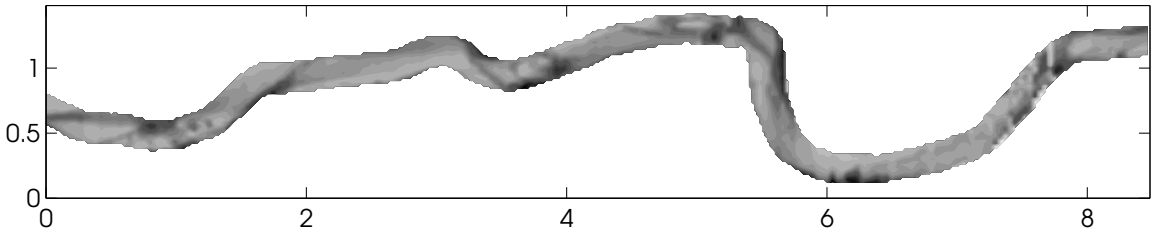

(j) Experiment 2: Hour 50

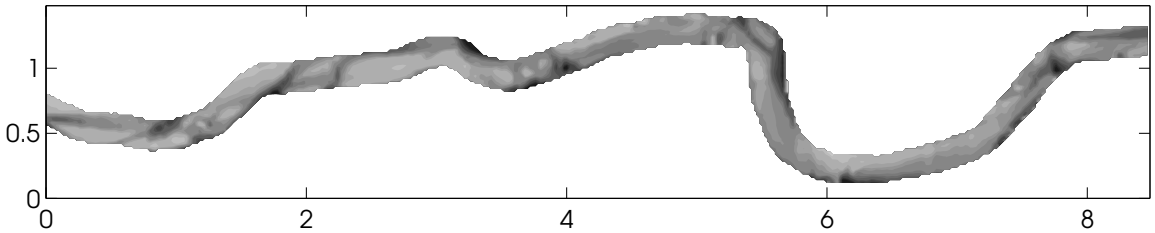

(k) Experiment 2: Hour 55

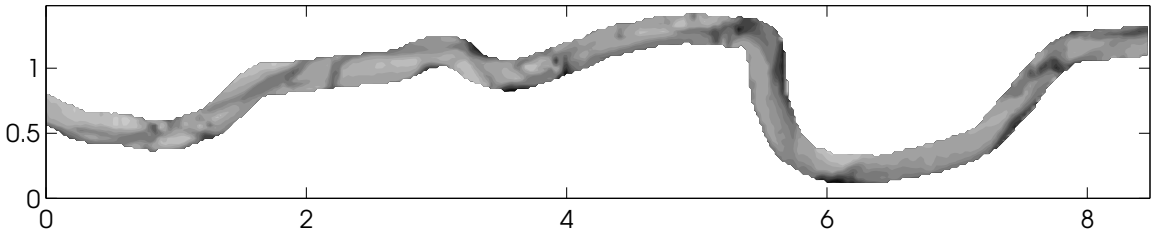

(l) Experiment 2: Hour 60

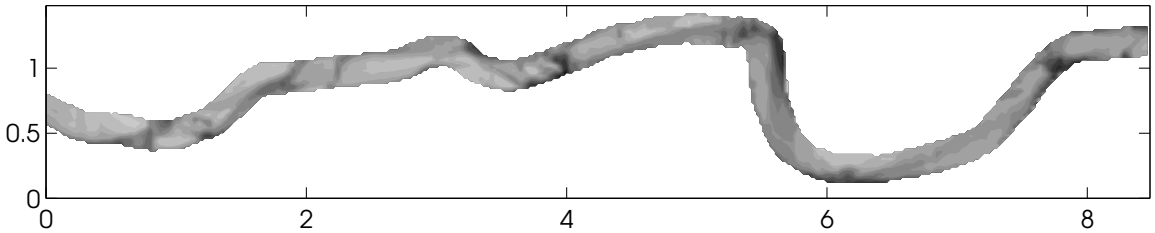

(m) Experiment 2: Hour 65

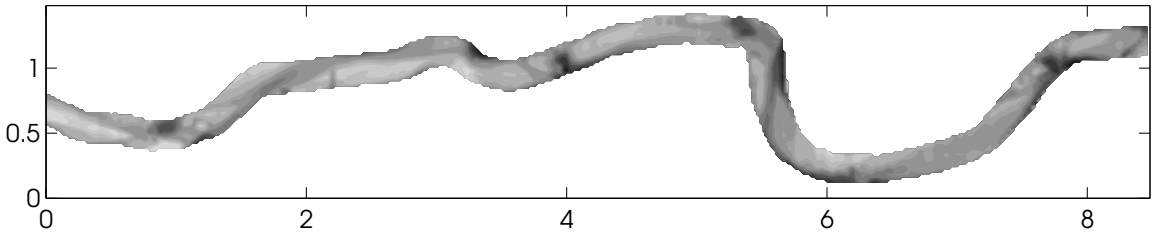

(n) Experiment 2: Hour 70

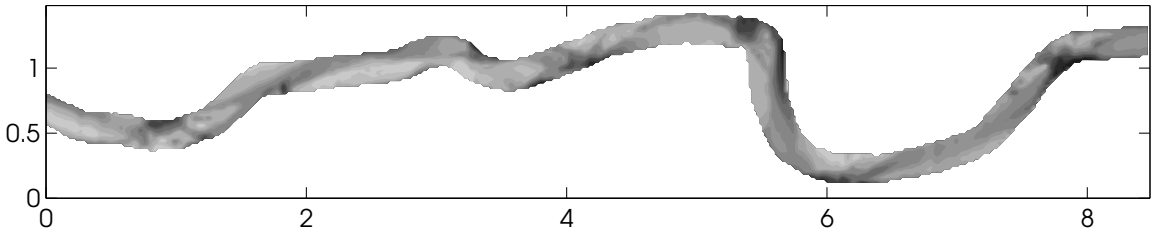

(o) Experiment 2: Hour 75

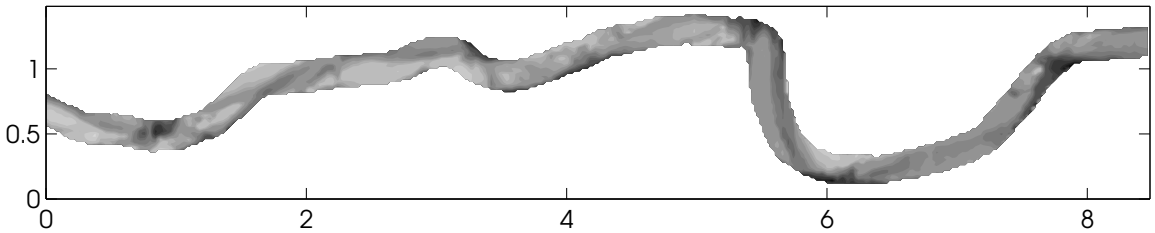

(p) Experiment 2: Hour 80

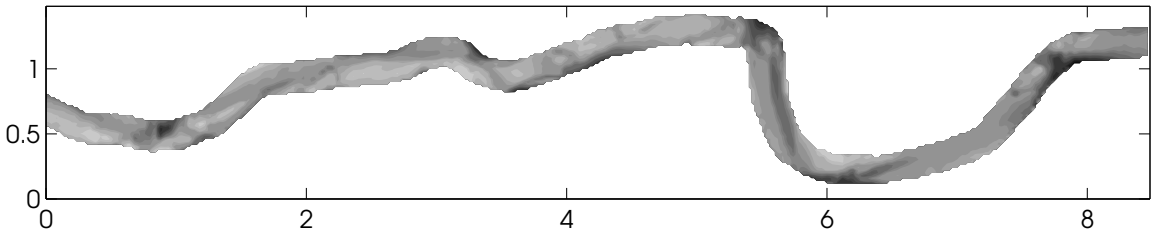

(q) Experiment 2: Hour 85

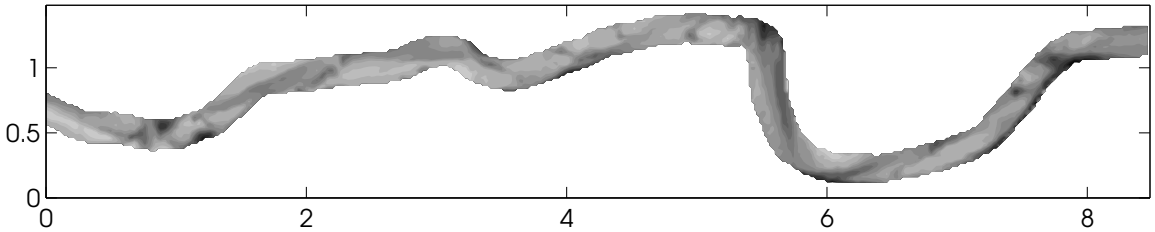

(r) Experiment 2: Hour 90

Figure B.3: Digital Elevation Models for Experiment 2

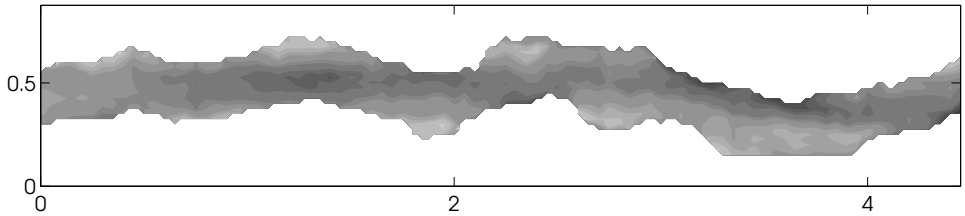

(a) Experiment 3: Hour 15

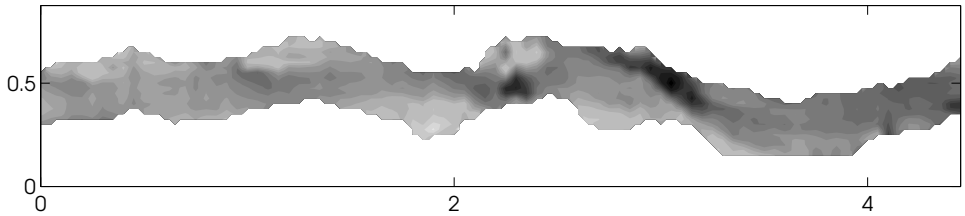

(b) Experiment 3: Hour 20

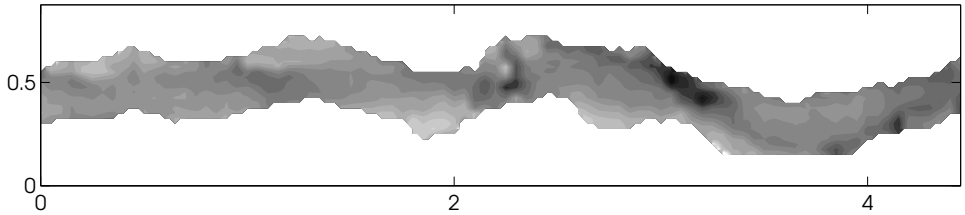

(c) Experiment 3: Hour 25

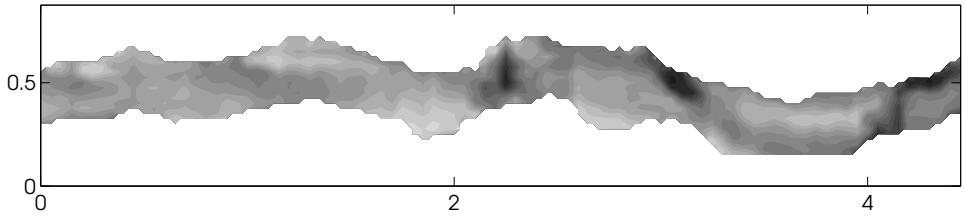

(d) Experiment 3: Hour 30

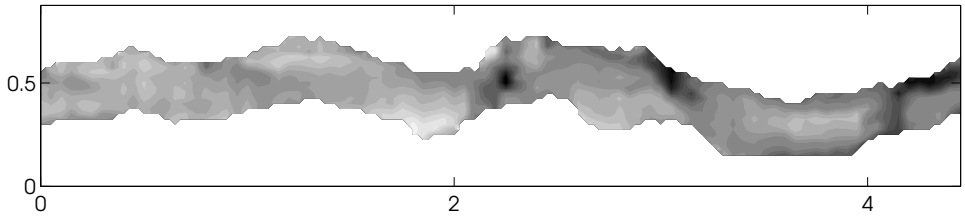

(e) Experiment 3: Hour 35

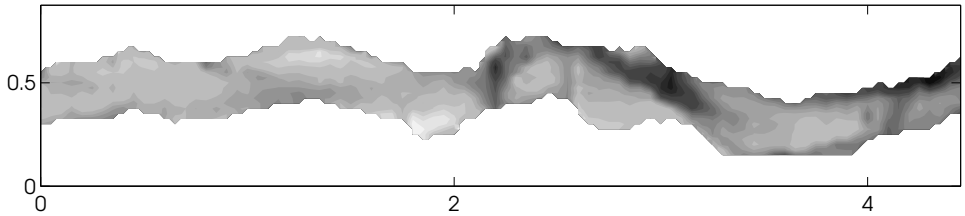

(f) Experiment 3: Hour 40

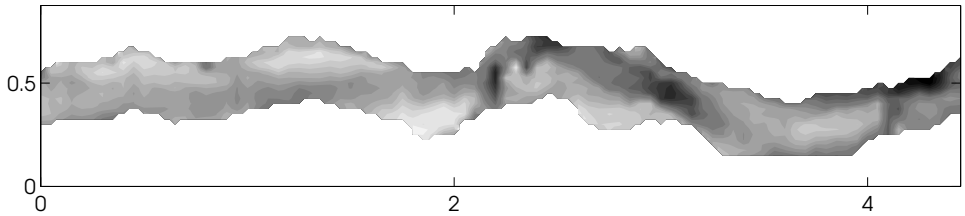

(g) Experiment 3: Hour 45

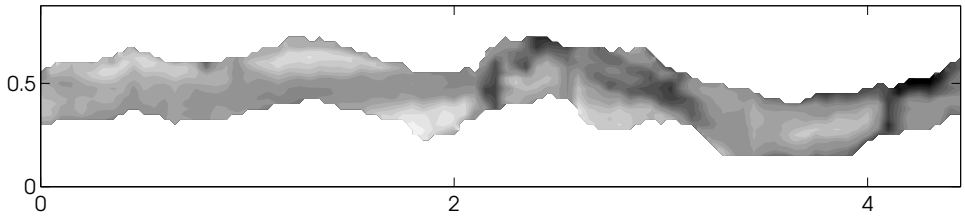

(h) Experiment 3: Hour 50

Figure B.4: Digital Elevation Models for Experiment 3

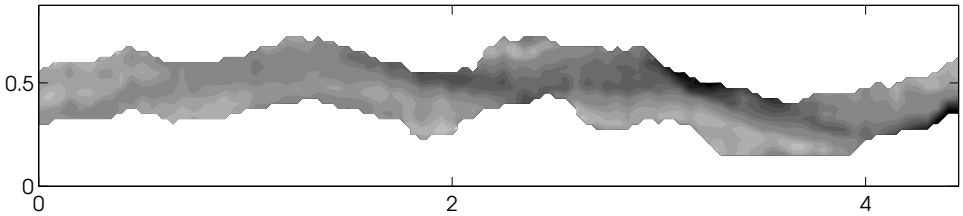

(a) Experiment 4: Hour 10

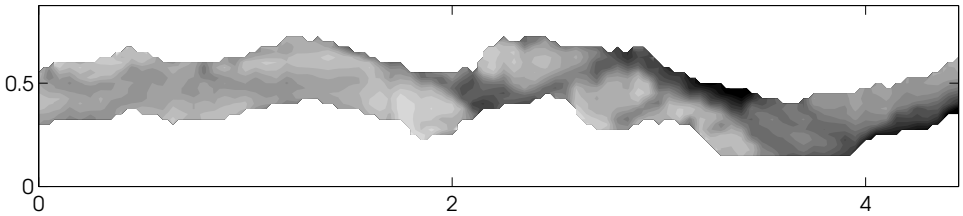

(b) Experiment 4: Hour 15

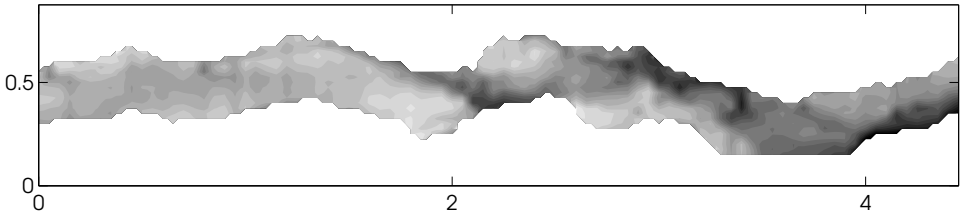

(c) Experiment 4: Hour 20

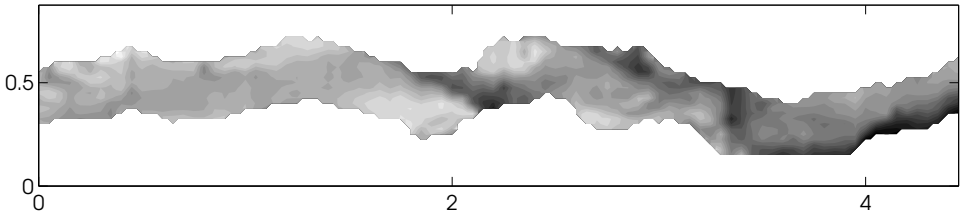

(d) Experiment 4: Hour 25

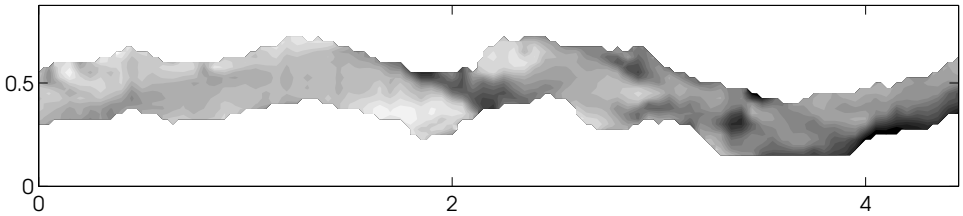

(e) Experiment 4: Hour 30

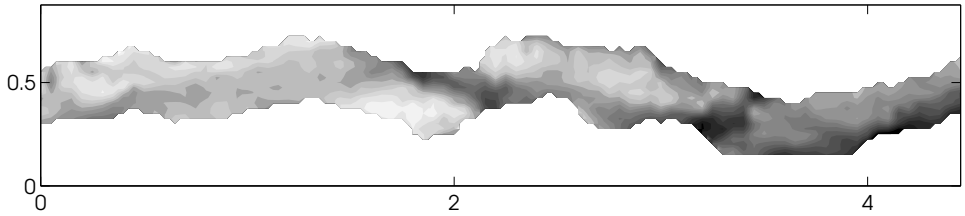

(f) Experiment 4: Hour 35

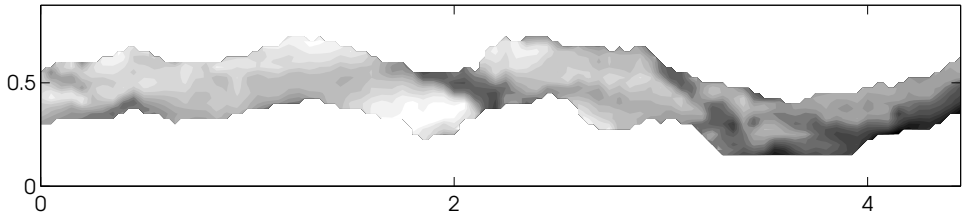

(g) Experiment 4: Hour 40

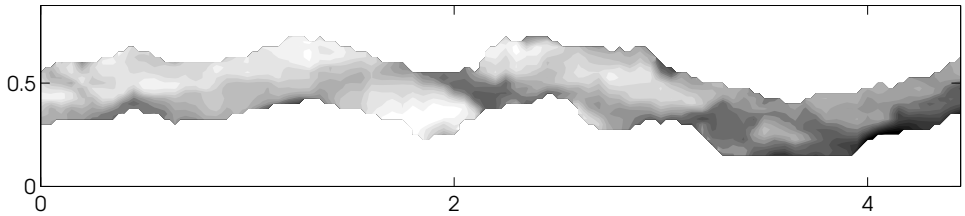

(h) Experiment 4: Hour 45

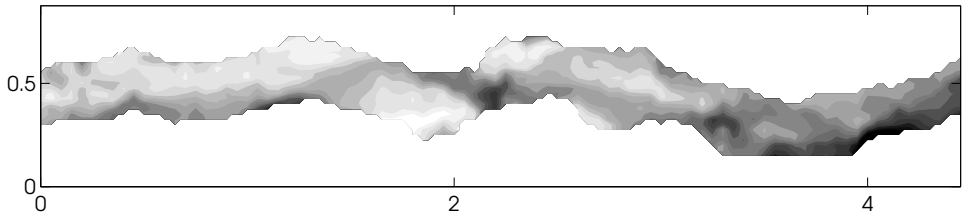

(i) Experiment 4: Hour 50

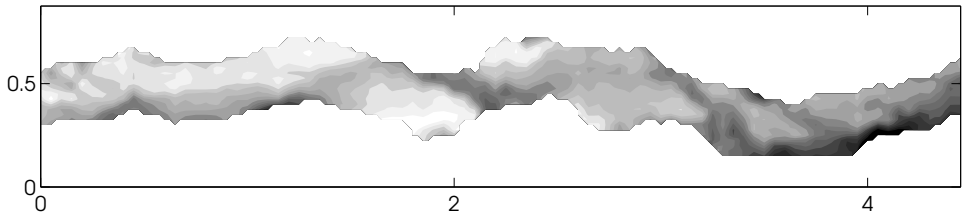

(j) Experiment 4: Hour 55

Figure B.5: Digital Elevation Models for Experiment 4

Appendix C

DEMs of Difference

DEMs of difference (DoDs) are created by subtracting two DEMs from one another. The DoDs presented in this appendix show the difference in elevation between subsequent runs in each experiment. All of the figures use the same legend (Figure C.1). The units of the x- and y- axes are meters and the units in the z- direction (elevation) are in millimeters.

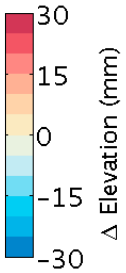

Figure C.1: Legend used for all DoDs presented below. Values show the difference in elevation between the two DEMs in millimeters.

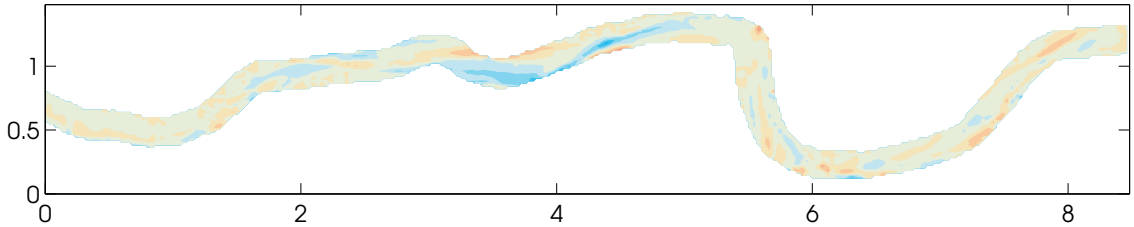

(a) Experiment 1: Hours 10 - 5

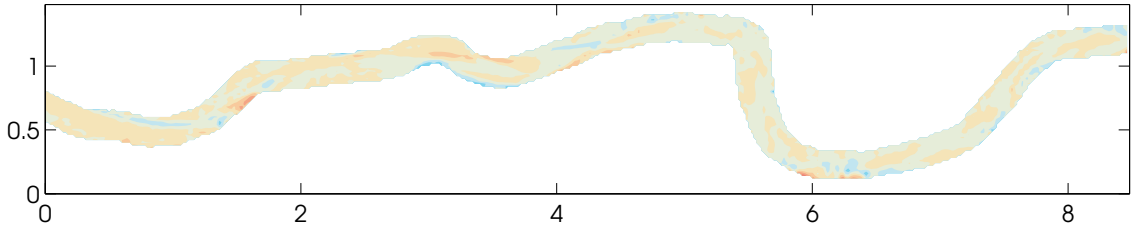

(b) Experiment 1: Hours 15 - 10

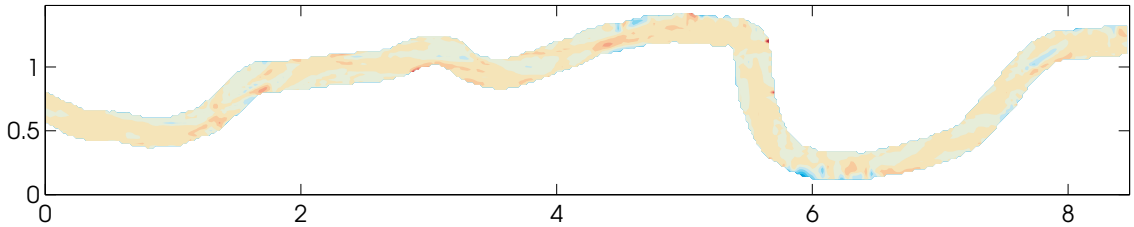

(c) Experiment 1: Hours 20 - 15

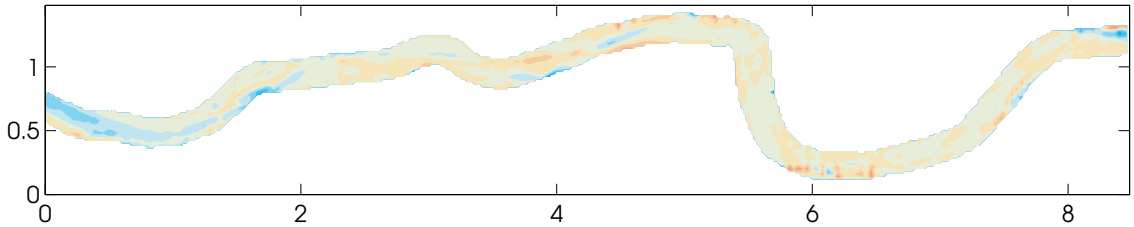

(d) Experiment 1: Hours 25 - 20

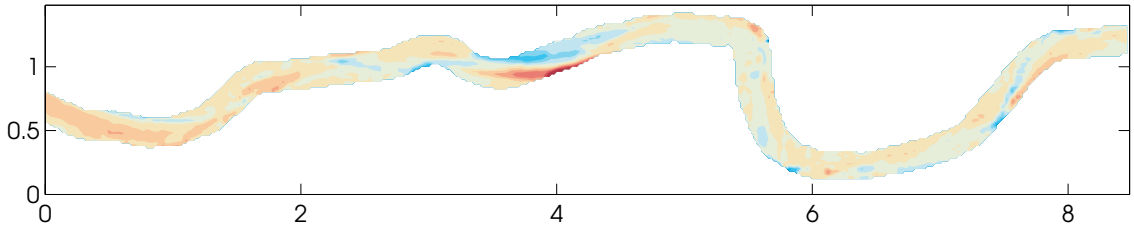

(e) Experiment 1: Hours 30 - 25

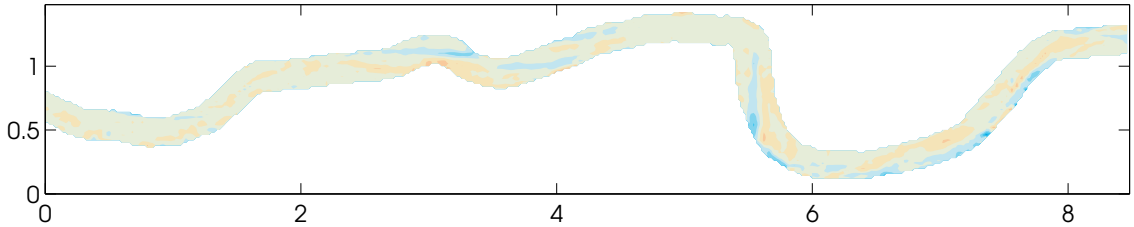

(f) Experiment 1: Hours 35 - 30

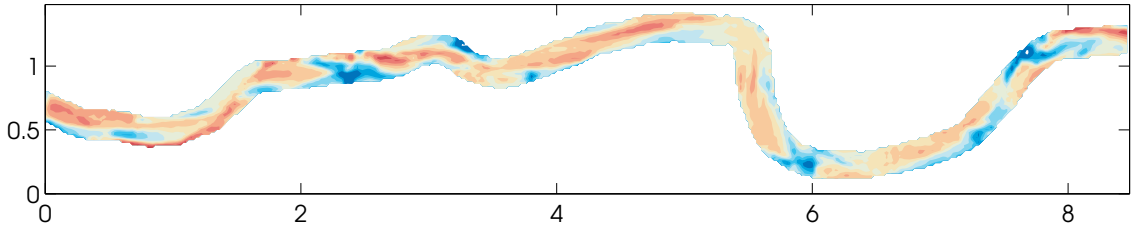

(g) Experiment 1: Hours 40 - 35

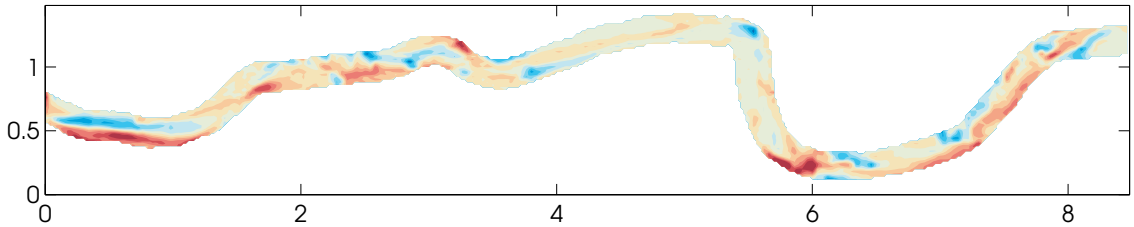

(h) Experiment 1: Hours 45 - 40

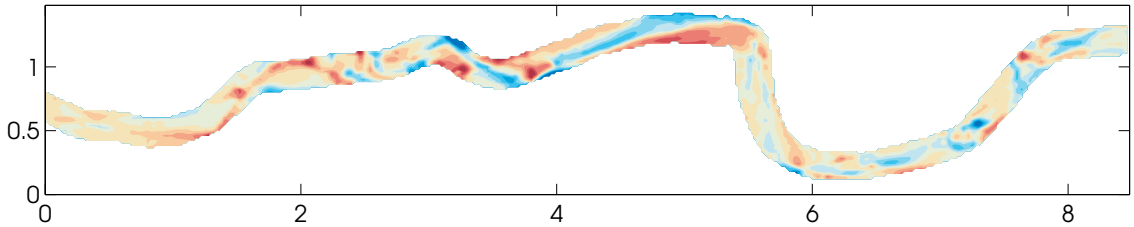

(i) Experiment 1: Hours 50 - 45

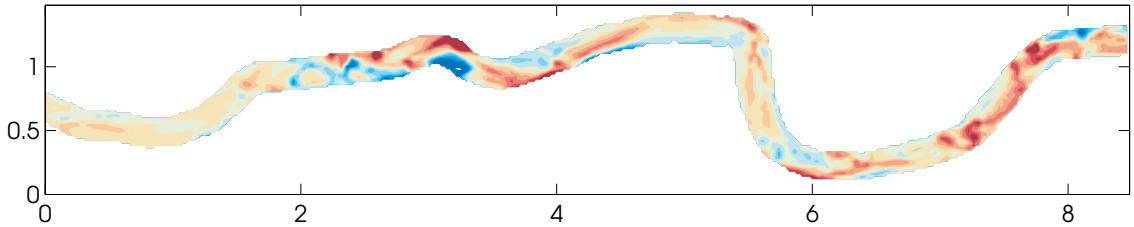

(j) Experiment 1: Hours 55 - 50

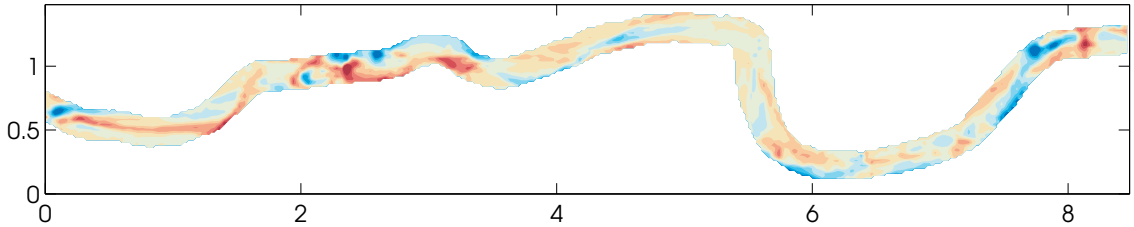

(k) Experiment 1: Hours 60 - 55

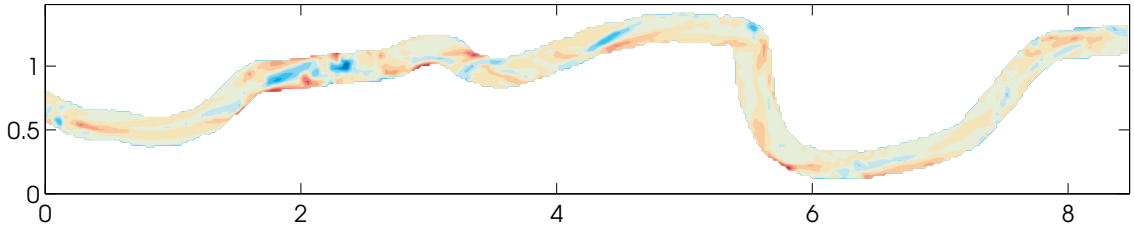

(l) Experiment 1: Hours 65 - 60

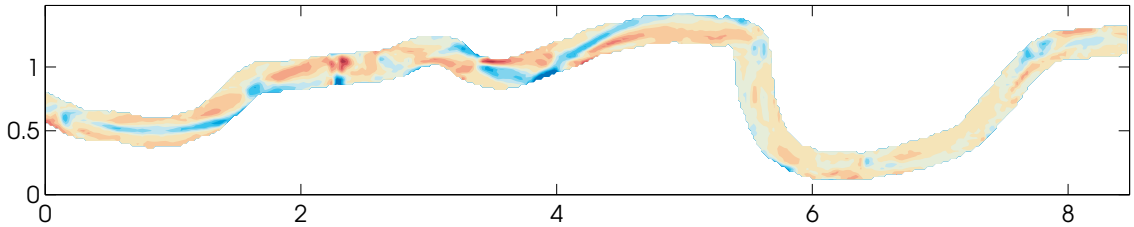

(m) Experiment 1: Hours 70 - 65

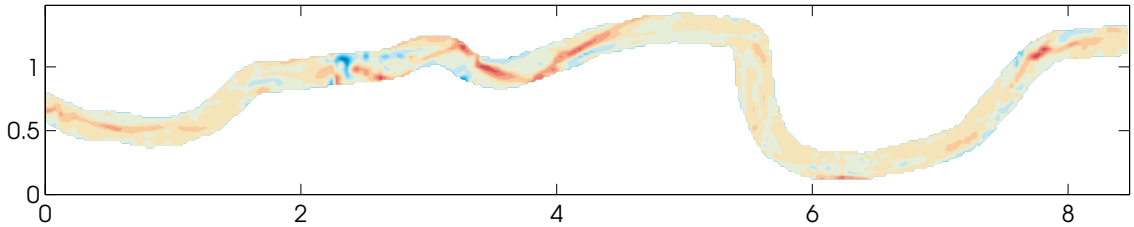

(n) Experiment 1: Hours 75 - 70

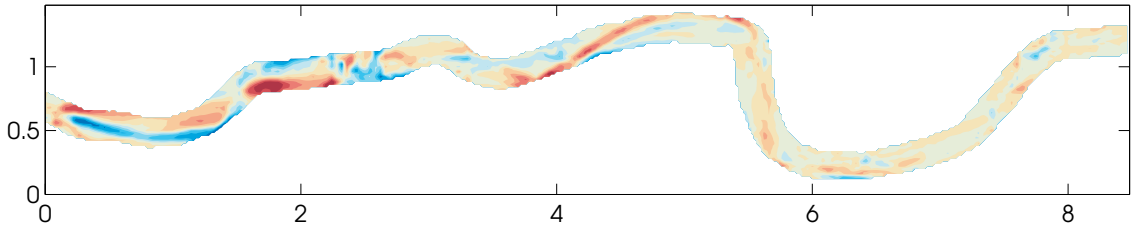

(o) Experiment 1: Hours 80 - 75

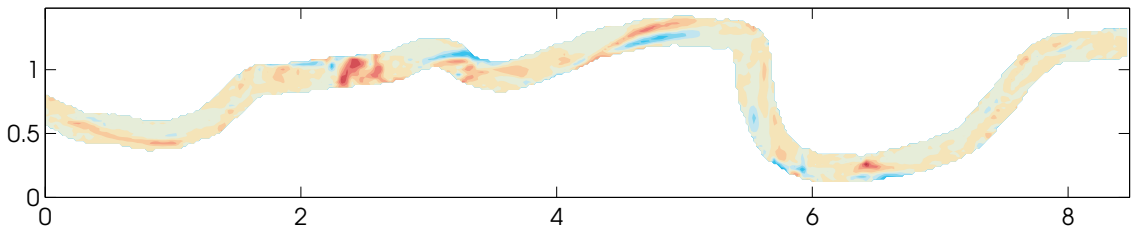

(p) Experiment 1: Hours 85 - 80

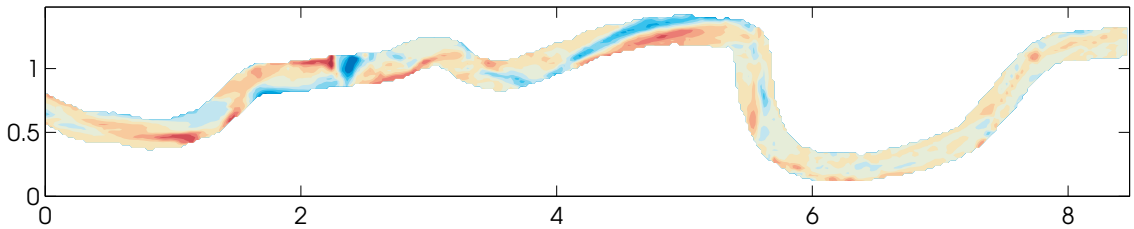

(q) Experiment 1: Hours 90 - 85

Figure C.2: DEMs of Difference for Experiment 1

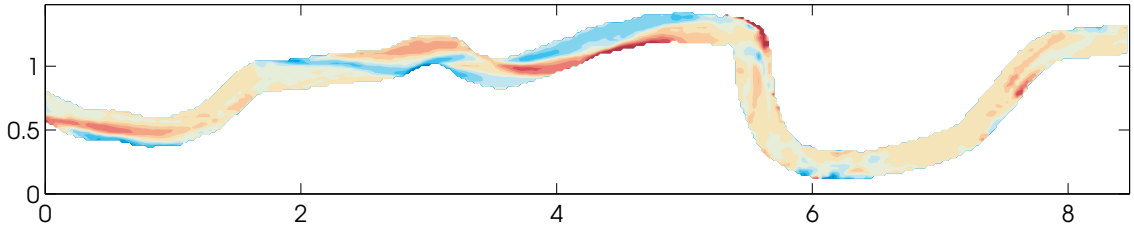

(a) Experiment 2: Hours 10 - 5

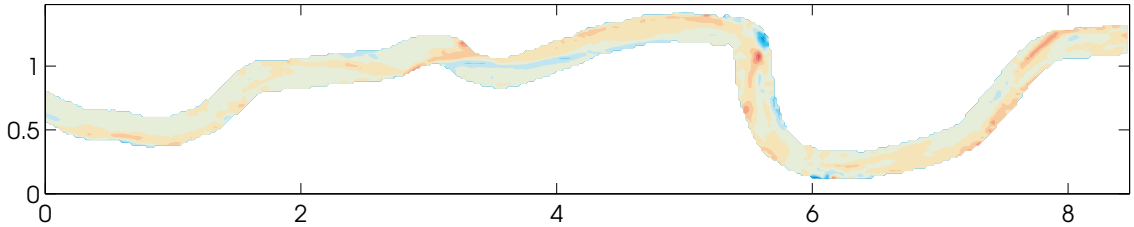

(b) Experiment 2: Hours 15 - 10

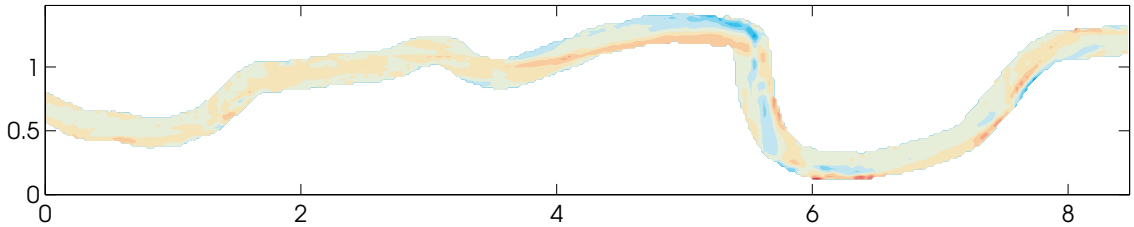

(c) Experiment 2: Hours 20 - 15

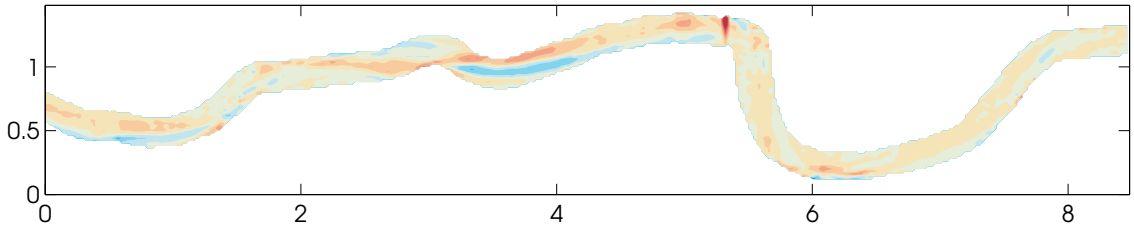

(d) Experiment 2: Hours 25 - 20

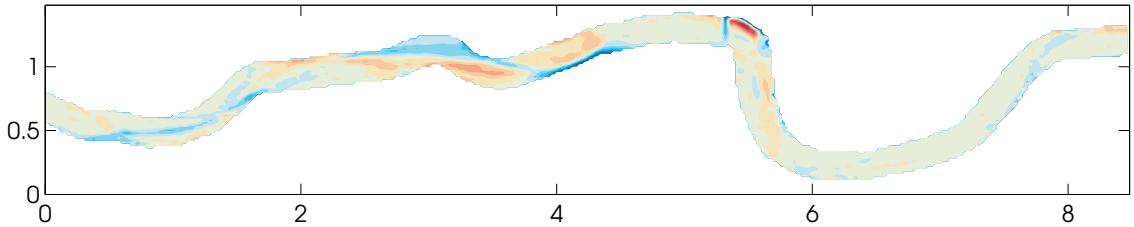

(e) Experiment 2: Hours 30 - 25

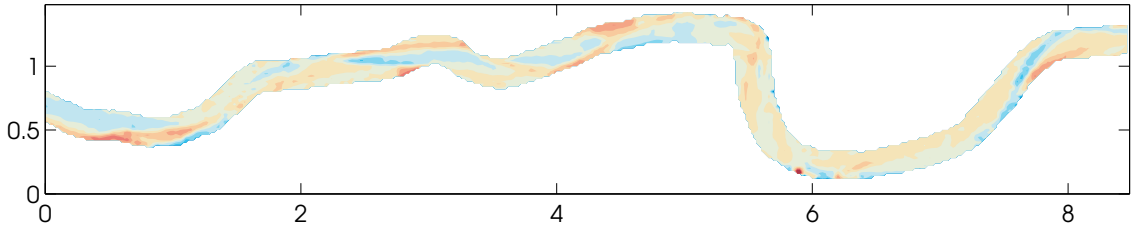

(f) Experiment 2: Hours 35 - 30

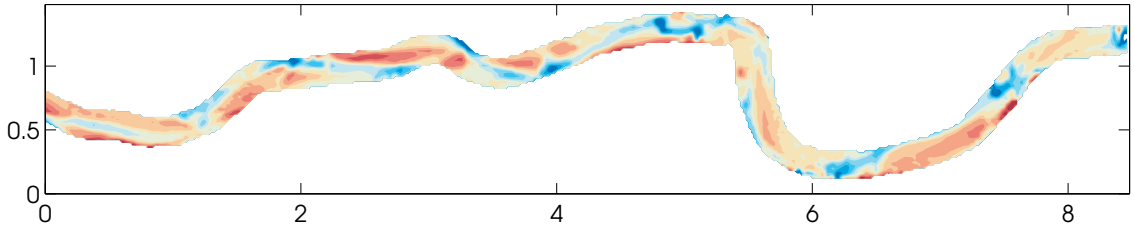

(g) Experiment 2: Hours 40 - 35

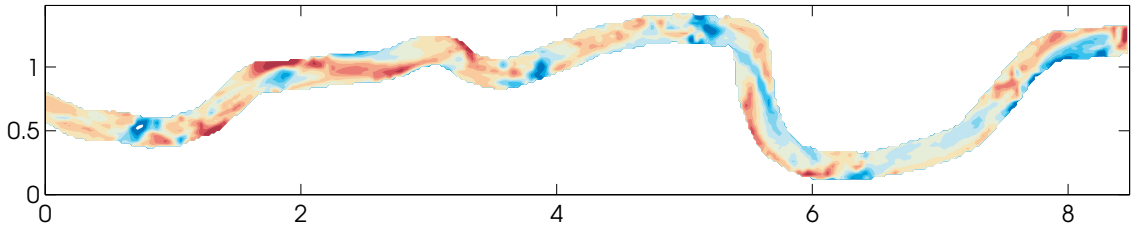

(h) Experiment 2: Hours 45 - 40

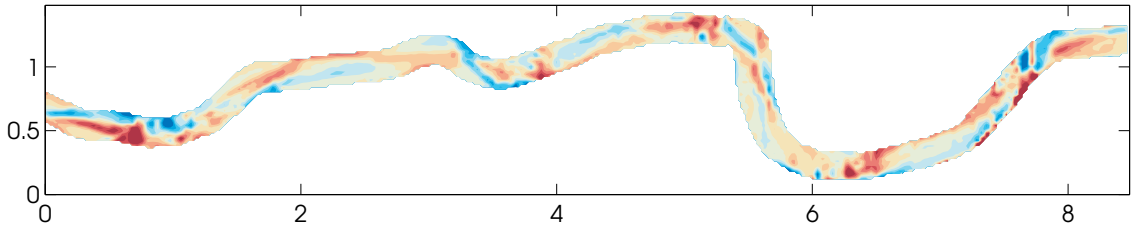

(i) Experiment 2: Hours 50 - 45

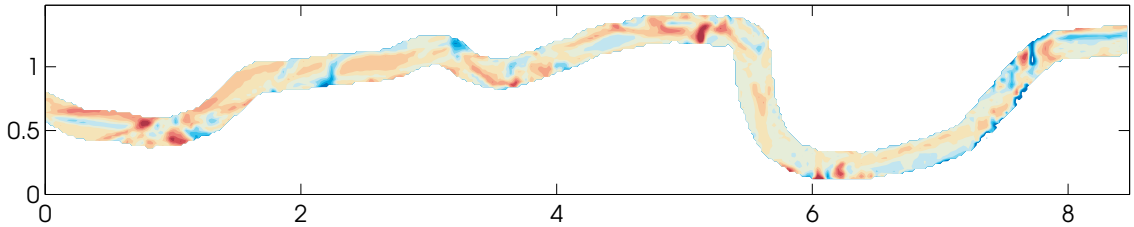

(j) Experiment 2: Hours 55 - 50

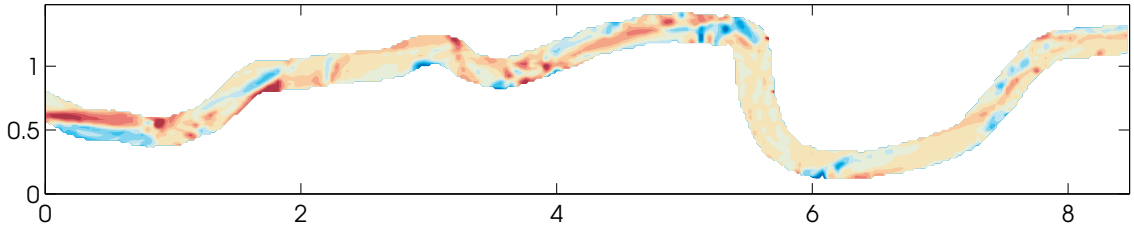

(k) Experiment 2: Hours 60 - 55

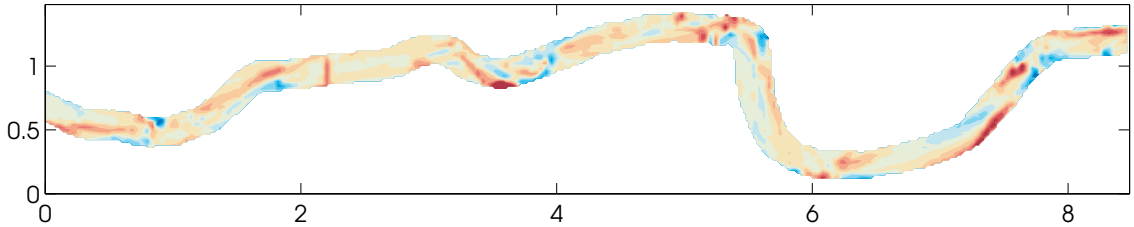

(l) Experiment 2: Hours 65 - 60

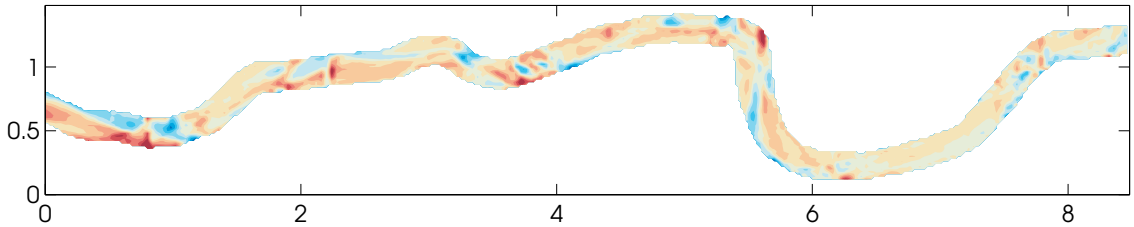

(m) Experiment 2: Hours 70 - 65

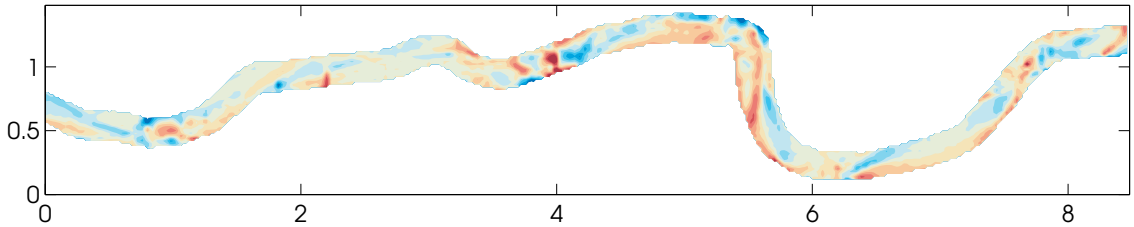

(n) Experiment 2: Hours 75 - 70

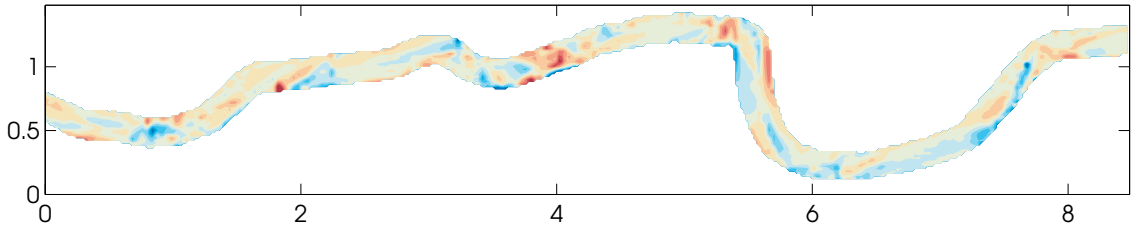

(o) Experiment 2: Hours 80 - 75

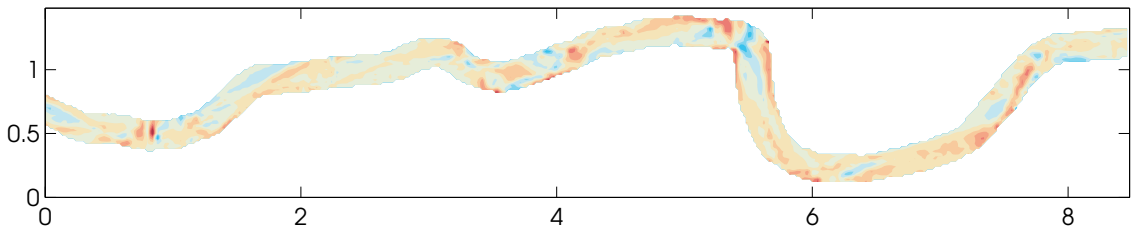

(p) Experiment 2: Hours 85 - 80

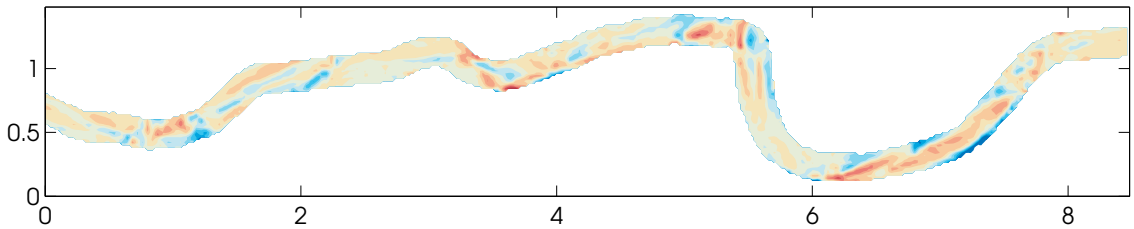

(q) Experiment 2: Hours 90 - 85

Figure C.3: DEMs of Difference for Experiment 2

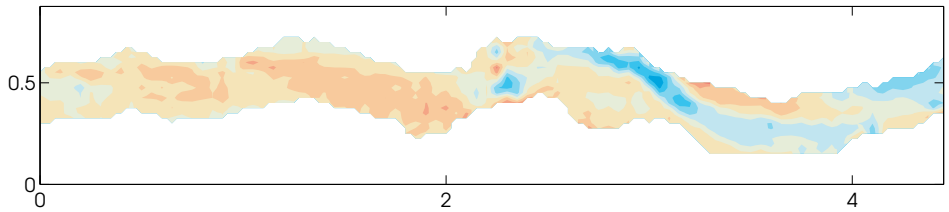

(a) Experiment 3: Hours 20 - 15

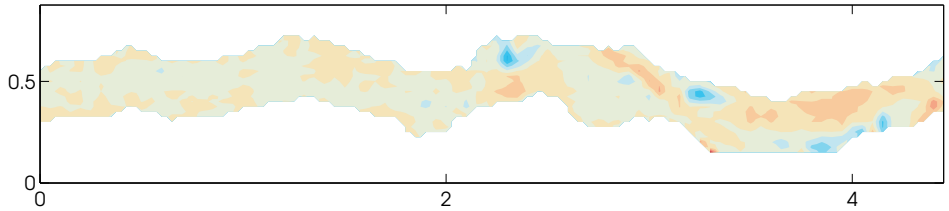

(b) Experiment 3: Hours 25 - 20

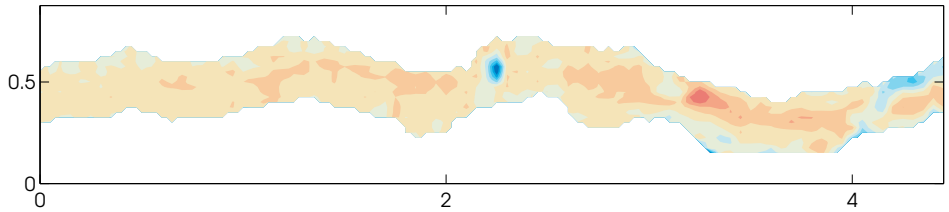

(c) Experiment 3: Hours 30 - 25

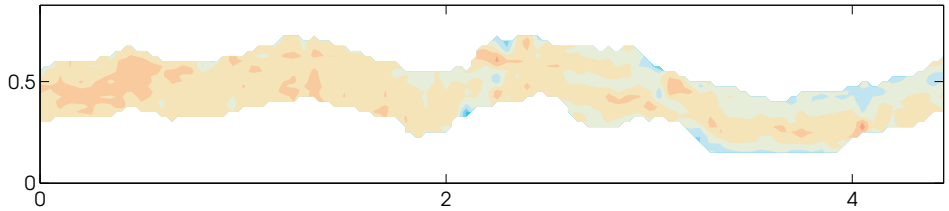

(d) Experiment 3: Hours 35 - 30

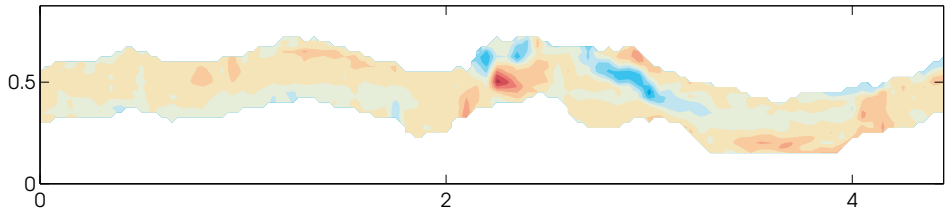

(e) Experiment 3: Hours 40 - 35

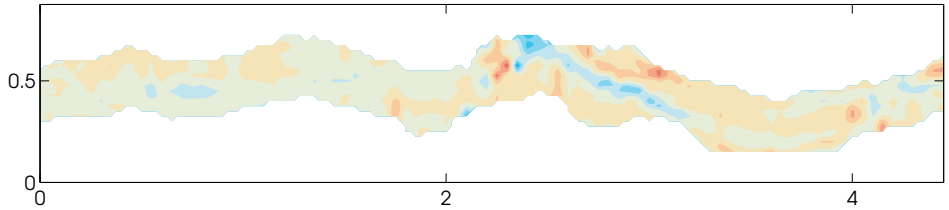

(f) Experiment 3: Hours 35 - 30

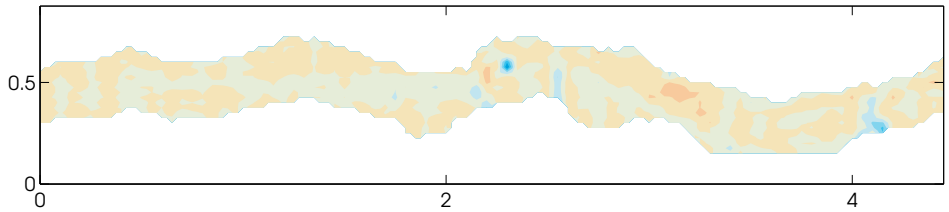

(g) Experiment 3: Hours 40 - 35

Figure C.4: DEMs of Difference for Experiment 3

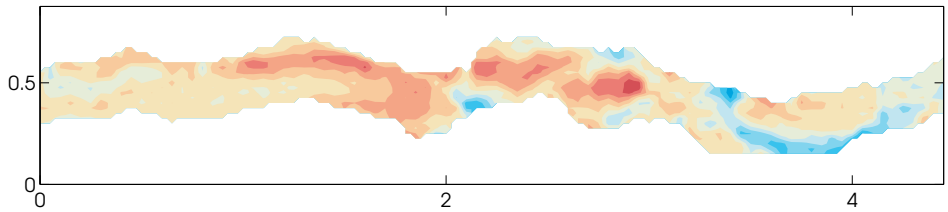

(a) Experiment 4: Hours 15 - 10

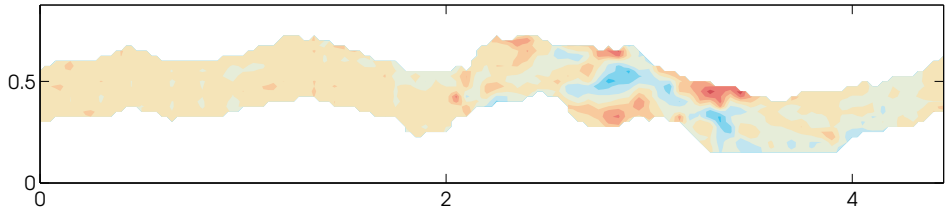

(b) Experiment 4: Hours 20 - 15

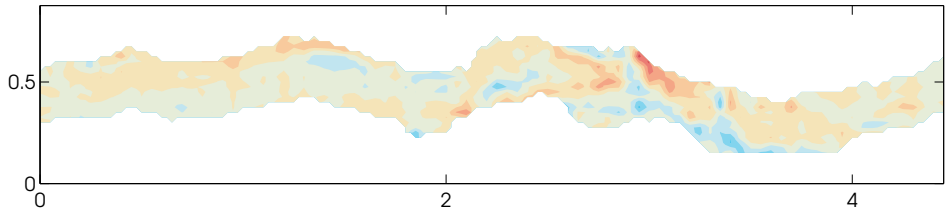

(c) Experiment 4: Hours 25 - 20

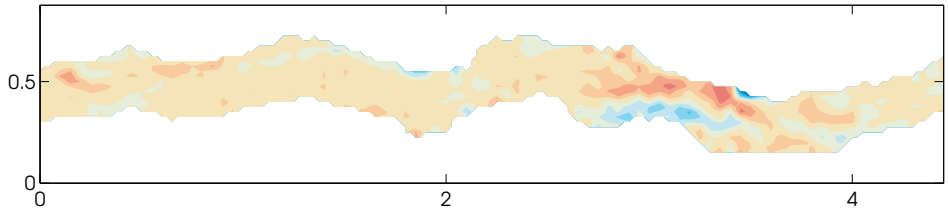

(d) Experiment 4: Hours 30 - 25

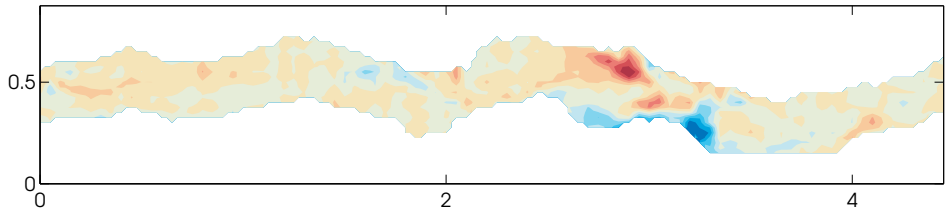

(e) Experiment 4: Hours 35 - 30

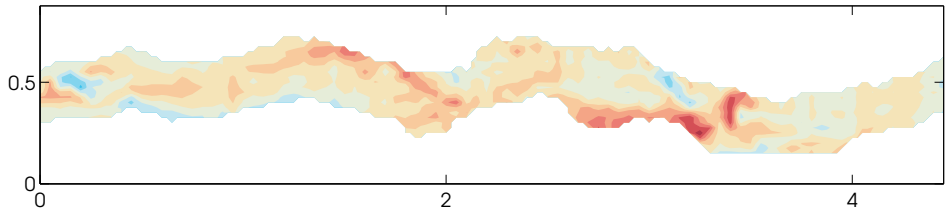

(f) Experiment 4: Hours 40 - 35

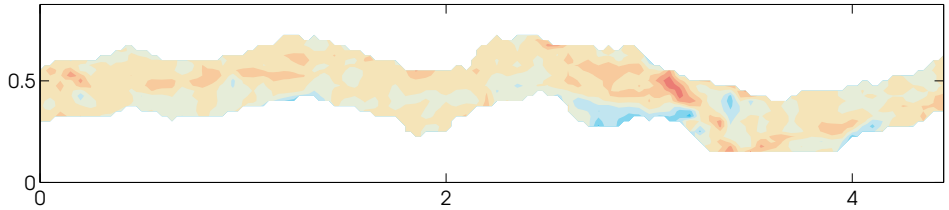

(g) Experiment 4: Hours 45 - 40

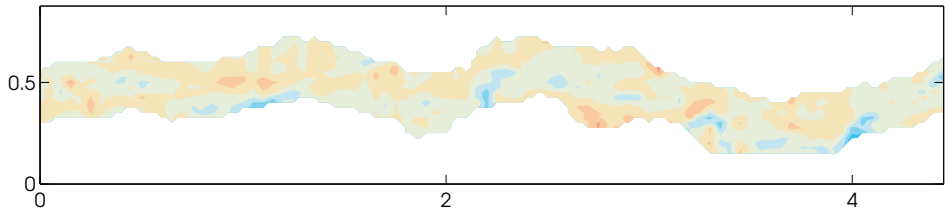

(h) Experiment 4: Hours 50 - 45

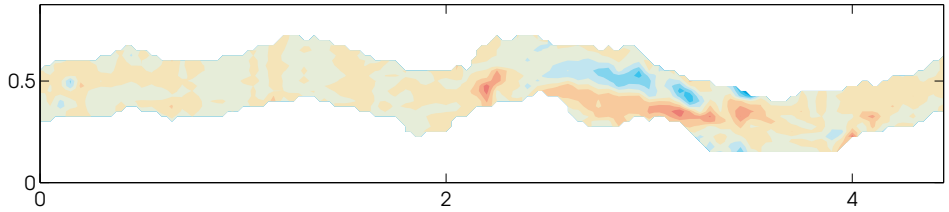

(i) Experiment 4: Hours 55 - 50

Figure C.5: DEMs of Difference for Experiment 4